PROGRESS REPORT ON SAFETY RESEARCH ON RADIOACTIVE
WASTE MANAGEMENT FOR THE PERIOD
APRIL 1993 TO MARCH 1995

March 1996

(Eds.) Keiichi SEKINE, Susumu MURAOKA and Tsunetaka BANBA

日 本 原 子 力 研 究 所
Japan Atomic Energy Research Institute

Progress Report on Safety Research on Radioactive Waste Management
for the Period April 1993 to March 1995

(Eds.) Keiichi SEKINE, Susumu MURAOKA and Tsunetaka BANBA

Department of Environmental Safety Research
Tokai Research Establishment
Japan Atomic Energy Research Institute
Tokai-mura, Naka-gun, Ibaraki-ken

This report summarizes the research and development activities on radioactive waste management at the Engineered Barrier Materials Laboratory, Natural Barrier Laboratory and Environmental Geochemistry Laboratory of the Department of Environmental Safety Research during the fiscal years of 1993 and 1994 (April 1, 1993 - March 31, 1995).

The topics are as follows:

1) As for waste forms and engineered barrier material, performance assessment studies were carried out on various waste forms, buffer materials and mortar.

2) In the safety evaluation study for shallow land disposal, migration behaviour of nuclides in the soil layer was studied.

3) In the safety evaluation study for geological disposal, chemical behaviour of radionuclides in water, nuclide migration in geosphere and groundwater flow system were studied. Migration of uranium series nuclides in uranium ore deposit was studied as a part of natural analogue study.

放射性廃棄物処理処分の安全性研究に関する平成5、6年度報告書

日本原子力研究所東海研究所環境安全研究部

（編）関根　敬一・村岡　　進・馬場　恒孝

（1996年2月15日受理）

　人工バリア研究室、天然バリア研究室及び地質環境研究室において、平成5、6年度に実施した放射性廃棄物処理処分の安全性に関する研究成果をまとめた。

　その内容は次の通りである。

1)　廃棄物固化体及び人工バリア材の研究開発では、各種固化体、緩衝材及びモルタルの性能評価試験を継続した。

2)　浅地中埋設に関する安全評価研究では、土壌中の核種移行試験を継続した。

3)　地層処分の安全性評価研究では、核種の水中での化学的挙動、地層中での核種移行、地下水流動に関する研究、並びに、ナチュラルアナログ研究を継続した。

# Contents

# 目　　　　次

Introduction

In order to achieve the safe disposal of radioactive wastes, it is necessary to promote the development of waste management and safety assessment methodology.

The Japan Atomic Energy Research Institute (JAERI) has been conducting safety assessment study and development of new technology to contribute to the establishment of national system for the radioactive waste management in Japan.

This report summarizes the status and results of studies performed in the fiscal years 1993 and 1994 at Engineered Barrier Materials Laboratory, Natural Barrier Laboratory and Environmental Geochemistry Laboratory of the Department of Environmental Safety Research, JAERI.

The progress report series have been issued in the following numbers: JAERI-M 82-145, 83-076, 84-133, 85-090, 86-131, 87-131, 88-201, 89-192, 91-019, 92-022, 93-037 and 94-027.

# 1. Research and Development of Waste Forms and Engineered Barrier Materials

## 1.1 Performance of Ceramic Waste Forms

### 1.1.1 Zirconia-Alumina Composite Ceramic Waste Forms Containing Ce and Nd Oxides

K. Kuramoto

## 1. INTRODUCTION

For the management of high level wastes (HLW) arising from reprocessing of spent nuclear fuels, it is very important to isolate some hazardous radionuclides, especially TRU elements e.g. from a group partitioning process, from the biosphere for a long time. These hazardous radionuclides are generally to be fixed into a suitable solid form with high water-resistance under hydrothermal conditions, and then to be disposed of an underground repository over several thousands years. In addition, the improvement of the properties of waste forms leads to reduction of multi-barrier system qualitatively and quantitatively, and to decrease of a cost of disposal sites.

In the previous works, the applicability of yttria-stabilized zirconia (YSZ)[1] and alumina[2] ceramics to waste forms for immobilizing high concentrated TRU elements were examined using TRU simulants with emphasis on phase stability and chemical durability. It is shown that YSZ and alumina waste forms indicated good phase stability, and that YSZ waste form was superior to alumina for chemical durability.

YSZ-alumina composite waste form is proposed in quest of not only maintenance of phase stability and chemical durability of YSZ and alumina waste forms, but also further improvement of its properties such as fracture strength, toughness and long term stability. According to French et al.[3], fracture strength and toughness of YSZ are improved by the addition of alumina. For long term stability, the composite ceramic forms are expected to remain stable crystallographically after a long time because alumina will react with Pb and produce MP[4] and PK[5] phases, and other phases with Bi[6], which are daughters of the TRU elements.

In this report, the application of zirconia-alumina composite waste form for immobilizing high concentrated TRU elements are investigated in terms of phase stability and chemical durability using TRU simulants of Ce and Nd.

## 2. EXPERIMENTALS

### 2.1 Composite Sample Preparation

As shown in Table 1, composite ceramic waste forms containing rare earth oxides were prepared. The YSZ (TZ-8Y; Toso Co. Ltd.), reagent grade of $\alpha$-alumina, $CeO_2$ and $Nd_2O_3$ were directly weighed, and mixed using an agate mortar. After pelletized the powder mixture, the obtained disks of about 20 mm $\phi \times$ 3 mm h were calcined at 1500°C for 25 hrs in flowing 3% $H_2$ + Ar. These pellets were crushed and re-mixed in a YSZ ball mill and were uniaxially pressed in a cylindrical die at 36 MPa. The pellets were sintered at 1500 °C for 80 hrs in the atmosphere.

### 2.2 XRD and EDX

Crystalline phases formed in composite ceramic waste forms were identified by XRD method using powdered samples. XRD patterns were measured using a spectrometer of RAD-IIC type (Rigaku Co. Ltd.) with CuK$\alpha$ radiation at 40 kV and 20 mA. Lattice parameters of YSZ solid solutions were determined by Nelson-Riley method[7]. Lattice parameters of other phases were corrected using the respective lattice parameters of YSZ solid solutions as the internal standard. The contents of Ce and Nd in each phase of the samples were also obtained using EDX (S-650; Hitachi).

### 2.3 Chemical Durability

In accordance with the procedure of MCC-2[8], chemical durability were measured in deionized water at 150°C for 114 days using powdered samples adjusted under 75 $\mu$m. Judging from the previous work, these powdered ceramic forms are attacked more in an early stage, probably owing to the selective dissolution of sharp edges produced by crushing ceramic forms. Thus in this work, the leachate in a miniature teflon autoclave were exchanged after the early stage. After following 114 days leaching, the powdered samples and leachates were separated by the ultrafiltration with a milipore filter of 0.45 $\mu$m size. The withdrawn powder samples were washed with deionized water and dried in a vacuum desiccator. 0.01M $HNO_3$ was added into empty teflon crucible to dissolve precipitations adhering to the crucible, and heated at 150 °C for a day. The concentrations of the separated leachates and the acid solutions for each element were analyzed by ICP-MS (TMS-2000; Yokogawa). The obtained leach rates $(LR_i, \; g \cdot cm^{-2} \cdot day^{-1})$ for Zr, Al, Ce and Nd were normalized by the following equation.

$$LR_i = A_i \cdot V/(F_i \cdot SA \cdot T),$$

where $A_i$ is the sum of the concentration of element i in the both solution in g/ml, V is the volume of the leachates (50 ml), $F_i$ is the mass fraction of element in the sample, SA is the initial surface area of the sample in $cm^2$ and T is the leaching time in day, respectively.

## 3. RESULTS AND DISCUSSIONS

### 3.1 Phase Stability of Composite Waste Forms

Figure 1 shows XRD patterns of a series of A3Z ($Al_2O_3$:YSZ = 3:1) powdered samples containing Ce and/or Nd oxides. As shown in Fig.1, the intimate mixing of YSZ into alumina is not influential in these new phase formation, as is expected from the phase diagram[9]. It is revealed that addition of Nd to the composites brings about the formation of YSZ solid solution and PK phase, on the contrary, Ce addition causes to grow YSZ solid solution and MP phase in the Ce-bearing samples. The results of alumina compound formation are in good agreements with those of alumina-based ceramics[2]. It is demonstrated that the radius of rare earth ion relates with the relative phase stability for MP and PK phase[10]. YSZ solid solution, PK and MP phases were formed in Ce+Nd-bearing samples. The lattice parameters of the phases are listed in Table 2, which do not depend on matrix content. The lattice parameters of YSZ solid solutions in the Ce- and/or Nd-bearing samples are larger remarkably than those without rare earth oxides. This indicates formations of YSZ solid solution with Ce and/or Nd ions. It is confirmed by EDX observation and lattice parameter measurement that Ce also exists in PK phase as well as Nd in MP phase as listed in Table 3. Namely, larger lattice parameters of PK phase in a series of Ce+Nd-bearings than those of Nd-PK phases imply the presence of larger Ce ion as well as Nd, and smaller lattice parameters of MP in the Ce+Nd-bearing forms than those of Ce-MP phase indicate the settlement of smaller Nd ions as well as Ce.

### 3.2 Chemical Durability of Composite Waste Forms

Figure 2 shows chemical durability in deionized water at 150℃ for 114 days from a series of AZ3 powdered forms. The variation of matrix contents did not cause remarkably change of $LR_{Ce}$ and $LR_{Nd}$ in the present examinations. These results revealed obviously that all the values of normalized leach rates are less than $10^9$ $g \cdot cm^{-2} \cdot day^{-1}$, which are smaller by several orders of magnitudes than those of lanthanide elements of a non-radioactive borosilicate waste glass performed in deionized

water. The value of $10^{-9}$ g·cm$^{-2}$·day$^{-1}$ means that more than 99% of $^{237}$Np ($\tau_{1/2}$ = 2.41 × 10$^6$ years) in the composite ceramic waste form with 1 m cube containing 10 mol% of $^{237}$Np will remain to immobilize inside the form and decay to non-radioactive $^{209}$Bi.

For YSZ phase, LR$_{Zr}$ are much lower than those of other elements as shown in Fig.2, so it is demonstrated that YSZ is excellent in chemical durability. The low LR$_{Ce}$ in AZ3-C also show that MP phase has good chemical durability, and relatively high LR$_{Al}$ is considerable to depend on dissolution of unreacted $\alpha$-Al$_2$O$_3$ phase. Relatively high LR$_{Al}$ and LR$_{Nd}$ in AZ3-N are due to the selective dissolution of PK phase, which are sufficiently larger than LR$_{Al}$ in AZ3-O. PK phase dissolution also influences LR$_{Al}$, LR$_{Ce}$ and LR$_{Nd}$ of AZ3-CN. In other words, chemical durability of composite ceramic waste forms depends on the existence of PK phase.

## 4. CONCLUSIONS OF COMPOSITE WASTE FORMS

The results of this work on YSZ-alumina composite ceramic forms containing Ce and/or Nd oxides up to 10 mol% are the followings;

(ⅰ) The maintenance of phase stability of composite waste form was confirmed, that is, the intimate mixing of YSZ into alumina is not influential in these new phase formation. Nd-perovskite or Ce-magnetoplumbite were formed in Nd- or Ce-bearing samples, respectively, and in Ce+Nd-bearing samples Ce also exists in perovskite and Nd in magnetoplumbite phases.

(ⅱ) The YSZ-alumina composite ceramic waste forms sintered at 1500℃ for 80 hrs in a reducing atmosphere show good chemical durability of less than $10^{-9}$ g·cm$^{-2}$·day$^{-1}$, however chemical durability of waste forms depend on the formation of perovskite phase.

(ⅲ) Compared with YSZ, alumina and YSZ-alumina composite waste forms, these forms have phase stability but the formation of perovskite decrease chemical durability of alumina and YSZ-alumina composite waste form.

## 5. FUTURE WORK

The effects of the variation of TRU elements' valences caused by the change of sintering atmosphere (several grades of oxidizing and reducing atmosphere) on crystallographic phase stability and chemical durability are also investigated using YSZ waste forms including $^{237}$Np and $^{241}$Am at Nuclear Fuel Cycle Safety Engineering Research Facility: NUCEF.

## ACKNOWLEDGMENTS

## REFERENCES

( 1 ) Kuramoto, K., et al. : Preprint 1993 Annu. Mtg. on Rare Earths, Tokyo, 2A07.

( 2 ) Yanagi, T., et al. : J. Nucl. Sci. Technol., $\underline{31}$[10], 1092(1994).

( 3 ) French, J. D., et al. : J. Am. Ceram. Soc., $\underline{75}$, 418(1992).

( 4 ) Morgan, P. E. D., et al. : J. Am. Ceram. Soc., $\underline{69}$, C157-159(1986).

( 5 ) Kuxmann, C., et al. : Erzmetall, $\underline{27}$[11], 533(1974).

( 6 ) "Phase Diagrams for Ceramists" : Vol. 3, ed. by Levin, E. M. and McMurdie, H. F., Am. Ceram. Soc. (1975).

( 7 ) "X-Ray Method" : ed. by Whiston, C., John Wiley & Sons (1985).

( 8 ) Strachan, D. M., et al. : Mat. Res. Soc. Symp. Proc. Vol. 3, 347(1980).

( 9 ) "Phase Diagrams for Ceramists" : Vol. 4, ed. by Roth, R. S., Am. Ceram. Soc. (1981).

(10) Iyi, N., et al. : J. Solid State Chem., $\underline{83}$, 8(1989).

## Table 1 Compositions of YSZ-alumina composite
### ceramic waste forms in mol%[a]

| Sample | Matrix | | | Simulated Waste | |
|--------|--------|--------|----------|--------|----------|
| | $ZrO_2$ | $YO_{1.5}$ | $AlO_{1.5}$ | $CeO_2$ | $NdO_{1.5}$ |
| AZ3-0 | 51.65 | 8.62 | 39.73 | — | — |
| AZ-0 | 28.79 | 4.80 | 66.41 | — | — |
| A3Z-0 | 12.36 | 2.06 | 85.57 | — | — |
| AZ3-N | 43.90 | 7.33 | 33.77 | — | 15.00 |
| AZ-N | 25.09 | 4.19 | 57.87 | — | 12.86 |
| A3Z-N | 10.97 | 1.83 | 75.94 | — | 11.26 |
| AZ3-CN | 45.62 | 7.61 | 35.09 | 3.89 | 7.78 |
| AZ-CN | 25.92 | 4.33 | 59.80 | 3.32 | 6.63 |
| A3Z-CN | 11.29 | 1.88 | 78.15 | 2.89 | 5.78 |
| AZ3-C | 47.47 | 7.92 | 36.51 | 8.10 | — |
| AZ-C | 26.81 | 4.47 | 61.85 | 6.86 | — |
| A3Z-C | 11.63 | 1.94 | 80.47 | 5.96 | — |

a ; Compositions of each constituent indicate the contents of each
cation to total cations in mol%.

Table 2　Lattice parameters of YSZ, perovskite (PK)
and magnetoplumbite (MP) phases in nm

| Sample | YSZ (a) | PK (a) | PK (c) | MP (a) | MP (c) |
|--------|---------|--------|--------|--------|--------|
| AZ3-0  | 0.5136  | —      | —      | —      | —      |
| AZ-0   | 0.5139  | —      | —      | —      | —      |
| A3Z-0  | 0.5137  | —      | —      | —      | —      |
| AZ3-N  | 0.5188  | 0.5313 | 1.2927 | —      | —      |
| AZ-N   | 0.5188  | 0.5312 | 1.2908 | —      | —      |
| A3Z-N  | 0.5189  | 0.5313 | 1.2920 | —      | —      |
| AZ3-CN | 0.5179  | 0.5322 | 1.2986 | 0.5559 | 2.1941 |
| AZ-CN  | 0.5182  | 0.5328 | 1.2953 | 0.5555 | 2.1980 |
| A3Z-CN | 0.5186  | 0.5324 | 1.2956 | 0.5551 | 2.1974 |
| AZ3-C  | 0.5164  | —      | —      | 0.5554 | 2.2004 |
| AZ-C   | 0.5156  | —      | —      | 0.5554 | 2.1992 |
| A3Z-C  | 0.5151  | —      | —      | 0.5552 | 2.2017 |

" — " of lattice parameter indicates nonexistence of the phases.

Table 3　Relative amounts of Ce and Nd in each phase

| Sample | YSZ Ce | YSZ Nd | PK Ce | PK Nd | MP Ce | MP Nd |
|--------|--------|--------|-------|-------|-------|-------|
| A3Z-CN | 31     | 69     | 42    | 58    | 59    | 41    |

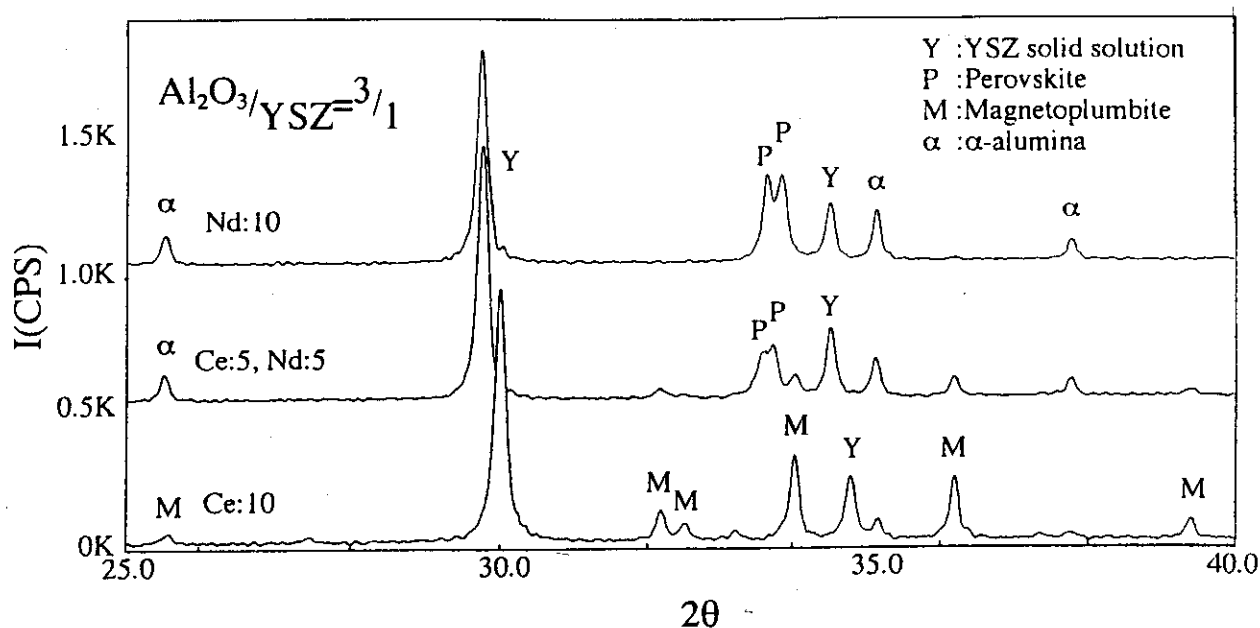Fig. 1 XRD patterns of composite ceramic waste forms of a series of A3Z
(Al$_2$O$_3$/YSZ=3/1) powdered samples.

Top:     A3Z-N (10 mol% of Nd oxide)
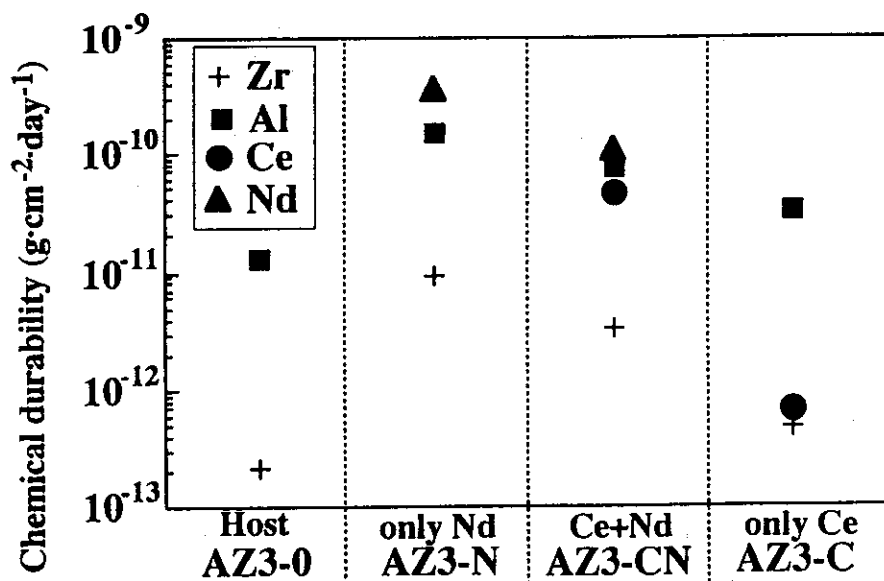Middle:  A3Z-CN (5 mol% of Ce and Nd oxides)
Bottom:  A3Z-C (10 mol% of Ce oxide)



Fig. 2 Chemical durability of composite ceramic waste forms in
deionized water at 150 ℃ for 114 days from a series of
of AZ3 (Al$_2$O$_3$/YSZ=1/3) powdered samples.

## 1.1.2 Radiation Damage of Cm-Doped Perovskite

H. Mitamura

### INTRODUCTION

In the polyphase titanate ceramic waste form, Synroc[1], a part of actinite nuclides would be incorporated in the perovskite phase. As microencapsulation by more durable phases could mask radiation-damage effects on less durable perovskite, single phase material is useful for getting direct information on this point. In the present study, $\alpha$-decay damage effects on Cm-doped perovskite were investigated through density measurement and MCC-1 leach testing. Since the Cm leach rate in pure water was not sensitive to accumulation of $\alpha$-decay damage, an acidic buffer solution was used in the present study to prevent adsorption of the curium on specimen surfaces and/or leach container wall as much as possible.

### EXPERIMENTAL

The Cm-doped perovskite that had its nominal composition of $Ca_{0.9892}(Cm, Pu)_{0.0108}$ $Al_{0.0108}Ti_{0.9892}O_3$ was made by hot-pressing at 1250 °C and 29MPa for 2 hours[2].

The density of a Cm-doped perovskite cylinder, was periodically measured at 30°C using the water displacement method. The half-disk specimens that had accumulated doses up to $8.3 \times 10^{17}$ $\alpha$ decays $\cdot g^{-1}$ were MCC-1 leach tested in pH~2 solution (0.05M KCl + 0.013M HCl) at 90°C for two months over four 7-day leach periods and a 28-day leach period. The leachate samples were analyzed by $\gamma$-ray spectrometry for $^{244}Cm$ and inductively coupled plasma atomic emission spectrometery (ICP-AES) for nonradioactive elements as in a previous study[2].

### RESULTS & DISCUSSION

#### Density

Change in density of the Cm-doped perovskite cylinder is shown in Fig. 3. The density changes are well fitted by a linear line. At a dose of $9 \times 10^{17}$ $\alpha$ decays $\cdot g^{-1}$, the fractional density decrease of the Cm-doped perovskite was 1.3%.

#### Leach Testing

The weight losses of half-disk specimens after two-month leach testing led to average leach rates of 1.7, 2.3, and 3.0 g $\cdot m^{-2} \cdot day^{-1}$ from the Cm-doped perovskite

material that accumulated doses of $1.6 \times 10^{17}$, $4.0 \times 10^{17}$, and $8.3 \times 10^{17}$ $\alpha$ decays$\cdot$g$^{-1}$, respectively (Table 4). This table implies that more damaged specimens are likely to give a higher leach rate. When the dissolution of perovskite proceeds through the following reaction:

$$CaTiO_3 + 2H^+ \longrightarrow Ca^{2+} + TiO_2(anatase) + H_2O \qquad (1),$$
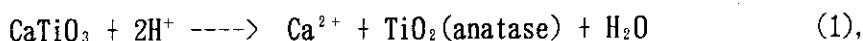
the CaO weight loss of a specimen would correspond to its total weight loss because TiO$_2$ precipitates on specimen surfaces[2] and contribution of the other minor elements would be negligible. Table 4 also compares normalized leach rates derived from the CaO and total weight losses of the Cm-doped perovskite specimens. Two different leach rates are similar to each other. Larger error of some specimens may be due to an additional weight loss during the specimen handling. That similarity implies that the simple reaction mentioned above can be adopted as the dissolution mechanism of Cm-doped perovskite in the acidic solution at 90 ℃.

Figure 4 compares changes in the normalized Ca leach rate and pH with time. In this figure, the Nos.(1), (2), and (3) indicate the data from leaching runs at doses of 1.6 $\times$ 10$^{17}$, 4.0 $\times$ 10$^{17}$, and 8.3 $\times$ 10$^{17}$ $\alpha$ decays$\cdot$g$^{-1}$, respectively. Unlike the normal leaching behavior of Synroc[1], the Ca leach rate from the Cm-doped perovskite increases with leach time. More damaged specimens tend to give a higher Ca leach rate. The most damaged samples give a constant leach rate after the first 7-day leaching run. At later stages of the leaching runs, the acidic leachant solution was neutralized by the leaching of Ca. At the final stage of the leaching runs, the Ca leach rate at three different doses converge to a similar value. This convergence may be due to solubility limit of Ca in the neutralized solution. Ti concentration in leachate was near the limit of detection. This is consistent with the replacement of perovskite by anatase on the surfaces of the as-leached perovskite specimens[2].

The $\gamma$-ray spectrometry also showed high leach rate of $^{244}$Cm (Fig.5). The Ca and Cm leach rates tend to rise with time in a similar manner to each other. Differences between both leach rates become larger at higher pH. In the final leaching run, both leach rates converged on each value, where the Cm leach rate was lower by a factor of >20. The lower Cm leach rate may be due to little solubilization at higher pH.

CONCLUSION

(1) Change in density of Cm-doped perovskite reached 1.3% at a dose of 9 $\times$ 10$^{17}$ $\alpha$

decays・g $^{-1}$.

(2) A simple dissolution mechanism was applied to leaching behavior of Cm-doped perovskite in acidic solution at 90℃.

(3) Cm and Ca leach rates at three different doses increased with leach time. In the final 28-day leaching run, both leach rates at three different doses converged to each lower value.

## REFERENCES

(1) A. E. Ringwood, S. E. Kesson, K. D. Reeve, D. M. Levins, and E. J. Ramm, "Synroc," pp. 233-334 in *Radioactive Waste Forms for The Future*, Edited by W. Lutze and R. C. Ewing, Elsevier Science Publishers, New York, 1988.

(2) H. Mitamura, S. Matsumoto, T. Tuboi, E. R. Vance, B. D. Begg, and K. P. Hart, "Alpha-Decay Damage of Cm-Doped Perovskite," pp. 1405-12 in *Scientific Basis for Nuclear Waste Management* XVIII. Edited by T. Murakami and R. C. Ewing. Materials Research Society, Pittsburgh, PA, 1995.

Table 4 Comparison of normalized leach rates derived from CaO and
weight losses of Cm-doped perovskite specimens

| Specimen Name | Normalized Leach Rate (g/m²/day) | | A/B | Dose |
|---|---|---|---|---|
| | CaO Loss (A) | Weight Loss (B) | (%) | (alpha decays/g) |
| P1-3B | 0.93 | 1.28 | 73 | 1.6E+17 |
| P2-2B | 1.47 | 1.77 | 83 | 1.6E+17 |
| P2-5B | 1.97 | 2.08 | 95 | 1.6E+17 |
| Average | 1.46 | 1.71 | | |
| P1-2B | 1.88 | 2.07 | 91 | 4.0E+17 |
| P1-4B | 2.22 | 2.43 | 91 | 4.0E+17 |
| P2-3B | 2.43 | 2.46 | 99 | 4.0E+17 |
| Average | 2.18 | 2.32 | | |
| P1-3A | 2.98 | 3.04 | 98 | 8.3E+17 |
| P2-2A | 2.94 | 3.02 | 97 | 8.3E+17 |
| P2-4A | 2.85 | 2.78 | 103 | 8.3E+17 |
| Average | 2.92 | 2.95 | | |
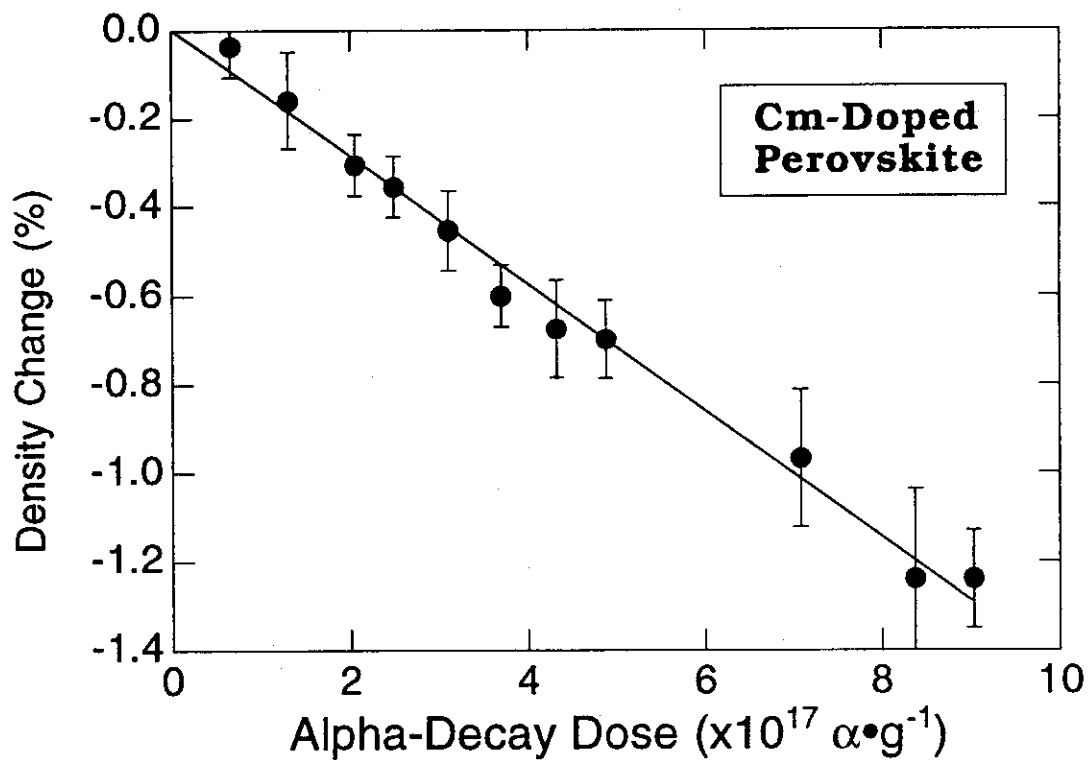


Fig. 3 Density change of Cm-doped perovskite versus alpha-decay dose.
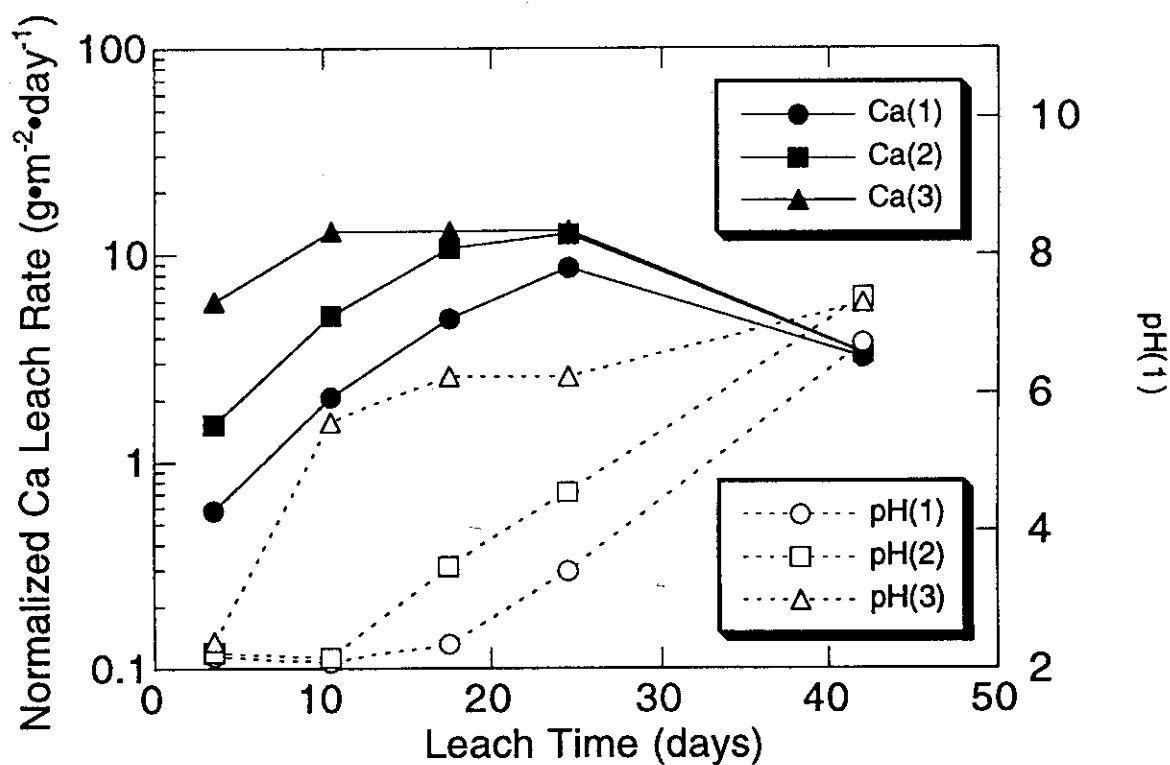
Fig. 4  Changes in normalized Ca leach rate and pH with time.
The specimens accumulated doses of (1) $1.6 \times 10^{17}$, (2)
$4.0 \times 10^{17}$, and (3) $8.3 \times 10^{17}$ $\alpha$ decays・$g^{-1}$.
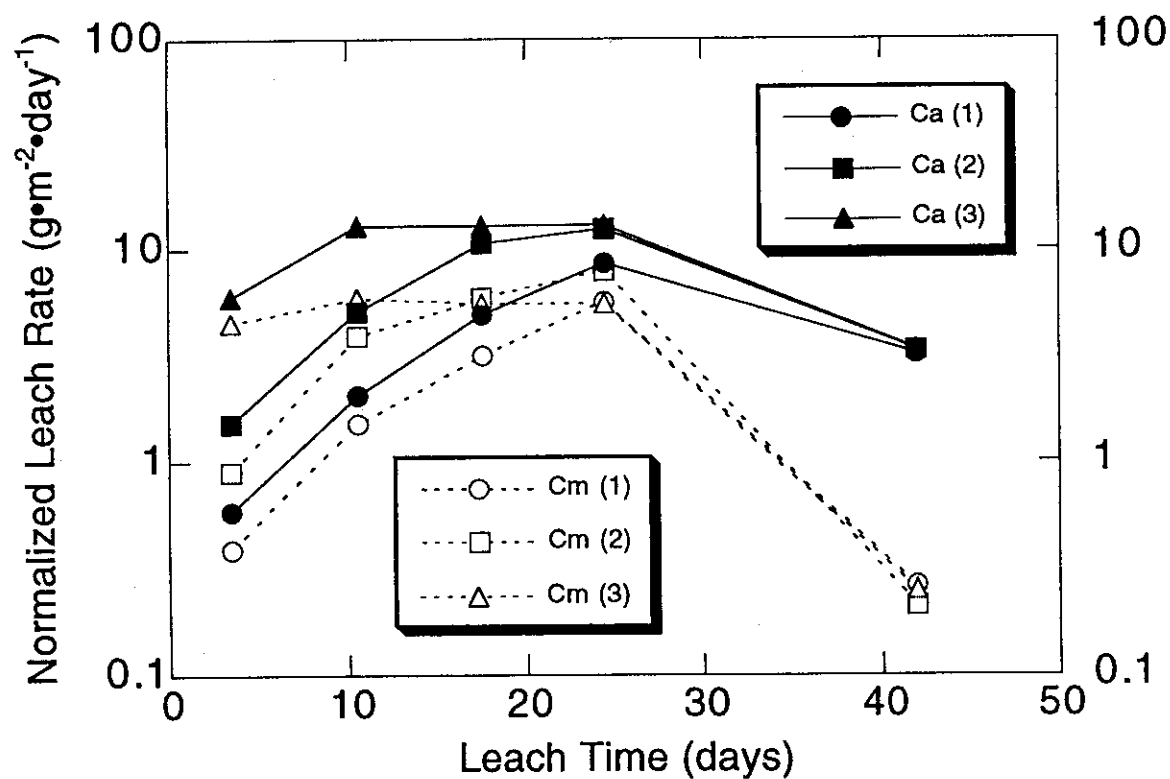


Fig. 5  Changes in normalized Ca and Cm leach rates with time.
The specimens accumulated doses of (1) $1.6 \times 10^{17}$, (2)
$4.0 \times 10^{17}$, and (3) $8.3 \times 10^{17}$ $\alpha$ decays・$g^{-1}$.

# 1.2 Performance of Engineered Barrier Materials

## 1.2.1 Sorption of Neptunium on Bentonite

N. Kozai

### INTRODUCTION

Transuranic elements (TRU) are particularly important in safety evaluations of high level radioactive waste disposal because of their long half lives and high toxicity. The use of bentonite as a backfill materials in radioactive waste disposal has been proposed because of its properties, that is, low permeability and large cation exchange capacity. Bentonite contains several minerals including smectite and quartz as a major components, and calcite and pyrite as minor phases. We have considered radionuclide sorption on bentonite to be discussed in a holistic fashion where the clay is considered as a complex assemblage of interacting minerals.

In the present work, we have investigated the sorption of neptunium on bentonite and on its components to clarify the role of each component of bentonite on the neptunium sorption on bentonite.

### EXPERIMENTAL

#### 2.1 Materials Preparation

The starting materials included:

(1) a pentavalent (Np(V)) neptunium solution from the Commissariat à l'Énergie Atomique (CEA) as $^{237}NpO_2NO_3$. This stock reagent was diluted with 0.01M $NaClO_4$ to yield a working solution having a neptunium concentration of $6 \times 10^{-7}$ M;

(2) Tsukinuno bentonite, Kunigeru V1 (Kunimine Industries Co. Ltd.) designated as $Na^+$-rich type bentonite. The bentonite contained smectite about 50 weight %, $\alpha$-quartz 40 weight %, pyrite 1 weight % and others. $Na^+$ and $Ca^{2+}$ were sorbed on the bentonite about 59 and 18 mol%, respectively.

(3) smectite provided as Kunipia F (Kunimine Industries Co. Ltd.) which had been separated from Kunigeru V1 bentonite. Before use, pure sodium- or calcium-smectite (Na-smectite or Ca-smectite) was prepared by substituting $Na^+$ or $Ca^{2+}$ for the exchangeable cation of smectite.

(4) $\alpha$-quartz powder sourced from India; and

(5) pyrite from Okayama, Japan. All sorbents were ground and sieved under less than 74 $\mu$m prior to use in the experiments.

## 2.2 Sorption-desorption Experiment

Sorption experiments were carried out to discuss the relationship between pH of the radioactive solution containing neptunium and the amount of neptunium sorbed on sorbent. The sorbent was added to the solution in polycarbonate centrifugation tube after the pH adjustment between 2 and 7, and the mixture was kept at 20℃ for 10 days. After the sorption experiment, the phase separation was carried out by centrifugation at 12000 rpm for 1 hr, and the pH and concentration of neptunium of the supernatant were measured.

Subsequently, desorption experiments using the sequential extraction procedure were carried out to clarify the association of neptunium with the sorbent. The sorbent on which neptunium was sorbed was firstly treated with 1 M KCl and secondary 1 M HCl solution at 20℃ for 2 days. At the end of each extraction step, the suspended solution was separated by the centrifugation mentioned above, and concentration of the extracted neptunium was measured.

## 2.3 Estimative Method

The relation between the amounts of neptunium before and after the sorption-desorption experiment will be expressed by

$$C_0 \cdot V = C \cdot V + Q, \tag{1}$$

$$Q = Q_K + Q_H + Q_R, \tag{2}$$

where $C_0$ = initial concentration of neptunium in solution $(\text{mol} \cdot \text{cm}^{-3})$, $C$ = concentration of neptunium in solution after the sorption experiment $(\text{mol} \cdot \text{cm}^{-3})$, $Q_K$ = the neptunium desorbed by KCl from sorbent (mol), $Q_H$ = the neptunium desorbed by HCl from sorbent (mol), $Q_R$ = the neptunium remained on sorbent after the desorption (mol), and $V$ = volume of solution $(\text{cm}^3)$. In an early study of neptunium, we showed that neptunium adsorbed ion-exchangeably on bentonite and smectite was desorbable by KCl solution and neptunium sorbed specifically was desorbed not by KCl but by HCl solution[1]. To evaluate the distribution of neptunium between solution and sorbent, the sorption ratio of the amount of neptunium sorbed on sorbent to initial amount of neptunium in the solution was defined as:

$$P_T = \frac{Q}{C_0 \cdot V} \cdot 100, \tag{3}$$

$$P_K = \frac{Q_K}{C_0 \cdot V} \cdot 100, \tag{4}$$

$$P_H = \frac{Q_H}{C_0 \cdot V} \cdot 100, \tag{5}$$

$$P_R = \frac{Q_R}{C_0 \cdot V} \cdot 100, \qquad (6)$$

where $P_T$ = the percent fraction of all the neptunium sorbed on sorbent, $P_K$ = the percent fraction of the neptunium adsorbed by ion-exchange mechanism, $P_H$ = the percent fraction of the neptunium sorbed specifically, and $P_R$ = the percent fraction of the sorbed neptunium remained on sorbent after the desorption experiment.

## RESULTS

The neptunium sorbed on all sorbents were desorbed completely by 1M KCl and 1M HCl solutions ($P_R$ = 0 for all sorbents). The sorption ratio of neptunium for bentonite is illustrated in Fig. 6 as a function of final pH of the solution. $P_T$ for bentonite was constant (~10%) at pH between 5 and 7 (Fig. 6a). Both $P_K$ and $P_H$ are almost constant and similar to each other (~5%) in this pH range (Fig. 6b).

The sorption ratio of neptunium for major components of bentonite, that is, Na-smectite, Ca-smectite, and quartz, are shown in Figs. 7, 8, and 9, respectively as a function of final pH of the solution. $P_T$ for Na-smectite was roughly constant at pH between 5 and 7 (20~30%) and increased with decreasing pH below pH5 (~65% at pH 2.5) (Fig. 7a). The increase in the $P_T$ is due to increase in the $P_H$ figure below pH5 (Fig. 7b). $P_T$ for Ca-smectite was roughly constant at pH between 3 and 7 (5~10%) and increased with decreasing pH below pH3 (~20% at pH2.5)(Fig. 8a). The increase in the $P_T$ is due to increase in the $P_H$ figure below pH3 (Fig. 8b). Both $P_K$ and $P_H$ were lower than those for Na-smectite. Little fraction on neptunium in the solution was sorbed on quartz powder ($\leq$ 3%, Fig. 9) and pyrite (~0%). Quartz and pyrite were negligible contributors to the neptunium sorption on bentonite.

## DISCUSSION

Differences of the sorption behavior of neptunium between the bentonite and Na-smectite are: (1) $P_K$ for the bentonite was smaller by a factor 1~5 than that for Na-smectite in the pH range between 2 and 7, and (2) $P_H$ for the bentonite did not increase with decreasing pH below pH5.

Since the smectite content and the Na$^+$ content of the "Kunigeru V1" bentonite are 50 weight% and 59 mol%, respectively, $P_K$ values for the bentonite would be calculated from the measured $P_K$ values for Na-smectite (5~25%) to be $\leq$ 7% (= $P_K$ for Na-smectite $\times$ 0.50 $\times$ 0.59). This is in accord with the experimental $P_K$ values for the bentonite. The ion-

exchangeable adsorption of neptunium on bentonite, therefore, would be estimated from the smectite content and the $Na^+$ content of bentonite.

As for the specific sorption of neptunium, we have reported the effect of $Ca^{2+}$, which is adsorbed on bentonite and contained in calcite, on the specific sorption on bentonite (smectite)[2]. The specific sorption of neptunium on smectite decreased with increasing the amount of $Ca^{2+}$ on smectite. When more than 13 mol% of $Ca^{2+}$ was adsorbed on Na-smectite, $P_H$ for the smectite of $Ca^{2+}$ 13 mol% became similar to that for Ca-smectite. Since the $Ca^{2+}$ content of smectite of the "Kunigeru V1" bentonite is 18 mol%, it is estimated that $P_H$ figure expected for the smectite of the bentonite would be similar to $P_H$ figure for Ca-smectite. Further, since the smectite content of the bentonite is 50 weight%, $P_H$ values expected for the "Kunigeru V1" bentonite would be calculated from the $P_H$ value for Ca-smectite (~20% at pH 2.5) to be ~10% at pH 2.5. This calculated $P_H$ figure for the bentonite is larger than the measured $P_H$ value for the bentonite of ~5% at pH 2.5. As for the difference between calculated and measured $P_H$ values for the "Kunigeru V1" bentonite, an attempt was made to examine the sorption of neptunium on the "natural" $Ca^{2+}$-rich smectite. No increase in the amount of the neptunium sorbed specifically was observed for the "natural" $Ca^{2+}$-rich smectite (Cheto montmorillonite). This result suggests that something of mechanism by which $Ca^{2+}$ is adsorbed on smectite might be different between the $Ca^{2+}$ adsorbed naturally for a long time and that adsorbed artificially within a short time. The smectite contained in the "Kunigeru V1" bentonite might have the nature of "natural" $Ca^{2+}$-rich smectite. As a result, no specific sorption of neptunium was occurred on the "Kunigeru V1" bentonite. This hypothesis will be examined in a future study.

REFERENCES

(1) N. Kozai et al., "Sorption Characteristics of Neptunium by Sodium-Smectite", J. Nucl. Sci. Technol., 30, 1153 (1993).

(2) N. Kozai et al., "Sorption Behavior of Neptunium on Bentonite - Effect of Calcium Ion on the Sorption-", Sci. Bas. Nucl. Waste Manage. XVIII, 1021 (1995).
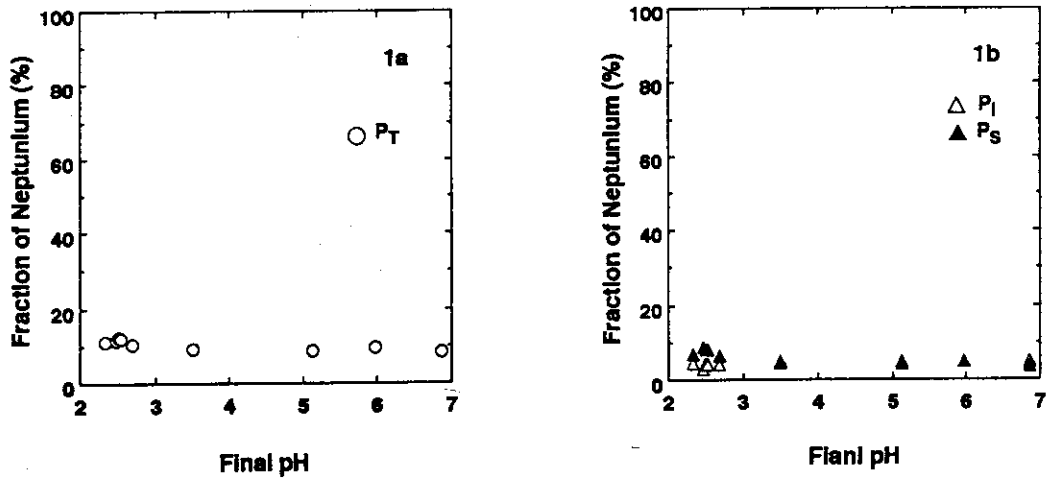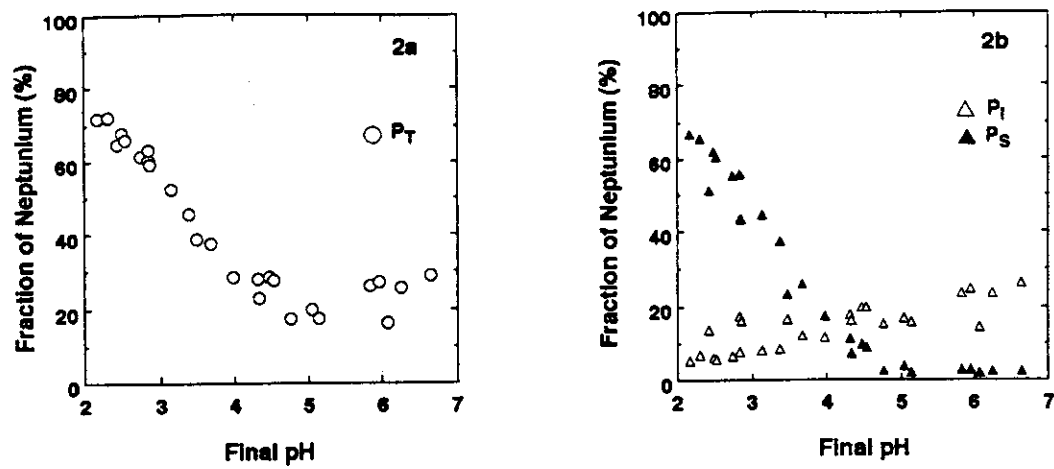
Fig. 6   Sorption ratio of neptunium for bentonite.


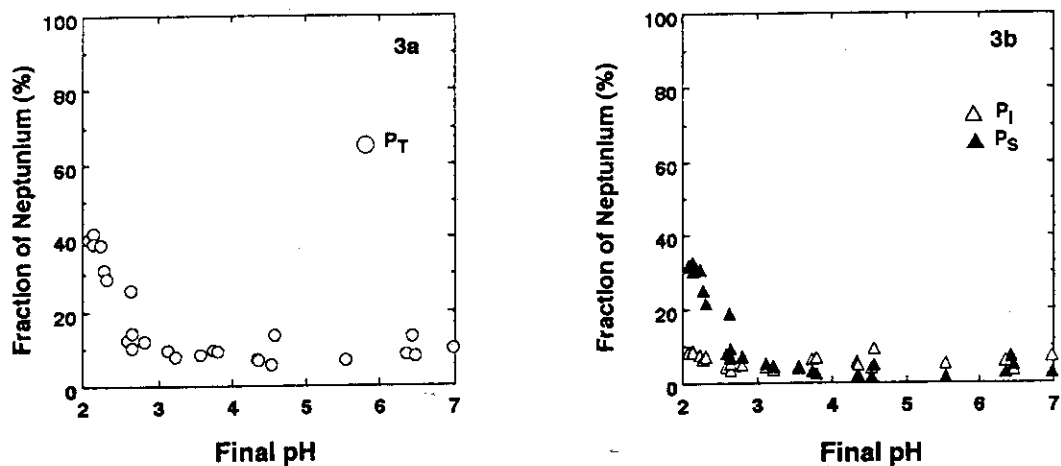
Fig. 7   Sorption ratio of neptunium for Na-smectite.

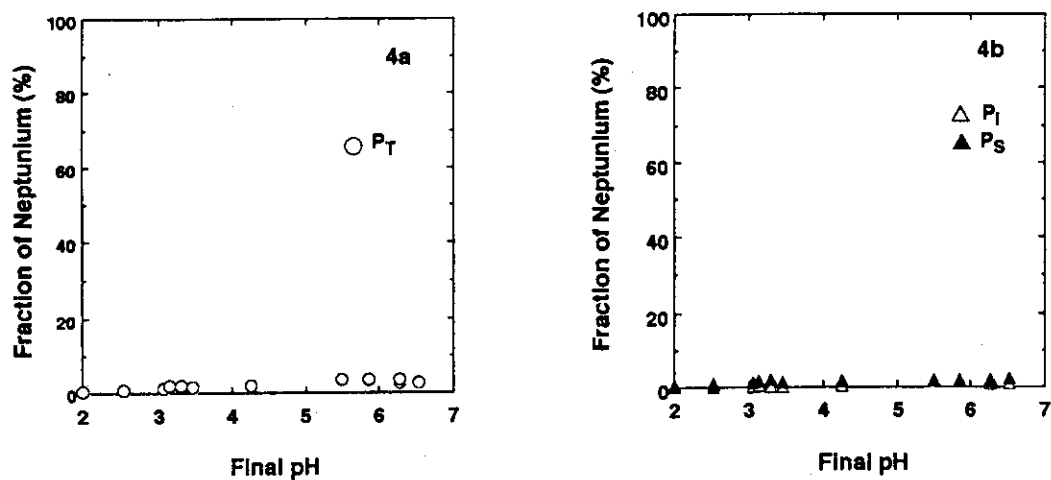Fig. 8 Sorption ratio of neptunium for Ca-smectite.



Fig. 9 Sorption ratio of neptunium for quartz.

## 1.2.2 Adsorption of C-14 on Mortar

J. Matsumoto

ABSTRACT

The sorption experiments of carbon-14 on the mortar grain (grain size: 0.50 ~ 1.0 mm) focused on the chemical form of the carbon-14 were carried out by the batch method. Four kinds of carbon-14 chemical form were used for the experiments: sodium carbonate, sodium acetate, acetaldehyde and arginine as the radiocarbons. 0.30 grams samples of mortar were soaked in the solution with carbon-14 at 15°C for periods of up to 20 days. At the end of each run, carbon-14 concentrations in the supernatants were determined before and after centrifugation (3,500 rpm, 1 hr).

In the mortar-sodium carbonate system, the retention process of carbon-14 related to reaction on the surface of the mortar was speculated as follows. First, $3CaO-SiO_2$, $2CaO-SiO_2$ of the mortar components contact with water and produce $Ca(OH)_2$. $Ca(OH)_2$ produces $Ca^{2+}$ and $OH^-$ in the solution. Then, calcite forms from $Ca^{2+}$ and $CO_3^{2-}$ in the solution. Thus, the sorption ratio of carbon-14 onto mortar will be high until mortar has been completely carbonated because $Ca^{2+}$ is rich in the mortar and the solubility of calcite is low.

In the mortar-organic system, the soluble organic carbon-14 is hardly sorbed on the surface of the mortar. Therefore, the cementitious materials may not inhibit the release of organic radiocarbons from the low-level radioactive wastes, contrary to the case of inorganic radiocarbon.

EXPERIMENTAL

### Materials

Three types of mortar samples used for the present sorption experiments were crushed mortar (grain size: 0.50 ~ 1.0 mm). First mortar was mixtures of ordinary portland cement, fine aggregate and water with mass ratio of 1:2:0.55 (OPC mortar). Second was mixture of ordinary portland cement, blast furnace slag, fly ash and fine aggregate and water with mass ratio of 1:3.15:0.7 (MC mortar). And the others was carbonated MC mortar (CMC mortar). Four kinds of carbon-14 sources were selected for the sorption experiment; sodium carbonate as inorganic carbon, and sodium acetate, acetaldehyde, arginine as organic carbon. These chemical forms normally comprise a large portion of carbon-14 contained in the low-level radioactive wastes (except arginine).

## Procedures

Experiments were conducted at 15℃ for up to 20 days in the distilled water. 0.30 grams of mortar sample and 9.0 ml distilled water were put into a sealed glass tube. The glass tube was preserved at 15℃ for 4 days. The pH of solution reached a constant value (about 12.5) for 4 days. After that, adjusted carbon-14 solution was added to the glass tube with mortar sample and water. The initial carbon-14 concentration of each run was determined by the liquid scintillation counter. The sorption experiments using different carbon-14 sources, that is, sodium carbonated, sodium acetate, acetaldehyde and arginine, were carried out under a carrier-free condition.

At the end of each run, 1 ml of supernatant was taken off and remains of sample solution was centrifuged under the condition of 3,500 rpm for 1 hr. Both the supernatants were determined by the liquid scintillation counter. X-ray diffraction pattern of the precipitates obtained from of carbon-14 free reference test, which was subjected to the sorption experiment under the same conditions, were obtained using copper X-ray tube.
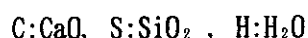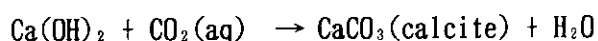
## RESULTS AND DISCUSSION

### Sorption of Carbon-14 in Mortar-Carbonate System

Figure 10 shows the normalized concentration of carbon-14 in the solution as a function of the elapsed time. In this experiment, the initial concentration of sodium carbonate is $7.4 \times 10^{-8}$ mol/l. The normalized concentrations of carbon-14 in the solutions before and after the centrifugation are shown by open and solid circles, respectively. Normalized concentrations of carbon-14 in both the solutions rapidly decrease with elapsed time in the initial stage of experiment. And there is some difference of carbon-14 concentration between the centrifuged solution and non-centrifuged solution.

This behavior of carbon-14 is similar to that in the leachate of the cementitious waste form containing carbon-14, which has been reported previously. Namely the apparent high concentration of carbon-14 in the non-centrifuged solution is attributable to the formation of suspended colloidal particles in the solution. The difference of carbon-14 concentration between the two solutions reduces grow in the solution with an increase in elapsed time and precipitate on the surface of the mortar. Identification of the suspended particles and precipitates obtained from the reference test was carried out by the X-ray diffraction analysis. An X-ray diffraction pattern from the precipitates reveals that the precipitates mainly consist of calcite ($CaCO_3$).

In the mortar-carbonate system, the retention process of carbon-14 closely related the reaction on the surface of the mortar is speculated as follows. First, $3CaO-SiO_2$ ($C_3S$) and $2CaO-SiO_2$ ($C_2S$) of the mortar components contact with water and process $Ca(OH)_2$. These solution, and consequently the pH of solution increases to about 12.5. Then, calcite ($CaCO_3$) forms from $Ca^{2+}$ and $CO_3^{2-}$ in the solution under a high pH condition. This reaction is expressed by equations.

$$2C_3S + 6H \rightarrow C_3S_2H_3 + 3Ca(OH)_2$$

$$2C_2S + 4H \rightarrow C_3S_2H_3 + Ca(OH)_2$$

$$Ca(OH)_2 + CO_2(aq) \rightarrow CaCO_3(calcite) + H_2O$$

$$C:CaO, \quad S:SiO_2, \quad H:H_2O$$
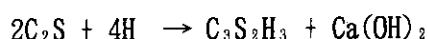
Most of the reaction product (calcite) is precipitated on the surface of the mortar. A small part of calcite is suspended in the solution. The reaction of formation of calcite on the surface of the mortar is the same reaction as the carbonation of cement. Thus, the sorption ratio of carbon-14 existing as carbonate ion ($^{14}CO_3^{2-}$) in the solution, onto mortar will be high until mortar has been completely carbonated because $Ca^{2+}$ is rich in the mortar and solubility of calcite is low.

## Sorption of Carbon-14 in Mortar-Acetic Acid, Acetaldehyde and Arginine System

Figures 11, 12 and 13 show the normalized concentrations of carbon-14 as a function of the elapsed time for all type of mortar - sodium acetate, - acetaldehyde and - arginine systems, respectively. In these experiments, initial concentrations of sodium acetate, acetaldehyde and arginine are $1.0 \times 10^{-3}$ mol/l (carbon-14 radioactivity concentration: $2 \times 10^5$ Bq/l), respectively. In the case of sodium acetate and acetaldehyde, there were little difference between the normalized carbon-14 concentrations in non-centrifuged and centrifuged solutions, which are indicated by open and solid circles in the figures. In contrast to the mortar-sodium carbonate system, the normalized concentrations of carbon-14 in both the organic radiocarbon solutions appear not to change with time. These results imply that the soluble organic carbon-14 is hardly sorbed on the surface of the mortar. However, in the case of CMC mortar - arginine, it was found that normalized concentration decreased. And there was a little difference between normalized concentration in non-centrifuged and centrifuged solutions. This behavior explained that arginine sorbed on mortar whenever arginine is present as cation in solution, however, the quantity is very low. Therefore, the cementitious materials, which are used as engineerekd barriers in the low-level radioactive waste repository, may be not excepted to inhibit the release of organic radiocarbons from the low-level radioactive wastes, contrary to the case of inorganic radiocarbon.

Fig. 10   Normalized $^{14}$C concentration versus elapsed time in the sorption experiment under the sodium carbonate. Error bars indicated the standard deviation from three measurements of each sample.
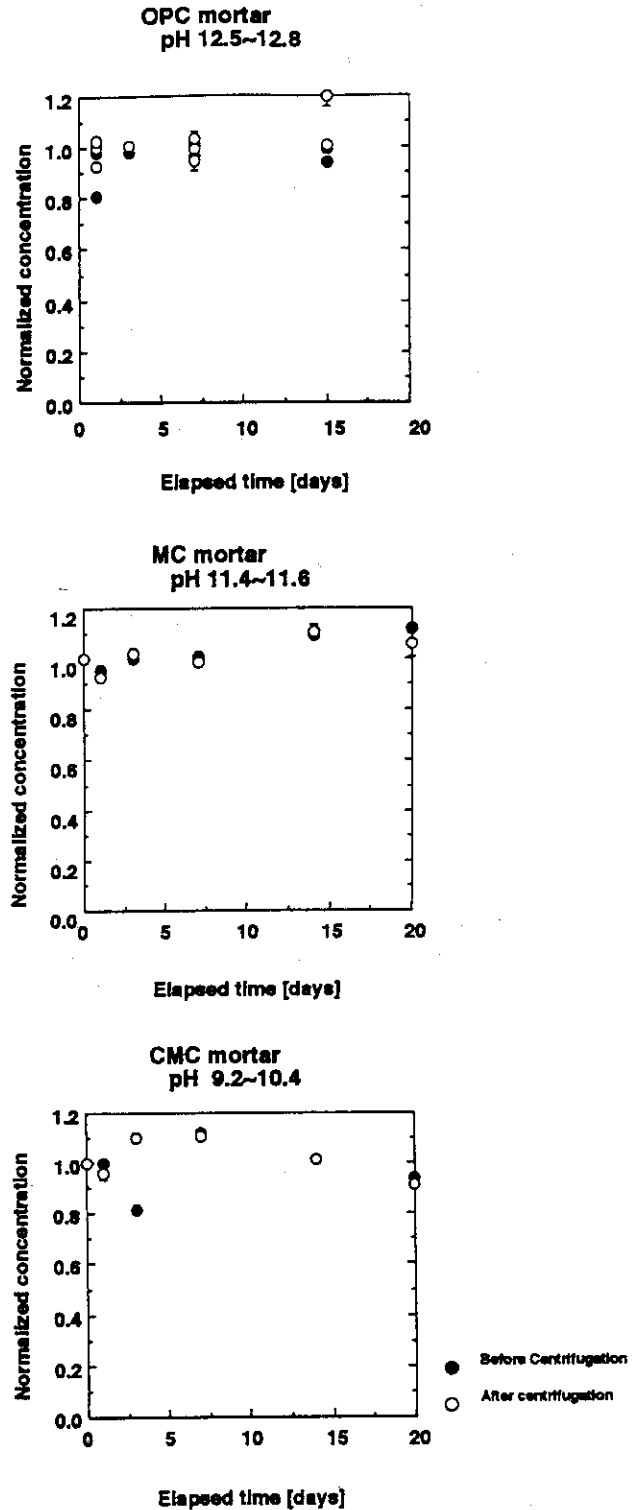
Fig. 11   Normalized $^{14}$C concentration versus elapsed time in the sorption experiment under the sodium acetate. Error bars indicated the standard deviation from three measurements of each sample.

Fig. 12 Normalized ^{14}C concentration versus elapsed time in the sorption experiment under the acetaldehyde. Error bars indicated the standard deviation from three measurements of each sample.
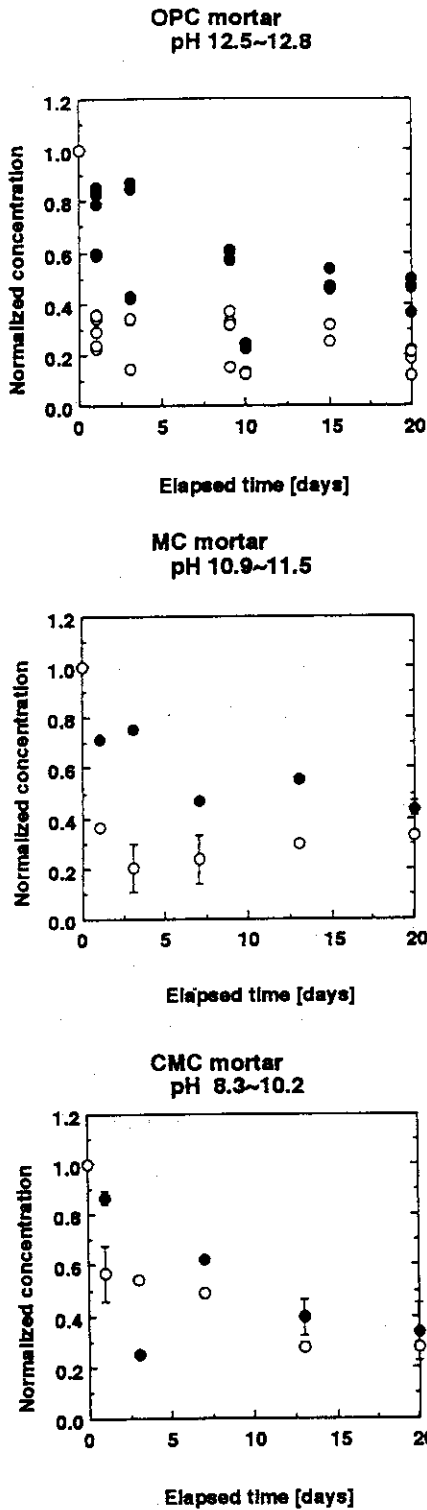
Fig. 13 Normalized ^{14}C concentration versus elapsed time in the sorption experiment under the arginine. Error bars indicated the standard deviation from three measurements of each sample.

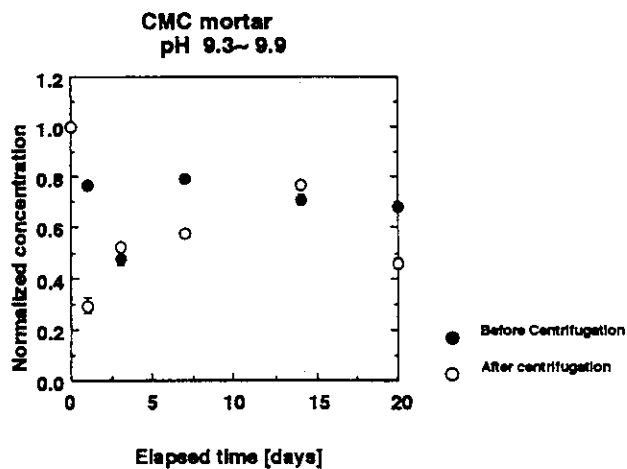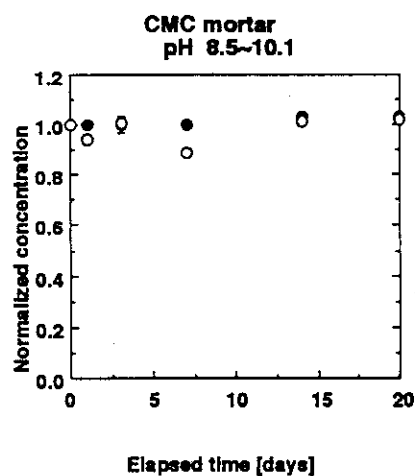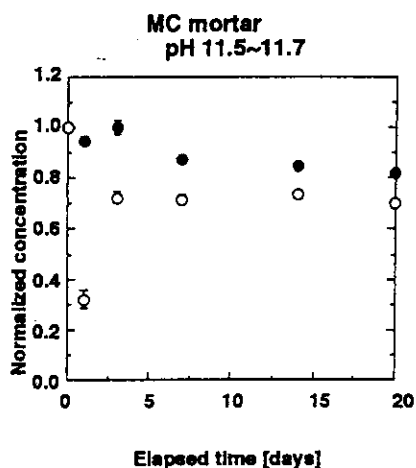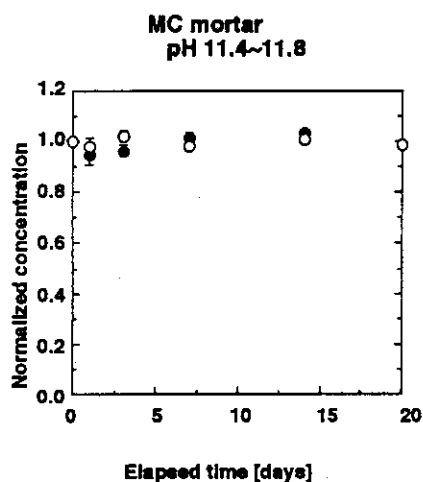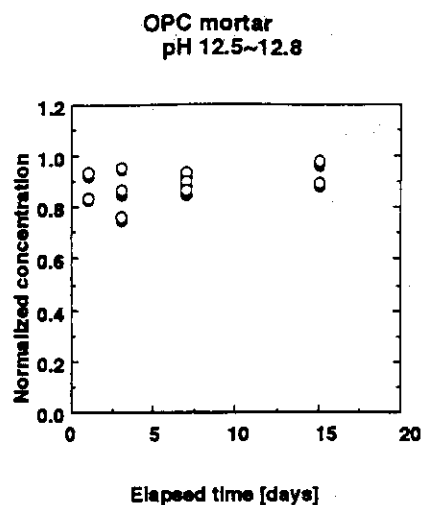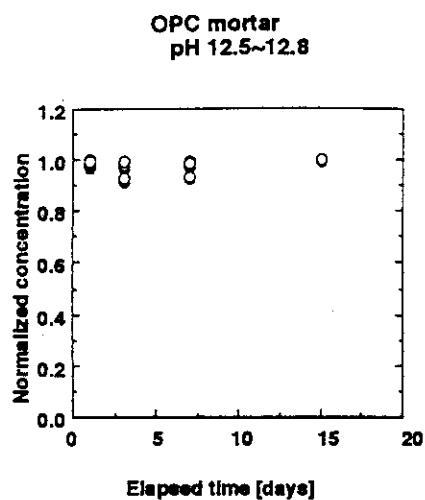# 2. Safety Evaluation Study on Shallow Land Disposal

## 2.1 Nuclide Migration Study

### 2.1.1 Evaluation of Wet and Dry Cycle Effects on Radionuclide Migration in Aerated Zone; Comparison between Laboratory Experiments and Field Tests

T. Tanaka

## 1. INTRODUCTION

In the case of disposal of low-level radioactive wastes (LLW) into a shallow land, it is necessary to grasp quantitatively the migration behavior of radionuclide released from disposal facility into the environment. In an aerated zone, which may be included in a promising layer for the disposal facility, amount of water infiltrated from ground surface depends on a season. The migration behavior of radionuclide in the aerated zone should be therefore evaluated under the unstationary and ununiform flow condition.

The authors take notice of a discontinuous water flow in an aerated zone and have previously found that the migratory mobility of cationic $^{85}$Sr and particulate $^{60}$Co and $^{137}$Cs species increases under a flow condition in which water is intermittently supplied into a soil layer *i.e.* Wet-dry cycle[1-5].

In this study, influence of Wet-dry cycle has been evaluated using results obtained from radionuclide migration tests performed in a natural field.

## 2. OUTLINE OF FIELD TRACING TESTS

To establish a safety evaluation methodology for shallow land disposal of low-level radioactive waste, field tracing tests had been carried out under a cooperative research between Japan Atomic Energy Research Institute and China Institute for Radiation Protection. In the field tracing tests, migration behavior of $^{60}$Co, $^{85}$Sr and $^{134}$Cs was examined during two years under both artificial and natural rainfall conditions, at the field test site of loess medium in Shanxi, China[6-9].

Two pits having the bottom depth of 30 cm were digged in the natural loess medium. After loess soil tagged with $^3$H, $^{60}$Co, $^{85}$Sr and $^{134}$Cs was placed on the bottom, the pits were refilled. To achieve continuous water flow condition, the artificial rain of 15 mm/d was supplied to one of the pits. Another pit was kept under a natural rainfall condition, in which rainfall and evaporation was repeated. Soil cores were periodically taken from the pits during 2 years and radionuclide distribution in them was measured.

Water movement in the pits was evaluated from the test results of $^3$H transfer.

## 3. FUNDAMENTAL EFFECTS OF WET-DRY CYCLE ON RADIONUCLIDE MIGRATION

### 3.1 Effects on $^{85}$Sr migration

In order to study the migration behavior of $^{85}$Sr under discontinuous water-flow condition, the migration experiments were carried out by a column method, in which deionized water was intermittently fed into a sandy soil layer traced with $^{85}$Sr [1, 3, 4].

The migration velocity of cationic $^{85}$Sr increased with increasing interruption times of water flow (Fig. 14) [3, 4]. This is caused by that the distribution coefficient of $^{85}$Sr decreases with increasing concentration of $Ca^{2+}$ which is eluted from the soil into interstitial water during the interrupted period [3, 5]. Values of the distribution coefficient were estimated from the concentration of coexistent $Ca^{2+}$ in effluent. The reducing tendency for distribution coefficient with the interruption times agreed well between the estimated values and the values determined from the migration velocity of $^{85}$Sr in the soil layer (Fig. 15) [3].

### 3.2 Effects on $^{60}$Co and $^{137}$Cs migration

Migration experiments of $^{60}$Co and $^{137}$Cs were carried out by the same column method as $^{85}$Sr. The concentration of $^{60}$Co and $^{137}$Cs in the deeper soil layer of the column increased when the times of flow interruption increased (Figs. 16 and 17) [2, 4].

This increase of $^{60}$Co is attributed to the increase of movable $\{^{60}Co(OH)_2\}_n$ which is formed by pH-rise in the interstitial water during the interrupted period due to buffer action of the soil [5]. A filtration model was developed and was found to be adapted to the concentration distribution of $\{^{60}Co(OH)_2\}_n$ fraction; the amount of $\{^{60}Co(OH)_2\}_n$ was estimated. About 1% of sorbed cationic $^{60}$Co was changed to $\{^{60}Co(OH)_2\}_n$ by one time of the interruption (Fig. 18) [2].

On the other hand, the increase of $^{137}$Cs is related to the concentration of fine soil particles in the interstitial water [1]. Particulate form of $^{137}$Cs, fixed on the fine soil particles, will move easily with water flow. The amount of particulate $^{137}$Cs increased by one time of the interruption was reduced with increasing interruption time (Fig. 19).

These results show that the effects of Wet-dry cycle on the $^{137}$Cs migration are smaller than those on the $^{60}$Co migration.

# 4. ANALYSIS OF FIELD TRACING TESTS UNDER WET-DRY CYCLE

## 4.1 Evaluation on [85]Sr migration

Results on concentration distribution of [85]Sr in both pits are shown in Fig. 20[9]. The distribution profile of [85]Sr under the artificial rainfall condition showed that peak position gradually moved to downward from the tracing layer for 1 year, while that under the natural rainfall condition moved little due to frequentative flow of water, and their features were symmetric.

Radionuclide migration process is controlled by both flow characteristics in soil and interactions of radionuclide with soil. Dispersion equation of radionuclide accompanying with water flow in soil layer can be described by

$$\frac{\partial C}{\partial t} + \rho \frac{(1-f)}{\theta} \frac{\partial Q}{\partial t} = D \frac{\partial^2 C}{\partial x^2} - V \frac{\partial C}{\partial x} \qquad (1)$$

where, $C$: radionuclide in pore water (Bq/ml), $Q$ : radionuclide adsorbed on soil (Bq/g), $f$ : porosity, $\theta$ : water content, $\rho$ : soil density (g/ml), $D$ : dispersion coefficient (cm$^2$/d), $V$: flow velocity (cm/d), $x$: length (cm), $t$: time (d).

On the assumption that a sorption of radionuclide onto soil is based on Henry's type sorption isotherm and equilibrium of the sorption is attained instantaneously, the interaction is described by using distribution coefficient $K_d$:

$$Q = K_d C \qquad (2)$$

The [85]Sr migration was predicted by soluting Eqs. (1) and (2), with $V$ and $D$ obtained from the test results of ^{3}H transfer[6-8]. Calculation result for simulation of [85]Sr migration in each pit, by assuming $K_d = 40$ ml/g, is shown in Fig. 20[9]. Under both the artificial and natural rainfall conditions, the $K_d$ of [85]Sr for the field test was roughly estimated to be 40 ml/g. This suggests that the migration velocity of [85]Sr under the natural rainfall condition can be evaluated by using test results obtained under continuous water flow condition.

## 4.2 Evaluation of ^{60}Co and [134]Cs migration

Results on concentration distribution of ^{60}Co and [134]Cs in both pits are shown in Figs. 21 and 22, respectively[9]. The distribution profiles of ^{60}Co under both the artificial and natural rainfall conditions were very similar, so that it could not be

found a promising difference for quantitative analysis between both distribution profiles. Peak position in the distribution remained almost around the tracing layer, and weak tailing to downward direction was observed. The distribution profiles of $^{134}$Cs were very similar to those of $^{60}$Co.

These results show that the effects of Wet-dry cycle on the migration of $^{60}$Co and $^{137}$Cs in the natural loess medium are much smaller than those found in the laboratory experiments.


5. CONCLUSION


The increase of migration velocity of cationic $^{85}$Sr and migration amounts of particulate $^{60}$Co and $^{137}$Cs were observed under Wet-dry cycle condition in the laboratory experiments, while were not observed in the field tests. It is very likely that the effects of Wet-dry cycle on the migration of $^{60}$Co, $^{85}$Sr and $^{137}$Cs can be neglected on the safety assessment for shallow land disposal of LLW into an aerated zone.


REFERENCES

(1) T. Tanaka, T. Yamamoto: *J.Nucl.Sci.Technol.*, 28, 239 (1991).

(2) T. Tanaka, T. Yamamoto: *ibid.*, 31, 308 (1994).

(3) T. Tanaka, T. Yamamoto: *RADIOISOTOPES*, 43, 389 (1994).

(4) T. Tanaka, T. Yamamoto: *JAERI-Research 94-010* (1994).

(5) T. Tanaka: *JAERI-Research 95-044*, (1995).

(6) S. Li, *et al.*: *"Proceedings of Asia Congress on Radiation Protection, Beijing"*, pp. 667 (1993).

(7) M. Mukai, H. Kamiyama and T. Tanaka: *ibid*, pp. 673 (1993).

(8) T. Tanaka, H. Kamiyama and M. Mukai: *ibid*, pp. 681 (1993).

(9) H. Kamiyama *et al.*: *JAERI-Research 94-009* (1994).
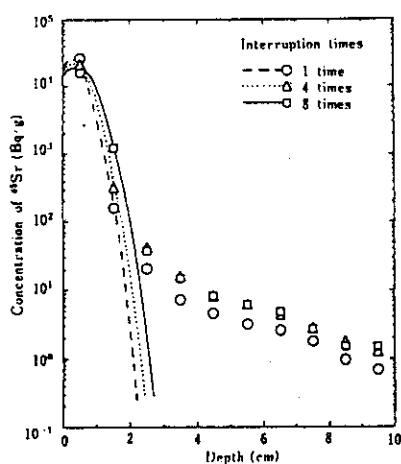
Fig. 14 Distribution profile of $^{85}$Sr in soil layer: lines represent fitted curves.
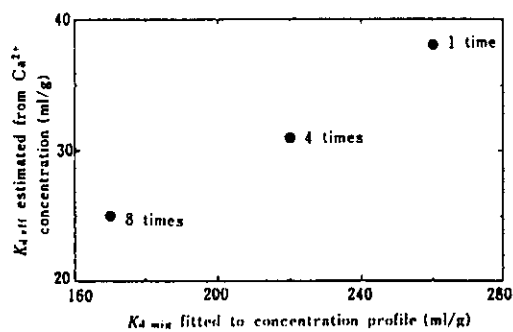


Fig. 15 Plots of $K_{d\ eff}$ vs. $K_{d\ mig}$.



.............: Estimated migration profile of cationic $^{60}$Co
——————: Filtration profile of particulate $^{60}$Co
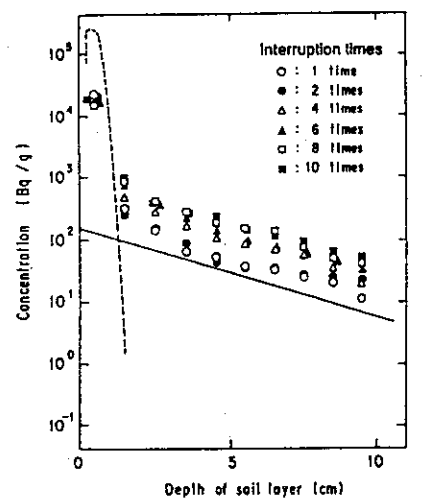
Fig. 16 Influence of interruption times on concentration distribution of $^{60}$Co in soil layer.
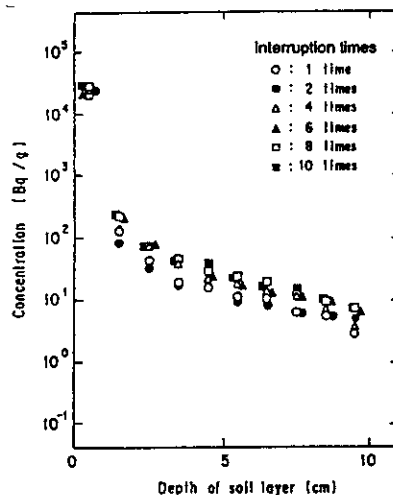


Fig. 17 Influence of interruption times on concentration distribution of $^{137}$Cs in soil layer.
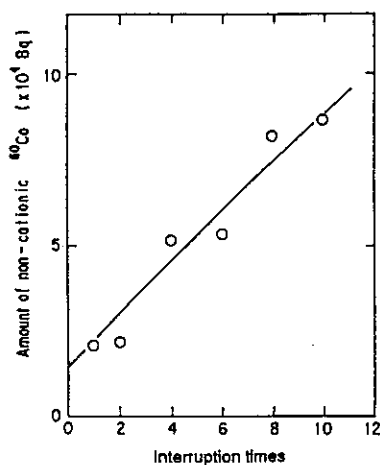


Fig. 18 Relation between amount of non-cationic $^{60}$Co and interruption times.
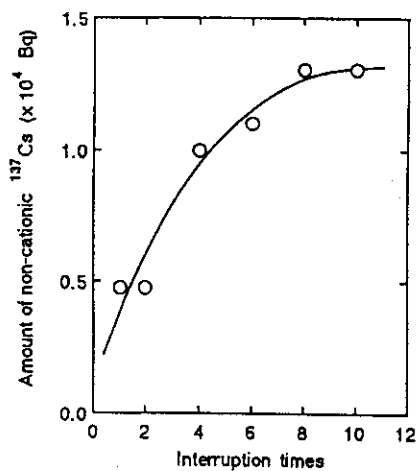


Fig. 19 Relation between amount of non-cationic $^{137}$Cs and interruption times.

Artificial rainfall condition

Natural rainfall condition
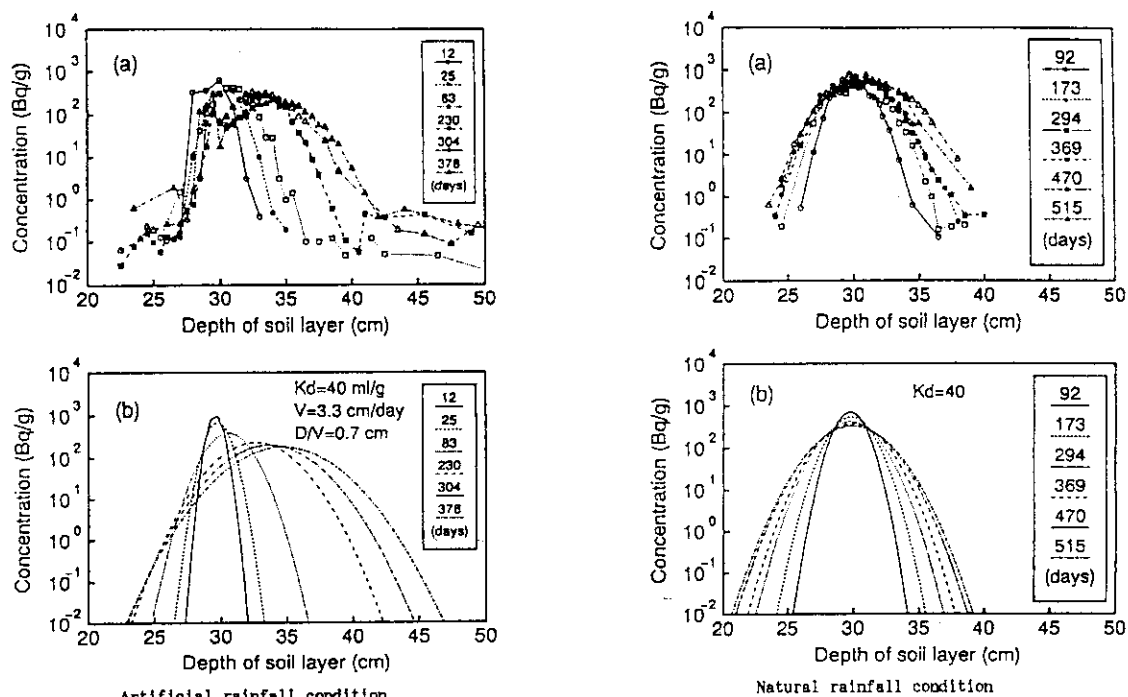
Fig. 20 Periodical change of distribution profile of $^{85}$Sr.
(a): Results obtained from the field tests
(b): Calculation results by equilibrium sorption model



Artificial rainfall condition

Natural rainfall condition
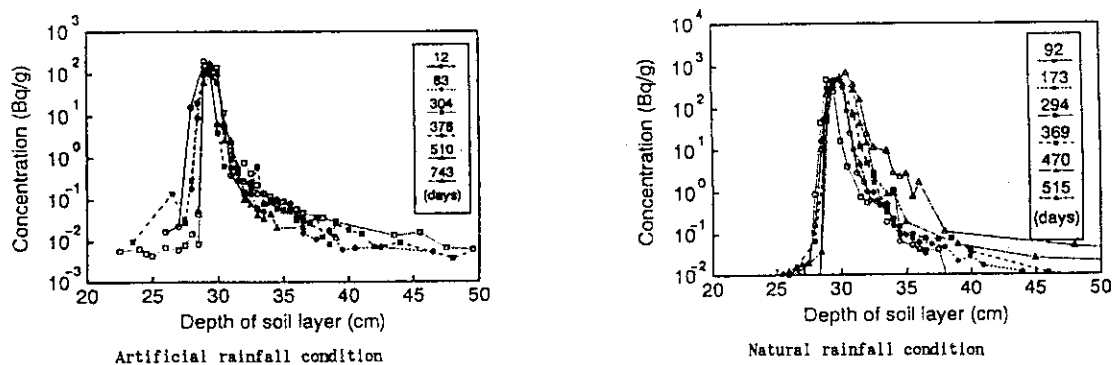
Fig. 21 Periodical change of distribution profile of $^{60}$Co.



Artificial rainfall condition

Natural rainfall condition
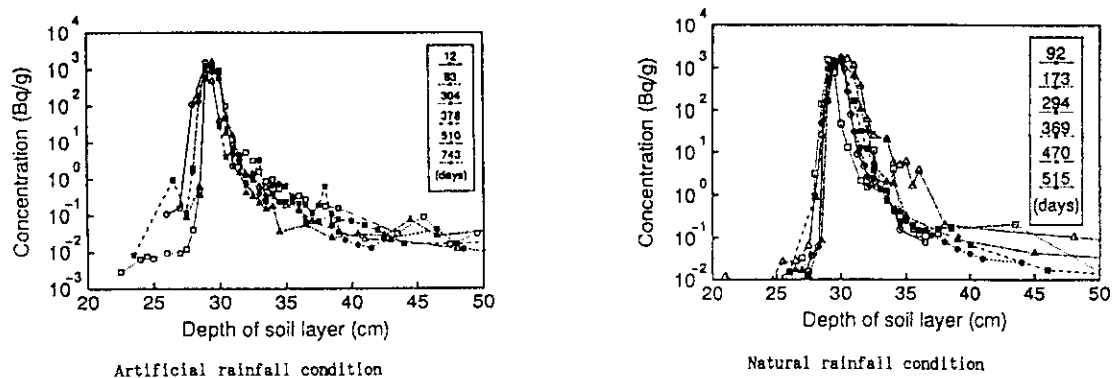
Fig. 22 Periodical change of distribution profile of $^{134}$Cs.

## 2.1.2  Migration Behavior of Inorganic and Organic $^{14}C$ in Soil Layer

S. Nagao and H. Ogawa

## 1.  INTRODUCTION

Carbon-14 ($^{14}C$) occurs in nature, but is also formed at nuclear power plants. Because of its long half-life (5730 years) and biological significance of carbon, releases of $^{14}C$ from nuclear facilities could have a significant radiological impact[1]. Bicarbonate and carbonate are major chemical forms of inorganic $^{14}C$ in low level radioactive waste[2]. Low level waste also contains organic $^{14}C$ such as hydrocarbon, carbohydrate and carboxylic acids etc.[2, 3]. Study on migration of bicarbonate, carbonate and organic $^{14}C$ in underground layer is important to evaluate environmental safety assessment for underground disposal of radioactive waste.

This study reports migration behavior of bicarbonate, carbonate and acetate $^{14}C$ (one of carboxylic acids) conducted by the closed column system with the constant feed of radiotracer. This method was applied to a tuffaceous sandy soil, as a porous media of geological materials. The desorption experiments were carried out with the column system by distilled water and NaF treatments to study the sorption mechanisms of $^{14}C$.

## A. Bicarbonate and carbonate $^{14}C$

## A. 2.  EXPERIMENTS

### A. 2. 1  Materials

A tuffaceous sandy soil sample was collected at northeastern part of Aomori prefecture, Japan. The sample was taken from a depth of 3 ~ 4 m below the ground surface. Grain size distribution of the soil sample is 2.3% gravel (2 mm<), 81.2% sand (2 mm - 74 $\mu$m), 11.2% silt (74 $\mu$m - 5 $\mu$m), and 5.3% clay (<5 $\mu$m) fractions. The main mineral components are quartz, feldspar, clinopyroxene, halloysite and allophane. The main chemical components are $SiO_2$ (78%) and $Al_2O_3$ (11%). The contents of CaO, $Fe_2O_3$ and organic carbon are 2%, 1.9% and 0.004%, respectively.

### A. 2. 2  Apparatus

A simple closed column system is shown in Figure 23. The system consists of a radioactive solution reservoir, magnetic stirrrer, syringe, gas bag, micro tube pump, column (2.5 cm I.D. and 5 cm long) and sample collector. The column system was designed to make it air-tight from reservoir bottle to soil column. A gas bag (1 liter TEDLAR

BAG) is connected to the reservoir bottle to prevent release of $^{14}C$ from solution to atmosphere. A disposal syringe is fitted with the reservoir bottle, and used to check variation of pH and concentration of $^{14}C$ in reservoir solution during the column experiment.

## A. 2. 3  Experimental procedures

### a. Column experiment

Migration experiments were carried out after the wetting of the soil column, which was dry packed to confirm bulk density of the column[4]. The 58 Bq/ml of $^{14}C$ radioactive solution (0. 12 mM H$^{14}CO_3^-$) at pH 8 was continuously introduced to top of the column by the micro tube pump at constant flow rate of 2 ml/min. The reservoir solution was gently stirred with the magnetic stirrer to prevent inhomogeneity during the experiment. The effluent was automatically collected into glass test tubes for 12. 5 min with the fraction collector. The glass test tube was sealed with a silicon rubber stopper after the collection immediately. The reservoir solution was collected with the syringe at regular intervals to monitor the pH and $^{14}C$. Migration experiments at pH 10 and 12 were carried out with the similar procedure after saturation of the soil column by carbonate solutions at pH 10 and 12, respectively. Tritiated water (HTO) was also introduced into the soil column to evaluate the column dispersion. The concentrations of HTO and $^{14}C$ were measured with a liquid scintillation counter.

### b. Desorption experiment

Desorption of $^{14}C$ sorbed on the tuffaceous sandy soil was carried out with distilled water (nonspecific sorption) and NaF solutions (specific sorption) after the migration experiment at pH 8. The desorbing agent solutions were introduced to top of the column by the micro tube pump at constant flow rate of 2 ml/min in order of distilled water, $10^{-4}$ M, $10^{-2}$ M and 1 M NaF solutions. These effluent solutions were automatically collected by the fraction collector at every 12. 5 min. Each desorption was carried out until the effluent volume of 550 – 590 ml. After the desorption column experiment, the soil was cut into 0. 5 cm section to obtain the concentration profile of $^{14}C$ in the soil column.

The effluent solutions were analyzed for concentrations of $^{14}C$ and pH as described above except for 1 M NaF effluent samples having yellowish color. The 1 M NaF effluent samples were measured with the liquid scintillation counter after the oxidation treatments[4]. The pH was not measured for the 1 M NaF effluent samples.

## A. 3  RESULTS AND DISCUSSION

### A. 3. 1  pH-dependent migration

Figure 24 shows breakthrough curves of bicarbonate and carbonate $^{14}C$ in the tuffaceous sandy soil, and effluent patterns of pH. The pH of effluent at three pH experiments is lower than reservoir values. This is considered to be buffering effect of the soil sample. The effect decreases with increasing influent pH.

The $^{14}C$ at pH 8 experiment shows delayed breakthrough compared to the tritiated breakthrough followed by relative concentration of less than unity within the experimental period. The $^{14}C$ relative concentration at pH10 experiment agrees with those of reservoir solutions above 400 ml effluent volume. The pattern of breakthrough at pH10 is similar with that at pH 8, but different from the synmmetry curves of other anions. The breakthrough curve at pH 12 experiment shows broad peak with relative concentration above unity. These effluents show yellowish color. This is considered to be desorption of $^{14}C$ sorbed on the soil at previous period and dissolution of soil components sorbed $^{14}C$. The retardation of $^{14}C$ by the soil sample becomes stronger in the order, pH 12, pH 10, pH 8.

The pH-dependence of migration of bicarbonate and carbonate $^{14}C$ is observed for the tuffaceous sandy soil at pH 8 to 12. In our batch experiments, the sorption of $^{14}C$ shows pH-dependence and maximum at about pH 6 [5]. The similar pH-dependence of bicarbonate and carbonate sorption exhibits for goethite and Al oxides [6-8]. These minerals and allophane have pH-dependent charge [9-11]. The tuffaceous sandy soil sample contains these soil minerals. Therefore, pH-dependence of retardation of bicarbonate and carbonate $^{14}C$ by the soil column experiments is considered to be pH-dependent sorption of $^{14}C$ onto the soil sample.

### A. 3. 2  Desorption behavior

The sorption mechanism of $^{14}C$ on the soil was studied by the desorption column experiment. The concentration of $^{14}C$ desorbed from the soil is maximum at first or second fractions and then decreases with the effluent volume (Fig. 25). The pH of effluent is almost constant with the effluent volume at distilled water and $10^{-4}$ M NaF desorptions, but in $10^{-2}$ M NaF treatment, the pH sharply increases with increasing the effluent volume until 100 ml and then constant (pH 8.5) with the volume. The increase in pH agrees with increase of desorption of $^{14}C$. Fluoride ion was sorbed on the soil, and then released OH- and $^{14}C$ from the soil surface.

The amount of $^{14}C$ desorbed from the soil sample is 14% (distilled water), 10% ($10^{-4}$ M

NaF), 12% ($10^{-2}$ M NaF) and 39% (1 M NaF). The $^{14}$C remaining the soil prepared by a Packard Oxidizer 307 is 6%. The desorption of $^{14}$C by NaF is 61% to total sorption $^{14}$C.

## A.3.3 Sorption mechanism

Desorbability of anions having specific desorption ability from soil is very low by addition of non-specific adsorption anions such as $Cl^{-}$ [12]. The amount of $^{14}$C desorbed with distilled water is 10% at column experiment and 12% at our batch experiment. And the $^{14}$C desorption is only 3% for 1M KCl at our batch experiments. The desorbability of $^{14}$C by distilled water and chloride ion is low.

On the other hand, the amount of $^{14}$C desorbed from the soil by fluoride ion is 66% for this column experiment and 77% for our batch experiment. Many soil chemists have shown that fluoride ion is strongly and selectively adsorbed by several hydrous oxides in soil because of the close to similarity in size of fluoride and OH ions. Fluoride ion, therefore, is an effective desorbing agent for previously adsorbed anions, especially specific adsorption anions. In addition, desorption of $^{14}$C by $HPO_4^{2-}$ (another specific adsorption anion, pH 9.0) is 75% at our batch experiments. Therefore bicarbonate $^{14}$C is mainly specifically adsorbed onto the tuffaceous sandy soil having goethite, allophane and halloysite.

## A.4 CONCLUSION

A simple closed column system was conducted to study the migration of bicarbonate and carbonate $^{14}$C in soil layer. This system was applied to a tuffaceous sandy soil with pH-dependent charge minerals such as haloysite, allophane and goethite. The $^{14}$C is delayed to tritiated water and the retardation is in the order, pH 12, pH 10, pH 8. This is considered to be pH-dependence adsorption of bicarbonate and carbonate $^{14}$C onto the soil sample.

## B. Acetate-$^{14}$C

## B.2 EXPERIMENTS

Migration experiments for the tuffaceous sandy soil, a same sample used in the bicarbonate and carbonate $^{14}$C experiments, were carried out with the simple column system [4]. The 166 Bq/ml of $^{14}$C radioactive solution ($10^{-5}$M, $10^{-4}$M, $10^{-3}$M and $10^{-2}$M $CH_3^{14}COO^-$) at pH 7.0-7.5 was introduced to top of the soil column by the micro tube

pump at constant flow rate of 2 ml/min. The effluent was automatically collected into glass test tubes for 12.5 mm with the fraction collector.

The desorption of $^{14}C$ from the tuffaceous sandy soil was carried out with distilled water and NaF solutions ($10^{-4}M$, $10^{-2}M$ and 1M NaF). After the migration experiment at the concentration of $10^{-3}M$, distilled water and NaF solutions were introduced to top of the column by the micro tube pump at constant flow rate of 2 ml/min. Each desorption was carried out until the effluent volume of 540 - 570 ml (350 ml for 1M NaF solution). These effluent solutions were automatically collected by the fraction collector at every 12.5 min. The concentrations of $^{14}C$ at the migration and desorption experiments were measured with the method described at A.2 EXPERIMENTS.

## B.3 RESULTS AND DISCUSSION

### B.3.1 Validity of the column experiments

The concentration of $^{14}C$ and pH in the effluent and influent are shown in Figure 26. Decrease in the concentration of $^{14}C$ in reservoir solutions after the column experiments is only 0.7% of initial value. The variation of pH is only 0.2 pH values. On the other hand, the pH of effluent at the experiments with the acetate concentration of $10^{-2}M$ and $10^{-3}M$ is lower than those of influent solutions. This is considered to be buffer reaction of the soil sample. In the case of the acetate concentration of $10^{-2}M$, the concentration of $^{14}C$ in the effluent sharply increases until 56 ml, and then agrees with those of reservoir solutions above 120 ml effluent volume. This result indicates that the column experiments for acetate $^{14}C$ can be performed without release of $^{14}C$ from the column system within the experimental period.

Differences in the concentrations of $^{14}C$ between influent and effluent are observed for the experiments with the acetate concentrations of $10^{-4}$ and $10^{-5}M$ (Fig. 26). It is difficult to explain by release of $^{14}C$ into atmosphere because of keeping mass balance of $^{14}C$. The distribution coefficient of the soil sample, obtained by batch experiment, is about 100 ml/g at the acetate concentration of $10^{-4}M$ and pH 6.3, but 13 mg/l at the concentration of $10^{-2}M$ and pH 6.5. The lower $^{14}C$ value of the effluent, therefore, is considered to be due to sorption of $^{14}C$ on the soil sample packed in the column.

### B.3.2 Effects of acetate concentration on migration of $^{14}C$

Breakthrough curves of $^{14}C$ at the four different acetate concentrations are shown in Fig.27. The relative concentration ($C/C_0$) estimates that the effluent concentration (C) is multiplied by average value ($C_0$) of the reservoir solution. The $^{14}C$ with acetate

concentrations of $10^{-5}M$ and $10^{-4}M$ shows delayed breakthroughs compared to the tritiated breakthrough followed by relative concentration of less than unity within the experimental period. The relative concentrations of $^{14}C$ at the acetate concentrations of $10^{-2}M$ and $10^{-3}M$ agree with those of reservoir solutions above 120 ml and 230 ml effluent volume, respectively. The retardation of $^{14}C$ by the soil sample becomes stronger as decreasing the acetate concentrations.

B. 3. 3  Desorption behavior

The desorption experiments were carried out by distilled water and NaF solutions after the migration column experiment with the acetate concentration of $10^{-3}M$ to study adsorption mechanism of the $^{14}C$ on the tuffaceous sandy soil. The concentration of $^{14}C$ desorbed from the soil by distilled water is maximum at 22 ml effluent volume and then sharply decreases with the effluent volume (Fig. 28).  The concentration of $^{14}C$ treated by $10^{-4}$ NaF solution gradually decreases with the effluent volume. The concentration of $^{14}C$ treated by $10^{-2}M$ NaF and 1M NaF solutions is maximum at 34 - 70 ml effluent volume and then sharply decreases with the volume.

The amount of $^{14}C$ desorbed from the soil sample is 34% for distilled water, 12% for $10^{-4}M$ NaF, 26% for $10^{-2}M$ NaF and 18% 1 M NaF solution. The desorption of $^{14}C$ by NaF is 56% to total adsorption of the $^{14}C$. The desorption behavior indicates that the sorption of acetate $^{14}C$ is mainly specific adsorption and similar with the bicarbonate $^{14}C$.

B. 4  CONCLUSION

Migration behavior of acetate $^{14}C$ in a tuffaceous sandy soil was investigated by the simple closed column system at the acetate concentration ranging from $10^{-5}M$ to $10^{-2}M$. The $^{14}C$ was delayed to tritiated water, and the retardation became stronger as decreasing the acetate concentrations. The typical groundwaters have the acetate concentration of less than $10^{-5}M$, so that acetate $^{14}C$ may be retarded by the tuffaceous sandy soil.

5.  SUMMARY

The breakthrough curve of bicarbonate $^{14}C$ with the bicarbonate concentration of $10^{-4}M$ at pH 8 is similar with that of acetate $^{14}C$ having the concentration of $10^{-4}$ at pH 7. The bicarbonate and acetate $^{14}C$ sorbed on the soil is mainly desorbed with NaF solutions. These results suggest that the migration of bicarbonate and acetate $^{14}C$ in

the tuffaceous sandy soil may be controlled with the similar sorption mechanisms.

REFERENCES

( 1 ) R. P. Bush, G. M. Smith and I. F. White, EUR 8749, Luxembourg 1984.

( 2 ) R. Hesbol, I. Puigdomenech and S. Evans, SKB Technical Report 90-02, Stockholm 1990.

( 3 ) R. Dayal, R. F. Pietrzak and J. H. Clinton, Nuclear Technology, 72, 158-177 (1986).

( 4 ) S. Nagao and M. Senoo, in Scientific Basis for Nuclear Waste Management XVIII edited by T. Murakami and R. C. Ewing (Mater. Res. Soc. Symp. Proc., Pennsylvania 1995) pp. 1093-1100.

( 5 ) S. Nagao, H. Ogawa, Y. M. Lee and H. Kamiyama, presented at 1993 Spring Meeting of the Atomic Energy Society of Japan, Kyoto, 1993 (unpublished).

( 6 ) J. M. Zacharka, D. C. Girvin, L. Schmit and C. T. Resch, Environ. Sci. Technol., 21, 589-594 (1987).

( 7 ) R. S. Rundberg and Y. Albinsson, LA-UR-91-3244, Los Alamos 1991.

( 8 ) C. P. Schulthess and J. F. McCarthy, Soil Sci. Soc. Am. J., 54, 688-694 (1990).

( 9 ) F. J. Hingstone, R. J. Atkinson, A. M. Posner and I. P. Quirk, Nature, 215, 1459-1461 (1967).

(10) K. W. Perrot, B. F. L. Smith and B. D. Mitchell, J. Soil Sci., 27, 348-356 (1976).

(11) K. Wada, in Minerals in Soil Environments, edited by J. B. Dixon and S. B. Weed (Soil Sci. Soc. of Am., Wisconsin 1977) pp. 603-638.

(12) F. J. Hingston, A. M. Posner and J. P. Quirk, J. Soil Sci., 25, 16-26 (1974).
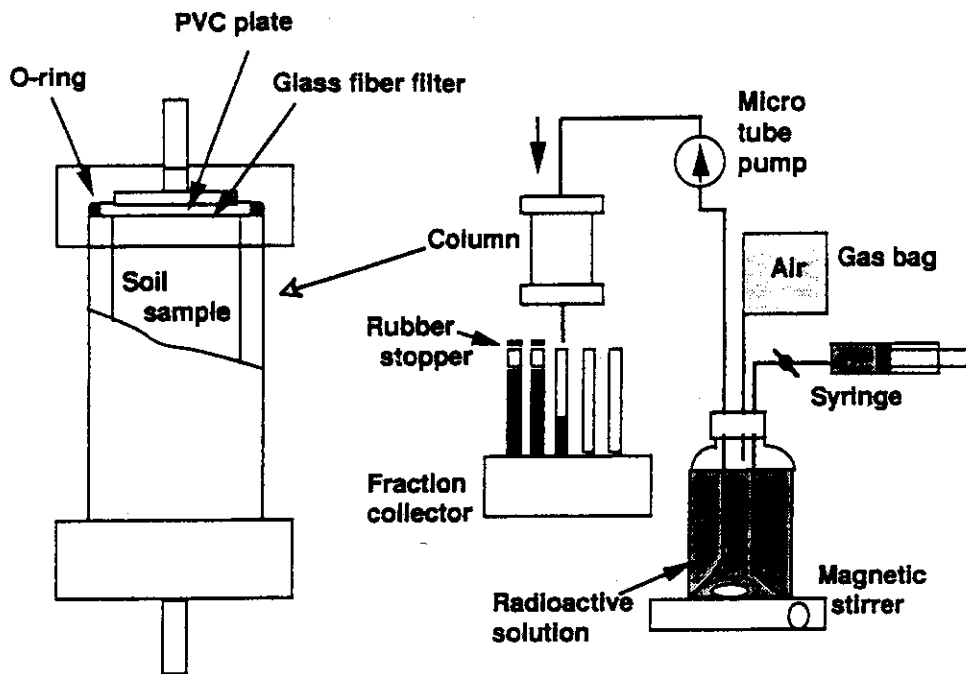
Fig. 23  Schematic illustration of a simple closed column system.
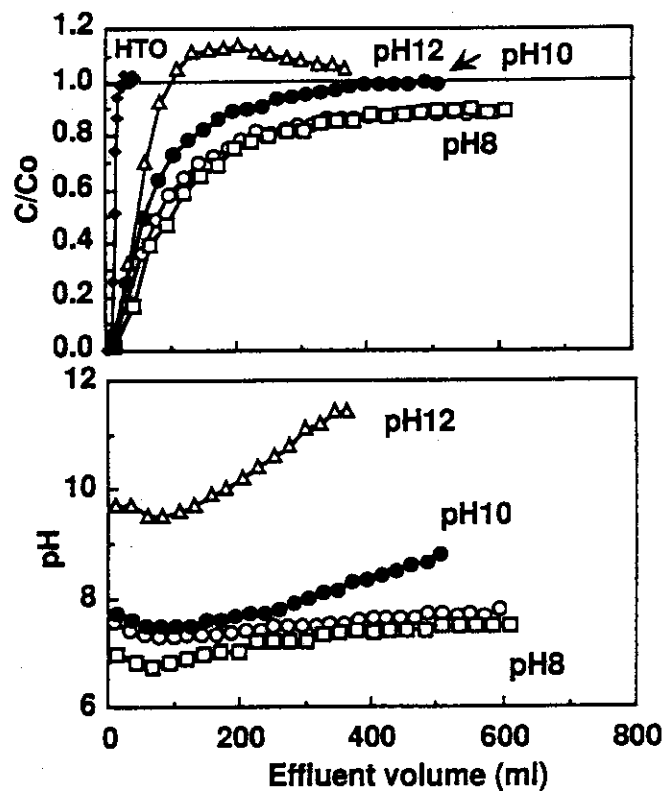


Fig. 24  Breakthrough curves of HTO (◆) and ¹⁴C (upper panel) and pH (lower panel) from the soil column packed with the tuffaceous sandy soil at pH 8(◯, □), pH10 (●) and pH12 (△). Porosity of three soil columns is 0.49. Flow rate is 1.73-2.08 ml/min at three experiments.

Fig. 25  Concentration of $^{14}C$ (upper panel) and pH (lower panel) in the effluents from the soil column at desorption experiments by distilled water (○), $10^{-4}$ M (◆), $10^{-2}$ M (▲) and 1 M NaF solutions (●). The flow rate is about 2 ml/min. The pH of effluent at 1 M NaF desorption experiment was not measured. These desorption experiments were carried out with the soil column after migration experiment at pH 8.
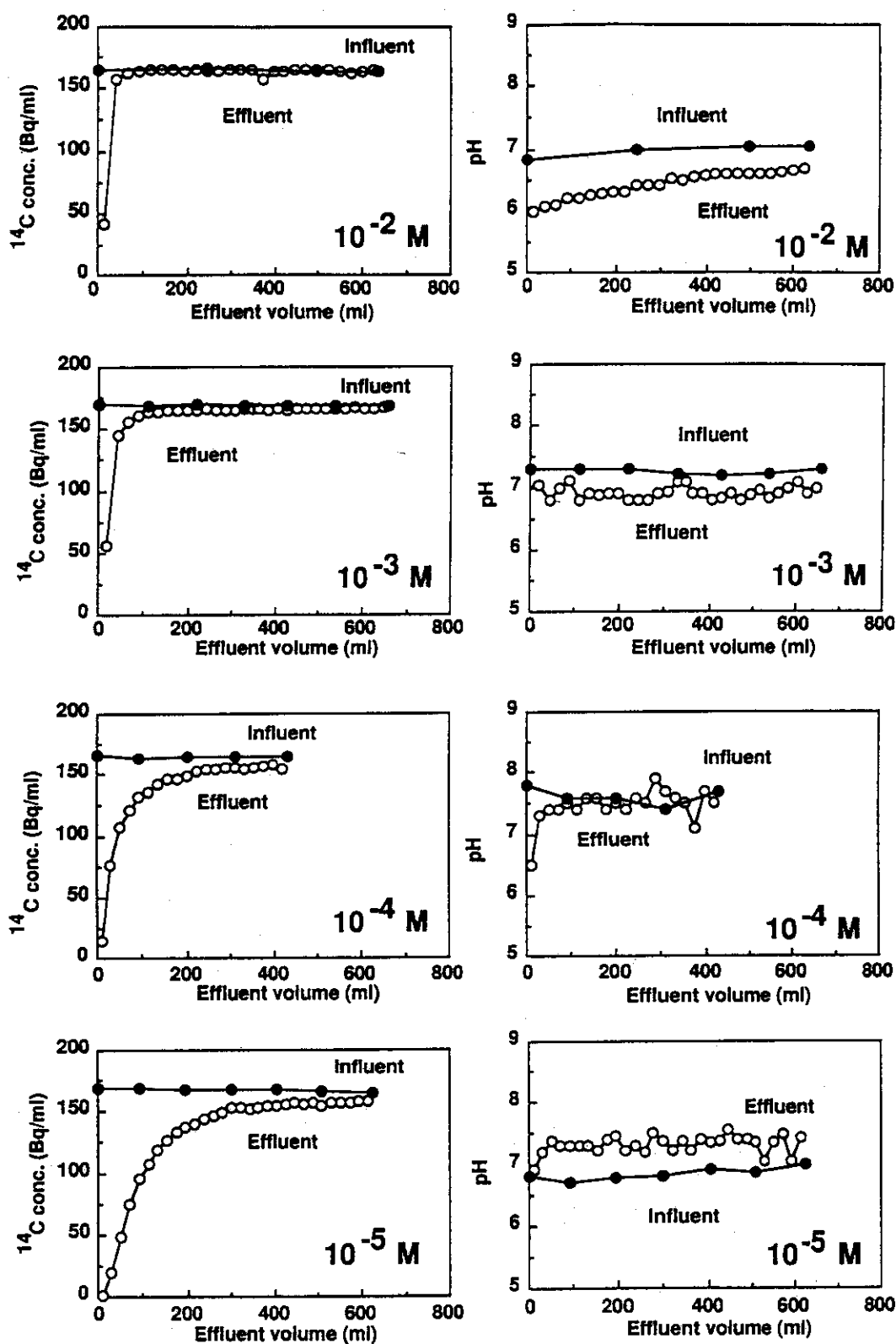
Fig. 26 Concentration of $^{14}$C (left side) and pH (right side) of influent and effluent from soil column packed with the tuffaceous sandy soil at the $^{14}$C concentration of 166 Bq/ml. The concentration of acetate is $10^{-5}$M, $10^{-4}$M, $10^{-3}$M and $10^{-2}$M. Porosity of the columns is 0.43-0.50. Flow rate is 1.7-2.0 ml/min. Open and closed circles indicate data for the effluent and influent, respectively.
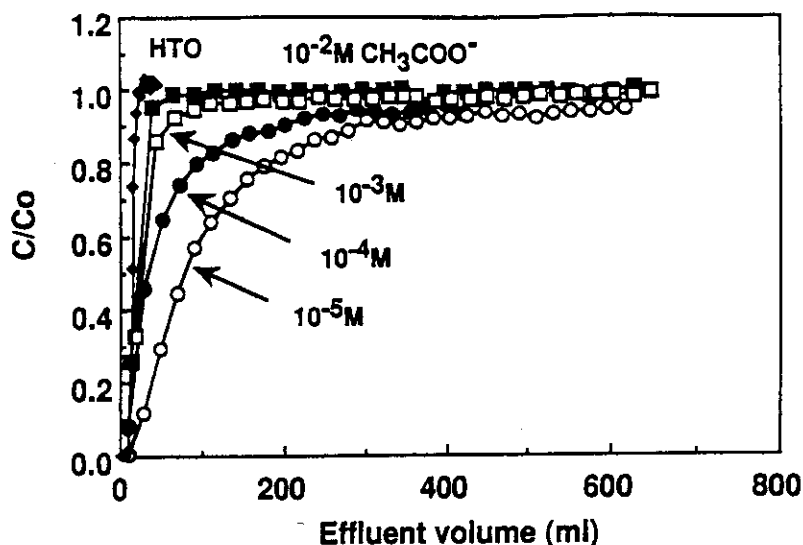
Fig. 27  Breakthrough curves of HTO (◆) and $^{14}C$ from the soil column packed with the tuffaceous sandy soil at pH 7.0-7.5. Concentrations of acetate were $10^{-5}M$ (○), $10^{-4}M$ (●), $10^{-3}M$ (□) and $10^{-2}M$ (■). Porosity of three soil columns is 0.43-0.50. Flow rate is 1.7-2.0 ml/min. The concentration of HTO in the effluent agrees with that of influent at 22 ml effluent volume.
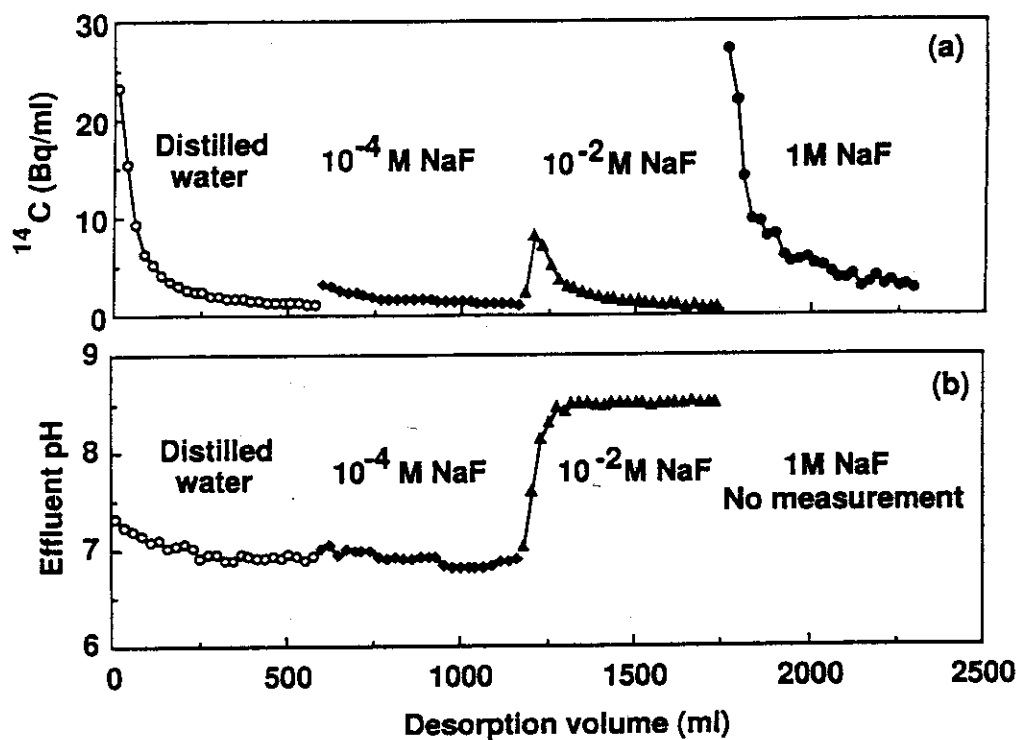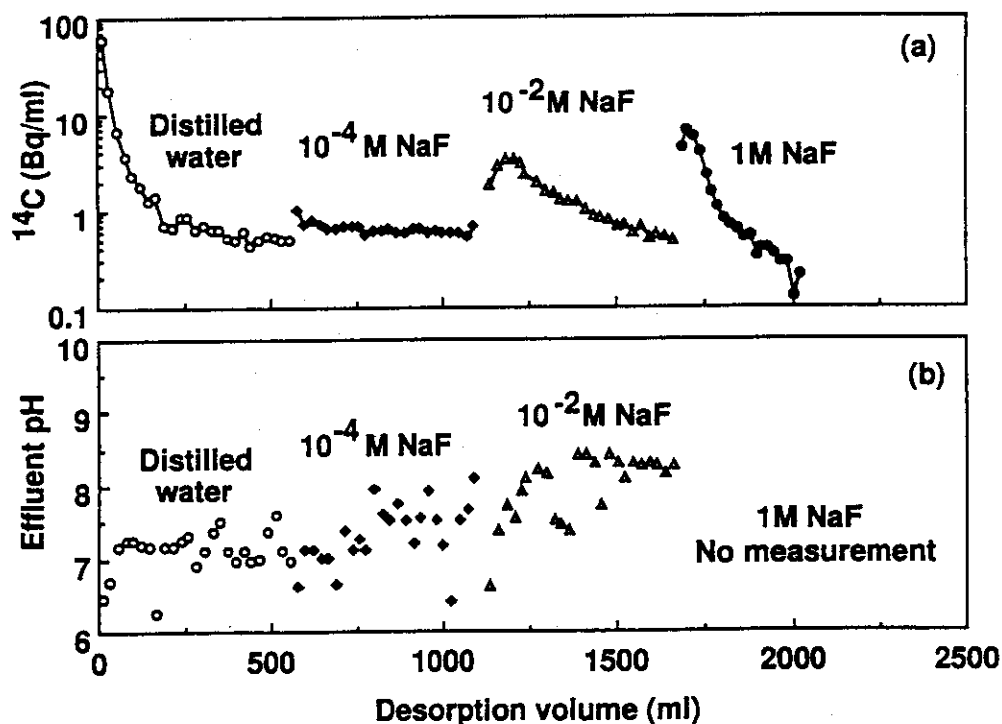


Fig. 28  Concentration of $^{14}C$ (upper panel) and pH (lower panel) in the effluents from the soil column at desorption experiments by distilled water (○), $10^{-4}M$ (◆), $10^{-2}M$ (△) and 1 M NaF solutions (●). The flow rate is about 2 ml/min. These desorption experiments were carried out with the soil column after migration experiment at the acetate concentration of $10^{-3}M$.

## 2.1.3 Influence of Humic Acid on Distribution Coefficients of $^{60}$Co, $^{85}$Sr, $^{137}$Cs, $^{237}$Np and $^{241}$Am for a Sand and an Ando Soil

T. Tanaka and M. Senoo

## 1. INTRODUCTION

The migration of radionuclides in a soil layer is controlled by both flow characteristics of interstitial water and interactions of the radionuclides with the soils. As humic acid has substantial chelatiion properties for metal ions, it considerably affects on the sorption and migration behavior of radionuclides in a soil layer. From a geochemical point of view, it is important to know reactivity of humic acid with the radionuclides released from radioactive-waste repository[1]. In this study, sorption experiments were performed by a batch method, to clarify an influence of humic acid on the sorption of $^{60}$Co, $^{85}$Sr, $^{137}$Cs, $^{237}$Np and $^{241}$Am on a sand and an ando soil.

## 2. EXPERIMENTAL

Humic acid was purchased from the Aldrich Chemical Co. and was purified to remove insoluble humin, fulvic acid and ash by the procedure described by Nash $et$ $al.$[2,3]. The purified humic acid was dissolved into small amount of 0.1 M NaOH, and the humic acid (HA) solution was prepared to desired concentrations by diluting with 0.01 M NaNO$_3$.

Soil samples used in this experiment were a coastal sandy soil and an ando soil, collected in Ibaraki-Pref., Japan. The ando soil and a sand fraction (250~350 $\mu$m in particle size) isolated from the sandy soil were washed with deionized water to remove fine soil particles.

The 2.5 g of prepared soils were contacted with 50 ml HA solution of 3~130 mg/L in concentration of dissolved organic carbon (DOC), in which the HA solution was spiked with $^{60}$Co, $^{85}$Sr, $^{137}$Cs, $^{237}$Np or $^{241}$Am, for 7 days at 0.01 M for ion strength of NaNO$_3$, 5.5 for pH and 25℃ for temperature, respectively. Concentrations of the radionuclides in the aqueous phase were measured before and after the sorption experiments. Distribution coefficient (Kd) of radionuclide was calculated from the concentrations before and after the sorption experiments.

The Kds of HA for the sand and the ando soil were also measured.

## 3. RESULTS AND DISCUSSION

The Kds in the sorption of $^{137}$Cs and $^{237}$Np onto both soils, were not changed at different concentrations of HA. The Kds of $^{60}$Co and $^{241}$Am decreased with increasing HA concentration (Fig. 29). Gradient of the decrease in the Kds of $^{60}$Co and $^{241}$Am for the sand was larger than that for the ando soil. The Kd of $^{85}$Sr for the sand was not changed at different concentrations of HA, while that for the ando soil increased with the HA concentration.

The solutions in a blank test not containing the soils were ultrafiltrated with Millipore filters of 5,000, 10,000, 30,000, 100,000 and 300,000 in cutoff molecular weight (MW). Figure 30 shows concentrations of HA and radionuclides in each MW fraction passed through the filters. The bulk of dissolved HA was in MW range from 30,000 to 100,000. Also the concentration of $^{60}$Co, $^{85}$Sr and $^{241}$Am was reduced by the filtration, with very similar to that of HA. These results indicate that most $^{60}$Co, $^{85}$Sr and $^{241}$Am form humic-complexes with the dissolved HA in the aqueous solution. However, $^{137}$Cs and $^{237}$Np were not trapped by all the five kinds of filters. Thus $^{137}$Cs and $^{237}$Np did not form humic-complexes.

Since the Kd of HA for the sand is nearly 0 ml/g (Fig. 31), the humic-complexes of $^{60}$Co, $^{85}$Sr and $^{241}$Am are hardly sorbed onto the sand[4]. This indicates that cationic $^{60}$Co, $^{85}$Sr and $^{241}$Am species dissociated from HA are sorbed on the sand[3,4]. On the other hand, the Kd of HA for the ando soil is rather large and is nearly equaled to that of $^{241}$Am (Fig. 31). This shows that the humic-complexes of $^{60}$Co, $^{85}$Sr and $^{241}$Am can be sorbed on the ando soil, as well as the cationic species. Hence the Kds of the radionuclides for the sand were significantly decreased by the increase of the HA concentration, compared with the ando soil, as shown in Fig. 29.

## 4. CONCLUSION

The results suggest that the migration of humic-complexable radionuclide in geologic media under presence of HA can be partly accelerated by formation of the humic-complexes and/or partly retarded by sorption of the humic-complexes onto a soil such as the ando soil.

# REFERENCES

(1) McCarthy, J. F. and Zachara, J. M. : *Environ.Sci.Technol.*, 23, 496 (1989).

(2) Nash, K., Fried, S., Friendman, A. M. and Sullivan, J. C. : *ibid.*, 15, 834 (1981).

(3) Tanaka, T. and Ni, S. : *JAERI-M 93-185*, (1993).

(4) Tanaka, T. and Senoo, M. : *Scientific Basis for Nuclear Waste Management* XVIII *(MRS94)*, p. 1013, Materials Research Society, (1995).
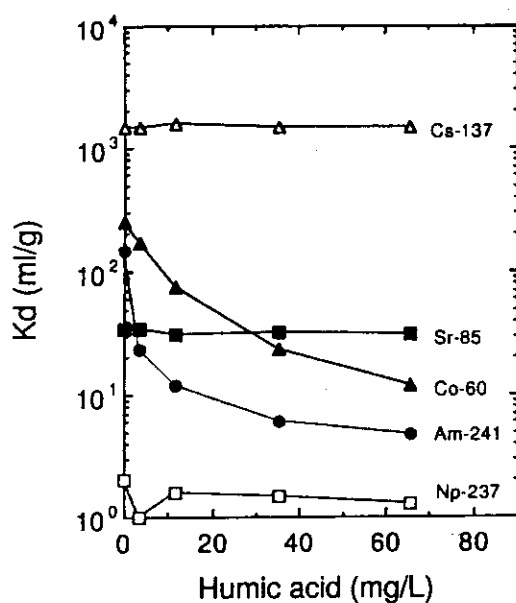
Sand
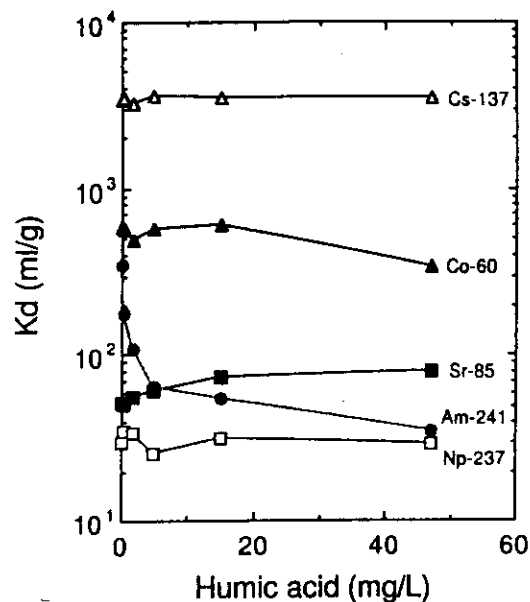
Ando soil

Fig. 29   Influence of humic acid concentration on Kd of radionuclides.
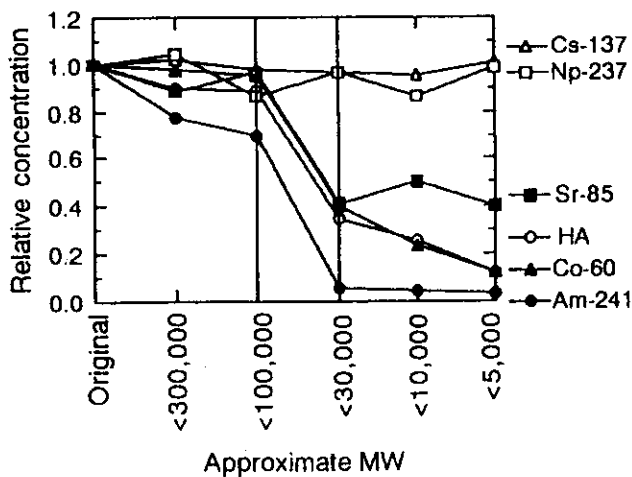


Fig. 30   Concentration of humic acid and   Fig. 31   Influence of concentration of Kd
radionuclides in each molecular-              of humic acid.
weight fraction before the
sorption experiment; Humic acid:
35 mg/L.

# 3. Safety Evaluation Study on Geological Disposal

## 3.1 Chemical Behavior of Radionuclides in Water

### 3.1.1 Influence of Humic Acid on Sorption Behavior of Np(V) onto Goethite

Y. Sakamoto*, A. Ohashi**, S. Sato** and H. Ohashi**

INTRODUCTION

Sorption behavior of [237]Np on geologic formation should be clarified for the safety assessment of the radioactive waste disposal because of its long half-life ($2.12 \times 10^6$ y) and high toxicity. Humic acid in ground water is one of the important factors to affect the sorption behavior of Np(V).

In the present work, a pH dependence of a stability constant of Np(V)-humate has been determined with a UV-VIS-NIR spectrophotometer to clarify chemical forms of Np(V) in the groundwater including of humic acid. Based on the information about speciation of Np(V) in solution including of humic acid, the influence of humic acid on the sorption behavior of Np(V) onto goethite, which is one of iron minerals to play important role of a retardation phenomenon for actinides, has been studied as a function of humic acid concentration.

EXPERIMENTAL

Humic acid

Humic acid(HA) purchased from Aldrich Co. was dissolved in an alkaline solution and precipitated at pH 1 with 1 M HCl solution. The precipitate was separated from the supernatant by centrifugation and redissolved into another alkaline solution. After this treatment was carried out three times, the precipitate was dispersed into deionized water for washing and the humic acid sample was recovered at pH 1. This washing process was also repeated. Final humic acid was freeze-dried for use in this work.

A proton exchange capacity of humic acid was determined by acid-base titration. Humic acid was dispersed into 0.1 M NaClO₄ solution to be 20 mg/l. It was titrated with 0.002 M NaOH (I = 0.1 M, NaClO₄) solution in the N₂ atmosphere. The obtained titration curve

was analyzed by the Gran method[1]. The proton exchange capacity of humic acid was 5.1 meq/g in the 0.1 M NaClO$_4$ solution. A value of pKa of humic acid was determined to be 4.0 by a plot of pH to log($\alpha$/(1-$\alpha$)), where $\alpha$ is the degree of dissociation of humic acid[2]. The E$_4$/E$_6$ ratio of humic acid in 0.1 M NaClO$_4$ solution was obtained as 7.8 by using the UV-VIS spectrophotometer.

## Stability constant of Np(V)-humate

The stability constant of Np(V)-humate in 0.1 M NaClO$_4$ solution was determined in the pH region from 5.3 to 8.7 with absorption spectra using the UV-VIS-NIR spectrophotometer. The concentration of $^{237}$Np in the solution containing humic acid was fixed as 1.2 $\times 10^{-4}$ M, and the concentration of humic acid was varied among 80 and 600 mg/l. Five ml of Np(V) solution containing humic acid was sealed in a tube and shaken at 25 ℃ for 7 days. After that, the solution was filtered by 0.45 $\mu$m Millexfilter. The concentrations of NpO$_2$$^+$ and NpO$_2$HA were determined by the spectrophotometer at 982.2 nm and 990.7 nm, respectively. An isosbestic point was 986.2 nm. Total Np(V) concentration was measured by a liquid scintillation counting. The concentration of carbonate in the solution that was measured by ion meter was 1.0×10$^{-4}$ M.

The stability constant of Np(V)-humate, $\beta$n(1/eq), is given by the equation as follows[3]:

$$\beta n = \frac{[NpO_2(HA)_n]}{[NpO_2{}^+][HA]_f{}^n} \tag{1}$$

$$\log \frac{[NpO_2(HA)_n]}{[NpO_2{}^+]} = \log \beta_n + n\log[HA]_f \tag{2}$$

where [HA]$_f$(eq/l) is the concentration of free uncomplexed functional groups of humic acid. The concentration of functional groups of humic acid was calculated from the proton exchange capacity (meq/g) and the concentration of humic acid (mg/l) that was measured with the UV-VIS spectrophotometer at 280 nm. The [HA]$_f$ was obtained by subtracting [NpO$_2$(HA)$_n$] from the total concentration of functional groups of humic acid. The stability constant is determined by correlation between log[NpO$_2$(HA)]/[NpO$_2$$^+$] and log[HA]$_f$.

## Sorption of Np(V) onto goethite

Synthesized goethite was purchased from Raremetalic Co.. The goethite sample was crushed and sieved to a particle size of less than 100 $\mu$m. Its specific surface area

was 15.5 m$^2$/g, which was measured by a BET method. Point of zero charge (PZC) of goethite sample was determined as 6.4 by an acid-base titration method in a N$_2$ atmosphere.

Sorption experiment of $^{237}$Np(V) on goethite was performed by a batch method. The pH of 0.1 M NaClO$_4$ solution was adjusted by the addition HNO$_3$ or NaOH to the prescribed value among 5 to 9. Humic acid concentration in this solution was adjusted from 0 to 200 mg/l. The glass vessel with 0.020g of solid sample and 20 ml of the solution was tightly sealed and shaken in an oven at 30 ℃ for 3 days. After the sorption run, the pH was measured by a pH meter and the solution was filtrated by 0.45 $\mu$m Millipore Miller filter.

The determination of $^{237}$Np radioactivity concentration in the solution was performed by the liquid scintillation counting. The percent sorbed $^{237}$Np onto the goethite was defined by the difference between the concentrations before and after the sorption experiment.

Sorption of humic acid

Sorption experiment of humic acid was also performed by the batch method. The sorption experiment conditions were same as that of the case of Np(V). The measurement of the humic acid concentration was carried out by the UV-VIS spectrophotometer at 280nm.

RESULTS AND DISCUSSION

Stability constant of Np(V)-humate and speciation of Np(V)

The value of $\log[NpO_2HA]/[NpO_2^+]$ is plotted in Fig.32 as a function of $\log[HA]_f$ to determine the stability constant of Np(V)-humate, according to eq.(2). The linear correlation was obtained for every pH conditions from pH 5.3 to 8.7. The slopes calculated by the least squares method were 1.42 at pH 5.3, 1.07 at pH 6.2, 0.99 at pH 7.3, 1.18 at pH 7.9 and 1.17 at pH 8.3. The averaged value of the slopes was 1.17. This result indicates that the interaction of Np(V) with the functional groups of humic acid yields the 1:1 complexation, as reported by Kim and Sekine[3]. Then, the stability constant was calculated as n=1.0 by the least squares method.

The pH dependence of the stability constant is shown in Fig.33. The logarithm of the stability constant inceased linearly with pH and was expressed in the form:

$$\log \beta_1 = (0.35 \pm 0.03pH) + 0.04 \pm 0.01. \qquad (3)$$

The pH dependence of the stability constant of Np(V) with humic acid has been

explained in terms of a loading capacity of humic acid[3]. In accordance with the Kim and Sekine treatment[3], the intrinsic stability constant of Np(V)-humate was determined to be $\log \beta_1^* = 3.66 \pm 0.05$. The loading capacities were calculated as 0.03 at pH 5.3, 0.05 at pH 6.3, 0.15 at pH 7.3, 0.19 at pH 7.9 and 0.25 at pH 8.7. The intrinsic stability constant of Np(V)-humate obtained in this work was in good agreement with that of Kim and Sekine ($\log \beta_1^* = 3.66 \pm 0.02$)[3], though their humic acid was extracted from Goreleben ground water in northern Germany and its characteristics were somewhat different from those of our humic acid. This fact may suggest that the loading capacity of humic acid is one of the useful concept to obtain the information of interaction of actinides with different kinds of humic acid.

With the stability constant expressed in Eq. (3), the distribution of the chemical forms of Np(V) in 0.1 M NaClO$_4$ solution was computed by using the geochemical code MINTEQ. The hydrolysis reaction[4] and the carbonate complexation[5] of Np(V) were taken into account for this calculation. The results in the presence of humic acid of 32 mg/l are illustrated in Fig.34 as a function of pH. The major chemical species of Np(V) is $NpO_2^+$ up to pH 8, and $NpO_2HA$ and $NpO_2CO_3^-$ become one of the dominant species beyond pH 8.


Sorption of humic acid on goethite

Figure 35 shows a pH dependence of humic acid sorption on goethite. The sorption of humic acid decreased with pH under every concentration of humic acid condition. This decreasing with pH is good agreement with the results reported by Tipping[6]. According to Tipping[6], the sorption isotherm of humic acid on goethite is of Langmuir type.

In the case of 5 and 10 mg/l of humic acid, in whose concentration the amount of sorbed humic acid was not saturated, the sorption of humic acid decreased beyond pH 6.4. Humic acid is negatively charged by dissociation of carboxylate and phenolate groups[7]. On the other hand, the negative charged sorption site density on goethite surface increases with pH over pH 6.4 that was the PZC of goethite used in this work. Consequently, electrostatic repulsion between the functional groups of humic acid and negative surface charge of goethite leads the decreasing in the sorption of humic acid over pH 6.4 as shown in Fig.34.


Sorption of Np(V) onto goethite

Before discussing about the influence of humic acid on the sorption of Np(V), the sorption behavior of Np(V) in the absence of humic acid should be confirmed. The

sorption of Np(V) acid has been explained by an interaction of Np(V) with the surface negative charge[8], which increases with pH by deprotonation of hydroxyl group on goethite surface[9]. The most typical sorption reaction is the electrostatic interaction of $NpO_2^+$ with the surface negative charge in the pH region where major chemical species in $NpO_2^+$ as shown in Fig.34. In addition to this sorption reaction, the sorption of $NpO_2CO_3^-$ and/or $NpO_2OH$ by the surface complexation reaction will be expected[10,11] in alkaline region.

The percentages of sorbed Np(V) are shown in Fig.36 as a function of humic acid concentration at pH5.0, 6.5 and 8.5. In the case of pH5.0, the sorption of Np(V) was low and not recognized the influence of humic acid on its sorption behavior. On the other hand, the sorption of Np(V) increased by addition of humic acid up to 10 mg/l and was subsequently reduced beyond 10 mg/l of humic acid at pH6.5 and 8.5.

According to some reports[6,12], the sorption of humic acid on sorbents will lead the increase in the surface negative charge density of sorbent in acidic and neutral region. Because this phenomenon corresponds to the increases in the sorption site for cation, it is probably that the sorption of $NpO_2^+$ increased with the humic acid concentration up to 10 mg/l at pH 6.5 and 8.5. Beyond 10 mg/l, however, the amount of available sorption site for $NpO_2^+$ does not increase with the humic acid concentration because the amount of sorbed humic acid achieves to be saturated. In addition, $NpO_2HA$ is formed in the solution as shown in Fig.34. The degree of sorption of $NpO_2HA$ is supposed to be low by the coulombic repulsion of negatively charged Np(V)-humate with surface negative charge on goethite. Then, the sorption of Np(V) onto goethite at pH6.5 and 8.5 has decreased with the humic acid concentration beyond 10mg/l because of the formation of Np(V)-humate and saturation of sorption site.

In the case of pH5.0, the sorption of Np(V) was lower than at pH6.5 and 8.5 because the goethite surface is positively charged to prevent the sorption of $NpO_2^+$. From the results shown in Fig.33, moreover, the interaction of Np(V) with humic acid is little at pH5. Then, although humic acid is sorbed on goethite surface to lead the increase in the negative surface charge density, the sorption of Np(V) has not been influenced by humic acid at pH5.


CONCLUSION


The pH dependence of the stability constant of Np(V)-humate was measured to obtain the information of speciation of Np(V) in the solution. The logarithmic stability constant of Np(V)-humate in 0.1 M $NaClO_4$ solution increased linearly with pH and the stability

constant was expressed by $\log\beta_1 = (0.35\pm0.03)\text{pH}+0.04\pm0.01$. The intrinsic stability constant was obtained to be $\log\beta_1^* = 3.66\pm0.05$ using the concept of the loading capacity by Kim and Sekine[3].

The sorption of Np(V) onto goethite was examined to study the correlation between chemical forms of Np(V), which were calculated with the stability constant obtained in this work. In the presence of humic acid up to 10 mg/l at pH6.5 and 8.5, the sorption of Np(V) onto goethite was enlarged by the bounding to goethite via humic acid sorbed on goethite surface, and beyond 10 mg/l of humic acid the sorption of Np(V) was reduced by the formation of Np(V)-humate in solution.

From these results, it is suggested that the change in the surface charge density by the sorption of humic acid and in the chemical species of Np(V) in solution must be taken into account for the influence of humic acid on the sorption behavior of Np(V).

## ACKNOWLEDGMENTS

## REFERENCES

( 1 ) G. Gran, Acta Chemica Scandinavia, 4, 559 (1950).

( 2 ) G. R. Choppin and L. Kullberg, J. Inorg. Nucl. Chem., 40, 651 (1978).

( 3 ) J. I. Kim and T. Sekine, Radiochim. Acta, 55, 187 (1991).

( 4 ) V. Neck, J. I. Kim and B. Kanellakopoulos, Radiochim. Acta, 56 (1992).

( 5 ) V. Neck, J. I. Kim and B. Kanellakopoulos, KfK-5301 (1994).

( 6 ) E. Tipping, Geochimica et Cosmochmica Acta, Vol. 45, 191 (1981).

( 7 ) F. J. Stevenson, in Humus Chemistry Genesis, Composition, Reactions, (A Wiley-Interscience publication, New York, 1982).

( 8 ) Y. Sakamoto, M. Konishi, K. Shirahashi, M. Senoo and N. Moriyama, Radioactive. Waste Man. and Nucl. Fuel Cyc., 15(1), 13 (1990).

( 9 ) R. G. Gast, in Minerals in Goethite Environmental, edited by J. B. Dixon and S. B. Weed (Sci. Society of America, Madison, 1977)p. 35.

(10) G. Bidoglio, P. Offermann and A. Saltelli, Applied Geochemistry, Vol. 2, 275 (1987).

(11) D. C. Girvin, L. L. Ames, A. P. Schwab and J. E. McGarrah, J. Colloid Interface Sci., Vol. 141, No. 1, 67 (1991).

(12) C. H. O and N. H. Miller, J. Colloid and Interface Sci., Vol. 106 No. 2, 281 (1985).
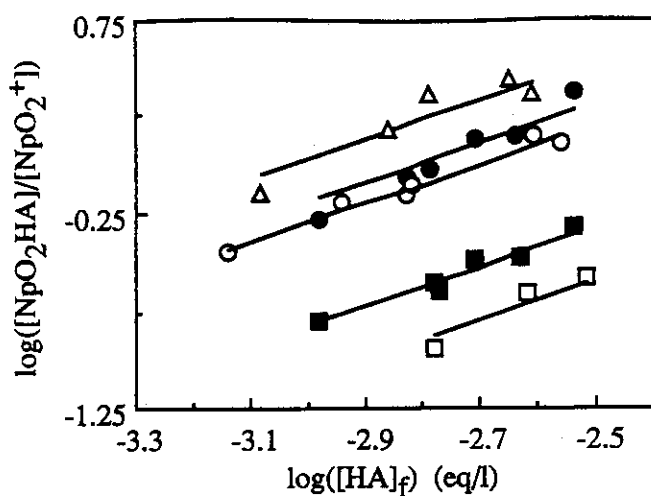
Fig. 32 Relationship between $[NpO_2(HA)_n]/[NpO_2^+]$ ratio and concentration of uncomplexed functional group of humic acid.

$\triangle$ pH 8.7; ● pH 7.9; ○ pH 7.3; ■ pH 6.2; □ pH 5.3
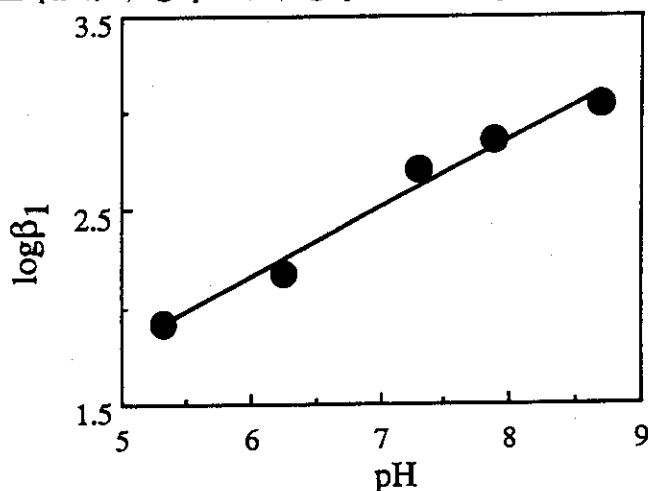


Fig. 33 pH dependence of stability constant of Np(V)-humate.
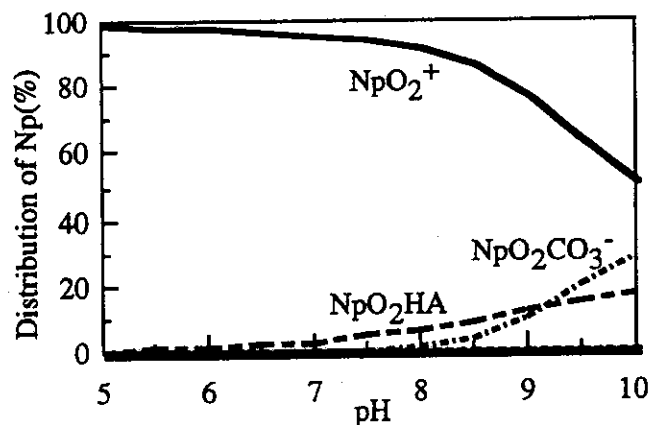


Fig. 34 Distribution of Np(V) in the 0.1 M $NaClO_4$ solution in the presence of humic acid of 32 mg/l (Calculated by MINTEQ). Total carbonate concentration is $1.0 \times 10^{-1}$ M.

$NpO_2^+ + nH_2O = NpO_2(OH)_n^{(1-n)} + nH^+$    $\log\beta_1 = 11.5$,   $\log\beta_2 = 23.84$   [4]

$NpO_2^+ + nCO_3^{2-} = NpO_2(CO_3)_n^{(1-2n)}$    $\log\beta_1 = 4.58$,   $\log\beta_2 = 6.60$   [5]
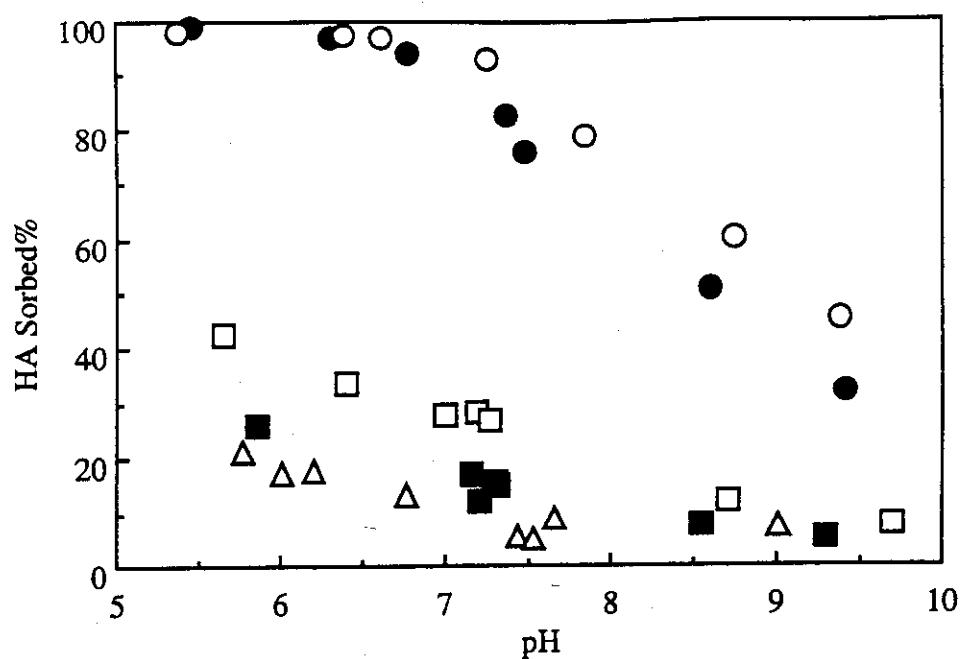
Fig. 35 pH dependence of sorption of humic acid on geothite.
　　　　○ HA: 5mg/l　　● HA: 10mg/l　　□ HA: 50mg/l
　　　　■ HA: 100mg/l　△ HA: 200mg/l
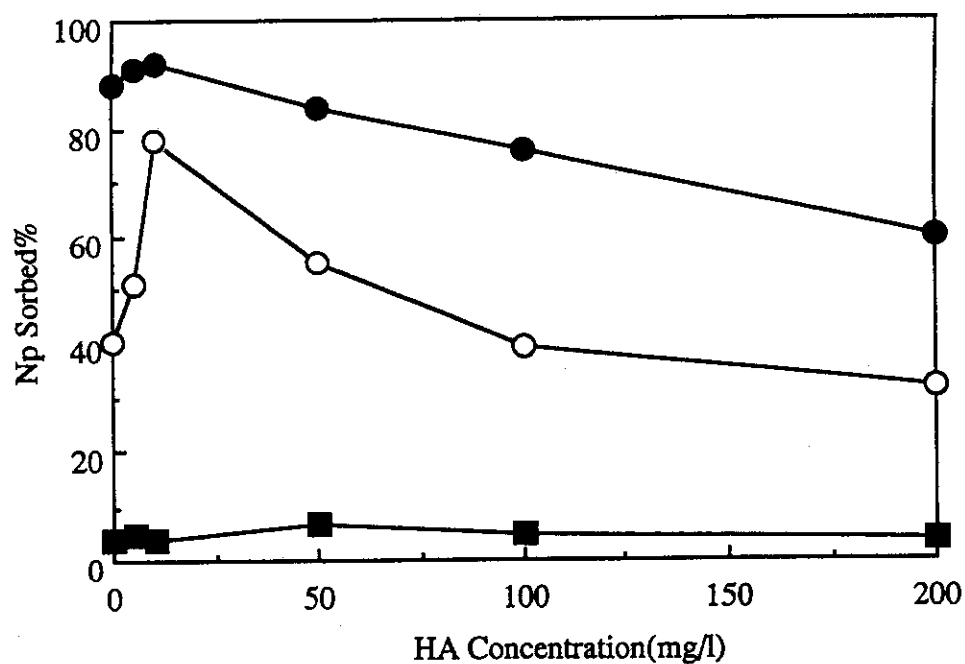


Fig. 36 Humic acid concentration dependence of sorption of Np(V) on goethite.
　　　　■ pH 5. 0　　○ pH 6. 5　　● pH 8. 5

### 3.1.2 Solubility of Neptunium(IV) Hydrous Oxide under Reducing Conditions[1]

S. Nakayama, T. Yamaguchi and K. Sekine

ABSTRACT

The solubility of neptunium(IV) hydrous oxide in water and $NaClO_4$ solutions was measured from over- and undersaturation directions at $25.0\pm0.2°C$ over a pH range of 5.30 to 13.7, in the presence of reducing agents ($Na_2S_2O_4$, metallic Fe or metallic Cu). Equilibration periods ranged from 1 to 119 days. All procedures were performed in a controlled atmosphere in a chamber containing high purity Ar ($<1$ ppm $O_2$). Steady concentrations appeared to be reached within 28 days from the over- and undersaturated directions in dilute solutions (ionic strength $< 0.1$ M), with the Np(IV) concentrations reaching approximately the same value from both directions. However, the concentrations decreased slowly to less than $10^{-9}$ M over subsequent periods of tens of days. The decrease in Np(IV) concentration was faster in a higher ionic strength medium, 1 M $NaClO_4$, reaching apparent equilibrium.

Keywords: Neptunium, Np(IV) Hydrous Oxide, Solubility

## 1. INTRODUCTION

The chemical conditions in and around a radioactive waste repository at depth are expected to be reducing and neptunium is expected to be present primarily as Np(IV). The environmental and safety assessment of geological disposal of radioactive waste requires solubility data of Np(IV) compounds to predict their concentration in groundwater near the repository. Because tetravalent actinides are susceptible to hydrolysis and have a strong tendency for complexation with carbonate ions[1], their solubilities are controlled by the concentrations of the hydrolysis products and/or carbonate complexes in natural aquatic environments.

The solubility of Np(IV) in neutral to alkaline water has been measured by a number of researchers, and fairly good agreement has been reported: log(solubility, $M^{2)}$) $<-8.3$[2], $-8.1$[3], $-8.5\pm0.1$[4], and $8.28\pm0.23$[5]. These values were obtained experimentally by approaching equilibrium solubility conditions either from

---

oversaturation[2-4] or from undersaturation[5], and over relatively short equilibration periods (<3 weeks). Ewart et al.[3] and Eriksen et al.[5] confirmed reaching equilibrium of the Np concentrations, but the durations of their experiments were shorter than <3 days and <4 days, respectively. In this study, the equilibrium solubility of Np(IV) hydrous oxide was approached from over- and undersaturation directions. The effects on solubility of equilibration periods of 100 days and ionic strength are reported in this paper.

## 2. EXPERIMENTAL

### 2.1 Preparation

A stock solution of Np(IV) was prepared from Np nitrate ([237]Np: 99.4%, [239+240]Pu: <0.3%, [238]Pu+[241]Am: <0.3%) obtained from AEA Technology, UK. The solid was dissolved in 1M $HNO_3$, evaporated to dryness, redissolved in 6M HCl, and diluted to 1M HCl. Reducing conditions in the solution were obtained by adding ferrous perchlorate and hydrazine monohydrochloride and heating at 50-60°C for approximately 30 minutes. The Np(IV) produced in this manner was extracted in 0.5M thenoylfluoroacetone (TTA) in xylene and back-extracted with 8M HCl. This extraction—back-extraction was repeated twice more to remove any residual Fe. The oxidation state of Np stock solution of 8M HCl was determined spectrophotometrically and by solvent extraction using 0.5M TTA in xylene. The Np(IV) concentration in the stock solution was found to be 0.038M. The Fe concentration in the stock solution was determined by inductively coupled plasma atomic emission spectroscopy (ICP-AES) to be approximately $4\mu g/g$.

Deionized water was deaerated by boiling and bubbling with Ar gas (>99.995%). This deaerated water was kept in an atmospheric control chamber with a high purity Ar (<1 ppm $O_2$) for at least a few months. Aqueous solutions of $NaClO_4$ and $Na_2S_2O_4$ as a reductant were prepared in the chamber with this thoroughly deaerated deionized water immediately before use. The 0.1 or 1.0M carbonate-free NaOH solutions used for pH adjustment were prepared in the same manner.

A number of reducing reagents were used to maintain Np in the reduced state, including $Na_2S_2O_4$, metallic Fe powder and metallic Cu powder. These chemicals were all reagent grade and used without further purification. Metallic Fe[2] and $Na_2S_2O_4$[2-5] were shown to be effective reductants to maintain Np in the tetravalent state.

## 2.2 General Procedures

All experiments were conducted under a controlled Ar atmosphere ($<1$ ppm $O_2$). In experiments performed from an oversaturation direction, aliquots of the Np(IV) stock solution were added to 15 mL of deaerated deionized water, 0.1 or 1.0M $NaClO_4$, 0.05 $Na_2S_2O_4$, or a mixture solution of $NaClO_4$ and $Na_2S_2O_4$ in 20-mL glass vial. The initial concentration of Np(IV) was around $10^{-5}$M with a few exceptions where the concentration was about $10^{-3}$M Np(IV). Metallic Fe or Cu powder (9-16 mg/15 mL) was added to the water and $NaClO_4$ sample solutions. The pH values were adjusted to cover a range of pH 5 to 14 with $HClO_4$ or NaOH solutions. The pH values for the $Na_2S_2O_4$ solutions were limited to the alkaline range where $Na_2S_2O_4$ effectively functions as a reductant. After preparation, the samples were kept at $25.0 \pm 0.2°C$.

Fresh precipitates of Np(IV) hydrous oxide was used in the experiments performed from an undersaturation direction. These precipitates were prepared by adding aliquots of the Np(IV) stock solution to a mixture of $Na_2S_2O_4$ and NaOH solutions. After several hours, the supernatant was discarded, the precipitate washed twice with deaerated deionized water and a fresh $NaClO_4$ solution or $Na_2S_2O_4$ solution, or a mixture of their solutions added. Precipitates formed in the experiments performed from the oversaturation direction were also used in the experiments performed from the undersaturation direction. In those cases the supernatant was removed after completion of the experiments ($<7$ days), and fresh $NaClO_4$ or $Na_2S_2O_4$ solution contacted with the precipitates. Equilibration periods ranged from 1 to 119 days for dilute solutions (ionic strength $< 0.1$M), and from 1 to 51 days for a higher ionic strength solution, 1M $NaClO_4$.

## 2.3 Measurements

The pH was measured with a ROSS combination-glass electrode calibrated with standard pH buffer solutions of 4.01, 7.00 and 10.013. For the higher pH values, 0.01, 0.1 and 1.0M NaOH solutions were used. Redox potentials were measured with a platinum electrode calibrated with a mixture solution of potassium ferricynide and potassium ferrocynide.

After predetermined equilibration periods, aliquots of the supernatant were withdrawn and filtered through a 10000-molecular-weight cutoff Millipore filter. Special care was taken to determine the concentration of dissolved Np. Rai and Ryan[2] used a pretreatment step (1) to avoid precipitation on or dissolution of the solid phase due to change in the pH during filtration. and (2) to saturate possible adsorption sites on the filters and filtration containers. Ewart et al.[3] and Eriksen et al.[5] used preconditioned filters. In the experiments described here, three steps were used: the

filters were pretreated by transferring 2 mL of the supernatants into a filter container, and allowed this to stand for 10 minutes to saturate the adsorption sites of the filters and the wall of filter containers. In the next step, the supernatant was filtered and the filtrates were left for 10 minutes to saturate the adsorption sites of the wall of the filtrate cup. Finally, the filtrates were discarded and new aliquots of the supernatant filtered using the same filters and containers.

The oxidation state of Np in the same solutions was determined by solvent extraction using 0.5M TTA in xylene. The filtrates obtained in the above step were acidified to 0.5M HCl, and mixed with equal volumes (1 mL) of 0.5M TTA in xylene. The initial, solvent-extracted, and non-extracted Np concentrations were determined by liquid scintillation alpha-counting using Packard Ultima Gold XR gel and Packard Tri-Carb 2550 TR/AB liquid scintillation analyzer. A 0.5-mL aliquot of the filtrate and aqueous phase was used for determinations of the total and non-extracted fraction of Np, respectively, and a 100-$\mu$L aliquot for the solvent-extracted fraction. These fractions were mixed with 3 mL scintillation gel. Sample solutions for background counts, containing solutions of the same composition as the corresponding Np samples, were prepared for each series of measurement. Measured background counts were equivalent to Np concentrations ranging from $4 \times 10^{-5}$M to $5.4 \times 10^{-9}$M.

## 3. RESULTS AND DISCUSSION

The (pe+pH) values obtained for the Np sample solutions ranged 0<pe+pH<6 (pe=0.0169Eh (mV) at 25°C). Some of the solutions that contained metallic Fe showed negative (pe+pH) values; under these conditions water is reduced to hydrogen. It is doubtful that uniform potentials at equilibrium were measured for the solutions. The results from the determination of oxidation states showed that Np(IV) was dominantly present in most samples. Samples in which showed Np(V) was predominantly present were not included in the interpretation of the data. The change in pH over the duration of the experiments was less than 0.5 of a pH unit in most of solutions except those containing metallic Fe. The pH values of Fe(m)-containing solutions that were initially adjusted below pH 7, rose to a pH of around 7. The reaction $Fe+2H^+ \rightarrow Fe^{2+}+H_2(g)$ proceeds at a pH <7.

The efficiency of the pretreatment of the filters is shown in Table 5. The filter unit used (a Millipore 10000-molecular-weight cutoff filter) consists of a filter container, the bottom of which is the filter and into which filtrant is placed, and a filtrate cup. The Np concentrations listed in the right four columns of Table 5 are those of (a) the supernatant, (b) the supernatant after 10 minutes in the filter containers, (c) the

filtrates immediately after filtration, and (d) the filtrates 10 minutes after filtration. These concentrations are relative to those in (a). Appreciable fractions of Np in the supernatants were sorbed on the filters and on the walls of the filter containers from solutions containing $Na_2S_2O_4$. Adsorption of Np from the filtrates on the wall of filtrate cups was generally less significant. The effects of filtration were observed to a greater or lesser extent in all solutions and was remarkably high in solutions containing 1M $NaClO_4$, $Na_2S_2O_4$ or metallic Cu powder. This observation suggests that the Np in these solutions was partially present in colloidal form.

The formation of colloidal particles of Np in $Na_2S_2O_4$ solutions has been reported by Pratopo et al. [4]. Metallic Cu powder was used as received without any pretreatment. Any fine Cu particles that might have sorbed Np appear to have been removed by filtration. The pretreatment of the filters and filtration unit reduced adsorption of Np. The results of this study suggest that saturation of surfaces that come into contact with solution is essential when determining equilibrium concentration of Np and that filtration is necessary to remove colloidal species.

Concentrations of Np(IV) in water and 0.1M $NaClO_4$ after equilibration periods less than 28 days are shown in Figure 37(a). The observed pH-independent solubility represents a dominant aqueous species of $Np(OH)_4(aq)$. Neptunium(IV) concentrations in the presence of metallic Fe approached from over- (6-10 days) and undersaturation (7 days) directions reached at a narrow range of $10^{-7.01\pm0.28}$ M, with the exception of one very low data point. The equilibrium concentrations of solutions in contact with metallic Cu also reached a nearly equal value ($10^{-7.53\pm0.32}$ M) from both directions (9 days for over- and 10 days for undersaturation directions). These observations suggest that steady-state conditions were reached in these solutions. In 0.05M $Na_2S_2O_4$ solutions with (undersaturation) and without (oversaturation) mettalic Fe, the Np(IV) equilibrium concentrations are $10^{-7.62\pm0.13}$ M.

The solubility values obtained in this study are listed in Table 6 together with data reported in the literature. The values obtained in this study from experiments with equilibration periods less than 28 days are more than 0.5 orders of magnitude higher than those reported elsewhere and are different for different reductants. Similar high concentrations of Np in $Na_2S_2O_4$ solutions were observed by Rai & Ryan [2] ($\sim10^{-7}$ M) and Pratopo et al. [4] ($\sim10^{-7.5}$ M). Both groups attributed their results to the ineffectiveness of $Na_2S_2O_4$ as a reductant at around pH 7 and the formation of Np(V). However, the values plotted in Fig. 37(a) represent Np(IV) concentrations and the high values in the figure cannnot be attributed to Np(V). The reason for the difference in measured solubility among different reductants is unknown. A possible explanation is

existence of fine particles of metallic Fe powder less than 10000-molecular-weight cutoff in size, on which large amounts of Np are sorbed. We observed yellow precipitates in a few samples, which suggests the formation of goethite. This observation provides evidence that iron particles functioned as an oxygen getter in these samples. Neptunium might be sorbed on the fine particles of the goethite, which was formed either by oxidation-precipitation of dissolved Fe(Ⅱ) or by surface oxidation of iron particles.

The measured solubilities decreased during longer equilibration periods (>51 days) as shown in Fig.37(b). The Np(IV) concentrations in the $Na_2S_2O_4$+Fe solutions and Cu-containing solutions (undersaturation, 119 days) attained the average value of $10^{-8.56\pm0.31}$ M. In 0.05M $Na_2S_2O_4$ solutions (oversaturation, 51 and 106 days) concentrations were near the limit of detection. Taking the limit values at the maximum concentrations, the equilibrium solubilities are $<10^{-9.2(\pm0.26)}$ M.

Figure 38 shows the measured Np(IV) concentrations in 1M $NaClO_4$ samples, most of which contained metallic Fe. The pH-independent solubility values are calculated to be $<10^{-8.48(\pm0.74)}$ M for 1-7 days and $<10^{-8.91(\pm0.66)}$ M for 8-45 days of equilibration. These two similar values, considering associated large errors, suggest that the concentration of Np(IV) approached the equilibrium much faster in 1M $NaClO_4$ solutions than in solutions of lower ionic strengths (Fig.37(a),(b)). It is not certain, however, that the solubility measured after 45 days of equilibration represents the equilibrium value.

Metal hydrous oxides precipitated from aqueous solutions gradually age with time to form crystalline oxides with time, and the solubilities of the crystalline oxides are in general lower than those of hydrous oxides. It has been found that initially X-ray-inactive precipitates of Np(IV) hydrous oxide showed X-ray diffraction peaks corresponding to crystalline $NpO_2$ within one month[6]. Because dissolution is a surface reaction, solubilities are controlled by the properties of the surface contacting the aqueous solutions. X-ray diffraction peaks are indicative of the development of crystalline phases in the bulk of the solids but do not necessarily reflect the property of the solid surface. Information on crystallinity and crystallization kinetics of the surface of Np(IV) hydrous oxide will be needed to relate the aging and the decrease in the solubilities observed in this experiment.

ACKNOWLEDGEMENT

REFERENCES

( 1 ) Kim, J. I. : Chemical Behavior of Transuranic Elements in Natural Aquatic Systems. In: *Handbook on the Physics and Chemistry of the Actinides*, Vol. 4 (A. J. Freeman and C. Keller, ed. ). Elsevier Science Publishers, New York, 1986.

( 2 ) Rai, D., Ryan, J. L. : Neptunium(IV) Hydrous Oxide Solubility under Reducing and Carbonate Conditions. *Inorg. Chem.* 24, 247 (1985).

( 3 ) Ewart, F. T., Gore, S. J. M., Williams, S. J. : The Solubility of Neptunium(IV) at High pH. AERE R 19975, Harwell, UK (1985).

( 4 ) Pratopo, M. I., Moriyama, H., Higashi, K. : The Behavior of Neptunium under Reducing Conditions. In: *Proc. of the 1989 Joint International Waste Management Conference*, Vol. 2, High Level Radioactive Waste and Spent Fuel Management (S. C. Slate et al., ed. ), Kyoto, Japan, October 22–28, 1989, The American Society of Mechanical Engineers.

( 5 ) Eriksen, T. E., Ndalamba, P., Cui, D., Bruno, J., Caceci, M., Spahiu, K. : Solubility of the Redox-sensitive Radionuclides $^{99}$Tc and $^{237}$Np under Reducing Conditions in Neutral to Alkaline Solutions. Effect of Carbonate. SKB Technical Report 93-18 (1993).

( 6 ) Strickert, R. G., Rai, D., Fulton, R. W. : Effect of Aging on the Solubility and Crystallinity of Np(IV) Hydrous Oxide. In: *ACS Symp. Ser. 246*, 135 (1984).

Table 5 Effect of filtration of Np suspensions (Millipore 10000-molecular-weight cutoff unit)

| Sample | Saturation Direction | Solution | Reductant | Equilibration (day) | pH | Relative concentration on Np (%) | | | |
| --- | --- | --- | --- | --- | --- | --- | --- | --- | --- |
| | | | | | | Before filtration | | After filtration | |
| | | | | | | 0 min (a) | 10 min (b) | 0 min (c) | 10 min (d) |
| 159 | over | 1M (e) NaClO$_4$ | Fe metal | 7 | 8.64 | 100 | 96 | 11 | 10 |
| 141 | under | 0.1M NaClO$_4$ | Fe metal | 7 | 8.24 | 100 | ND (f) | 96 | 70 |
| 135 | under | water | Fe metal | 7 | 7.71 | 100 | 110 | 73 | 85 |
| 153 | over | water | Fe metal | 9 | 7.55 | 100 | 91 | 68 | 69 |
| 168 | under | 0.05M Na$_2$S$_2$O$_4$ | Fe metal +Na$_2$S$_2$O$_4$ | 10 | 9.69 | 100 | 68 | 10 | 11 |
| | | | | 119 | 9.51 | 100 | 63 | 53 | 56 |
| 148 | over | 0.05M Na$_2$S$_2$O$_4$ | Na$_2$S$_2$O$_4$ | 13 | 12.77 | 100 | 94 | 61 | 44 |
| 151 | over | 0.05M Na$_2$S$_2$O$_4$ | Na$_2$S$_2$O$_4$ | 13 | 7.87 | 100 | 107 | 56 | 59 |
| 162 | over | 1M NaClO$_4$ +0.05M Na$_2$S$_2$O$_4$ | Na$_2$S$_2$O$_4$ | 7 | 6.31 | 100 | 69 | 3.2 | 2.4 |
| 156 | over | water | Cu metal | 9 | 11.36 | 100 | 110 | 28 | 22 |
| 165 | under | water | Cu metal | 10 | 9.67 | 100 | ND | 7.0 | 6.8 |
| | | | | 119 | 9.40 | 100 | 94 | 46 | 57 |

The Np concentrations are those of (a) the supernatant, (b) the supernatant after 10 minutes in the filter containers, (c) the filtrates immediately after filtration, and (d) the filtrates 10 minutes after filtration. These concentrations are relative to those in (a). The difference between (a) and (b) represents sorption on the filters and the walls of the filter containers, that between (b) and (c) indicates the amount of filtered Np, and that between (c) and (d) represents sorption on the walls of the filtrate cups. (e) M : mol/ℓ. (f) ND : Not determined.

Table 6 Solubility of Neptunium(IV) Hydrous Oxide

| Solution | Saturation Direction | Reductant | Equilibration (day) | Temperature (°C) | pH | $\log[\mathrm{Np(IV)}]$ (M[a]) | Reference |
|---|---|---|---|---|---|---|---|
| 0.05M Na₂S₂O₄ | under | 0.05M Na₂S₂O₄ | 9-12 | RT[b] | 11.24-14.18 | <-8.3 | [2] |
| water | under | Fe, Zn | NR[c] | RT | 6.2-8.4 | <-8.3 | [2] |
| concrete water | over | 10⁻³ or 10⁻⁴ M Na₂S₂O₄ | 1,3 | RT | 9.9-13.0 | -8.1 | [3] |
| 0.1M Na₂S₂O₄ | over | 0.1M Na₂S₂O₄ | 1-3 weeks | RT | 8.5-12.5 | -8.5±0.1 | [4] |
| NR | under | NR | 3-4 | RT | 6.05-12.05 | -8.28±0.23 | [5] |
| water or 0.1M NaClO₄ | over | 0.05M Na₂S₂O₄ | 10-28 | 25 | 7.87-13.67 | -7.62±0.15 | This study |
| | over | 0.05M Na₂S₂O₄ | 51,106,119 | 25 | 8.33-13.55 | <-9.0 | This study |
| | over & under | Fe | 6-9 | 25 | 7.22-12.07 | -7.01±0.28 | This study |
| | over & under | Cu | 9-10 | 25 | 7.91-11.36 | -7.53±0.32 | This study |
| | under | Cu | 119 | 25 | 8.41-9.40 | -8.66±0.43 | This study |
| 1M NaClO₄ | over & under | 0.05M Na₂S₂O₄, Fe | 45 | 25 | 5.30-11.38 | <-8.9 | This study |

(a) M : mol/ℓ, (b) RT : Room temperature. The temperatures are not reported in Refs. [2-5] for which their experiments were performed under inert gas atmosphere;(c) NR : Not reported.

Fig. 37 Measured solubility of neptunium (IV) hydrous oxide in water and 0.1 M NaClO$_4$ in the presence of a reductant (0.05 M Na$_2$S$_2$O$_4$, metallic Fe or metallic Cu). Equilibration periods: (a) 6, 7, 9, 10, 13 or 28 days; (b) 51, 106 or 119 days. Bars on the marks denote the concentrations of detection limits.
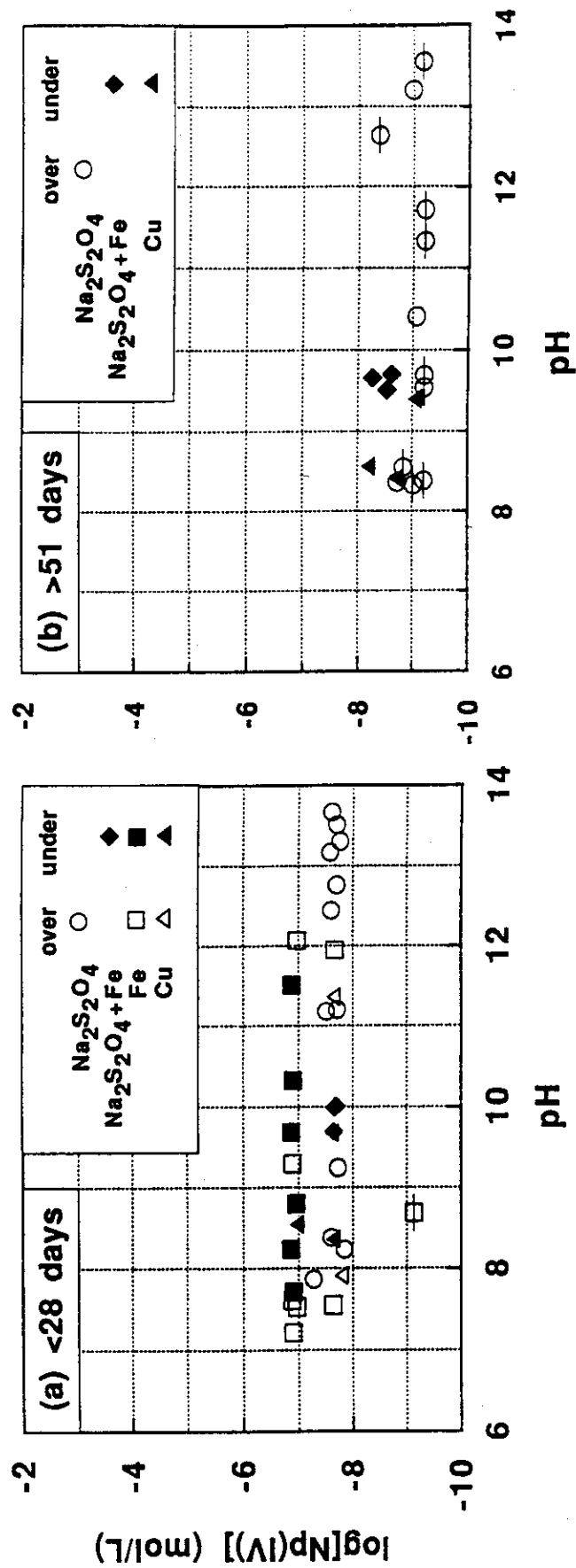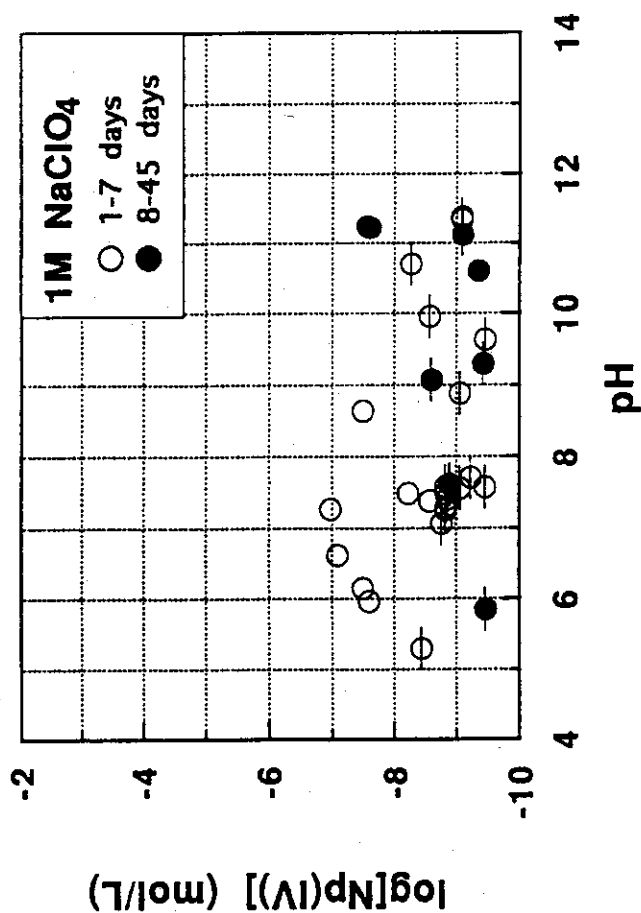
Fig. 38 Measured solubility of neptunium (IV) hydrous oxide in 0.1 M NaClO₄ in the presence of a reductant (0.05 M Na₂S₂O₄ or metallice Fe). Equilibration periods were 1, 2, 4-8, 10, 17, 34 or 45 days. Bars on the marks denote the concentrations of detection limits.

## 3.2 Nuclide Migration

### 3.2.1 Effective Diffusivity of the Uranyl Ion in a Granite from Inada, Ibaraki, Japan - Theoretical Relation to the Diffusivity in Water

T. Yamaguchi

Abstract

The effective diffusivity of uranium(VI) in Inada granite has been determined by through-diffusion. Experiments were performed at room temperature (20 - 25 ℃) in a 0.1 mol/L KCl solution where uranium is present predominantly as the poorly sorbing $UO_2^{2+}$. An effective diffusividy ($De$) of $(3.6 \pm 1.6) \times 10^{-14}$ m²/s was obtained, close to that for uranine (nonsorbing organic tracer), but one order of magnitude lower than those obtained for $Sr^{2+}$ and $NpO_2^+$, and two orders of magnitude lower than that obtained for $I^-$. According to well established theory, a proportional relationship exists between $De$ and the diffusivity in the bulk of the solution ($Dv$). The effective diffusivity obtained in granite was not proportional to $Dv$. This agrees with results obtained for effective diffusivity in a Swedish granite. The ratio $De/Dv$ was found to be not constant but increased with $De$ or $Dv$. This result suggests a limit to applying the theory.

## I. INTRODUCTION

After emplacement of high level radioactive waste in a deep underground repository, long-lived radionuclides may be leached from the wastes and may subsequently be transported through the surrounding rock mass. Major water bearing fractures in the rock surrounding the geosphere are considered to form the main transport paths. It is known that sorption onto mineral surfaces and diffusion into the pores or micro fissures in the rock matrix are important processes leading to the retardation of radionuclide transport through the geosphere. To evalute the migration of radionuclides in deep geological formations, it is important to quantify the diffusion of radionuclides into the rock matrix and to understand the diffusion mechanisms. Granite was used in these experiments, as it is widely occurring in Japan and is being considered as a potential host rock for the disposal of high level wastes.

The diffusivity of an aqueous species through the interconnected pore space in a rock matrix is often assumed to be proportional to its diffusivity in bulk solution ($Dv$) and to the geometric parameters of the rock: $\varepsilon$ (porosity), $\delta$ (constrictivity) and $\tau^{-2}$ ($\tau$ : tortuosity)[1-8]. This relationship has been proposed for diffusion in macroporous media by Brakel and Heertjes[9] and has been applied to the diffusion in rock matrix by Neretnieks[1]. Although it is convenient to use this relationship to describe diffusion in rock, it is very difficult to verify the relationship because of micro-inhomogeneity of intact rock. The authors studied the relationship between $De$ and $Dv$ for divalent cations[10]. However this relationship was not clearly presented due to the limited $Dv$ range and experimental error. In this study, the effective diffusivity of $UO_2^{2+}$, whose diffusivity in bulk solution is known, was determined for an Inada granite, a typical granite in Japan. The present $De$ for $UO_2^{2+}$ and previously obtained $De$'s for $I^-$[11], $Sr^{2+}$[10], $NpO_2^+$[6] and uranium[6] are compared.

## II. EXPERIMENTAL

The rock used in this study was a biotitic granite obtained from the Inada mine in the Ibaraki prefecture, eastern Japan. The chemical and mineral compositions are given elsewhere[8, 10]. The procedures for preparing the rock samples have been described in a previous paper[10]. The porosity of the granite, as determined by water saturation, was 0.7%.

The acrylic diffusion cells used in this study are shown in Fig. 39. A granite disk was fitted. tightly into the central part of the cell and any gap between the rock disk and the acrylic filled with a silicone gasket. The granite disk was soaked in a 0.1 mol/L KCl solution at pH 4 under vacuum to evacuate all air from the interconnected pores, and then kept under atmospheric pressure for 30 days to pre-equilibrate the disks with the solution at the same pH. The central support member containing the granite disk was sandwiched between the two reservoirs, each with a capacity of 116 mL. Solutions were prepared from reagent grade chemicals (Wako Pure Chemical Industries, Ltd., Tokyo) and deionized water (Milli-Q Labo System, Millipore). Uranium-233 was chemically purified by anion exchange and prepared as a $8.9 \times 10^{-4}$ mol/L solution in 1 mol/L HCl. The source solutions for the diffusion experiments were prepared by adding a 3 mL volume of the stock solution to 345 mL 0.1 mol/L KCl in a polypropylene bottle. The pH was adjusted to 4.0 with dilute KOH. The concentration of uranium in the source solution was $7.7 \times 10^{-6}$ mol/L.

The diffusion experiments were started by placing the source solution in the source reservoir and an equal volume of the 0.1 mol/L KCl solution at pH 4 in the other, measurement reservoir. Experiments were performed in triplicate at room temperature (20-25℃). At 10 day intervals, a 50 $\mu$L aliquot was taken from the measurement reservoir and diluted to prevent the salt from interfering with alpha spectrometry of the samples. A 50 $\mu$L aliquot of the diluted sample solution was evaporated on a stainless planchet and its activity determined by alpha spectrometry. The statistical error of the determination of the activity was 3 - 14%. The 50 $\mu$L aliquot removed from the measurement reservoir was replaced by an equal volume of 0.1 mol/K KCl to maintain the balance between the water levels in the two reservoirs. The concentration of uranium in the source reservoir was determined periodically to monitor its U-233 concentration. At the termination of each experiment, the inner wall of the measurement reservoir was rinsed with 10 mol/L HCl to determine the amount of uranium adsorbed on the cell walls. This amount of sorbed uranium was found to be 3% of the final uranium inventory in the measurement reservoir and can be ignored.

## III. RESULTS AND DISCUSSION

In aerated solutions, the dominant oxidation state of uranium is hexavalent. Speciation of uranium was calculated by using the stability constants of the hydrolysis species expected to be present around pH 4 shown in Table 7. Complexation of $UO_2^{2+}$ by chloride anion is negligible[12] as is carbonate complexation at pH 4[12]. The calculation shows that the uranium concentration in solution is limited by precipitation of $UO_2(OH)_2H_2O$ above pH 6. In the present study, the uranium concentration in the source reservoir remained virtually constant as shown in Fig.40, which suggests no significant removal of uranium by precipitation and/or sorption on reservoir walls. More than 93% (96±3%) of the uranium was calculated to be present as $UO_2^{2+}$ throughout the experiment although the pH of the solution had increased to 4.1 by the end of the experiment.

The method of analysis have been given previously[10]. As shown in the above reference, a plot of the concentration of diffusing species in the measurement reservoir against time yields $De$, from the slope, and the rock capacity factor, ($\varepsilon + \rho Rd$), from the intercept on the time axis of the extrapolated linear portion, where $\rho$ is the bulk density of the rock and $Rd$ is the distribution coefficient. Figure 40 shows the time dependence of the uranium concentration in the measurement reservoir for the triplicate experiments. The uranium concentrations increased linearly with time after

50 days. The effective diffusivity and the rock capacity factor were determined by the least square fitting and are presented in Table 8 together with literature data. The average $De$ value obtained in this experiment was $(3.6 \pm 1.6) \times 10^{-14}$ m$^2$/s for the triplicate experiments. This value is close to that for uranine, but one order of magnitude lower than those obtained for $Sr^{2+}$ and $NpO_2^+$, and two orders of magnitude lower than that obtained for $I^-$. The effective diffusivity differs significantly between $UO_2^{2-}$ and $NpO_2^+$, although they are similar in the ionic structure.

The effective diffusivity is related to the "apparent diffusivity" $Da$ by the rock capacity factor:

$$Da = De / (\varepsilon + \rho Rd). \qquad\qquad (1)$$

Using this equation, an apparent diffusivity of $(1.7 - 3.7) \times 10^{-12}$ m$^2$/s is obtained for uranyl ion in the present study. This range is similar to that reported by Idemitsu et al. [8, 16, 17].

As was pointed in reference 10, both pore diffusion and surface diffusion contribute to the diffusion of sorbing species in the interconnected pore space of the granite. The surface diffusion is expected to be only significant when large amounts of species are adsorbed on the solid. As discussed in our previous paper [10], surface diffusion contribution was less significant from a 0.1 mol/L KCl solution because of the competing effect for sorption sites by the high concentration of $K^+$ ions. In the present $UO_2^{2+}$ diffusion experiments, a 0.1 mol/L KCl solution was also used. The rock capacity factor $(\varepsilon + \rho Rd)$ was therefore very close to the $\varepsilon$, which denotes poor sorption of uranium on the rock and smaller effect of the surface diffusion than that of the pore diffusion.

In the case where pore diffusion is dominant and surface diffusion can be ignored, the effective diffusivity can be expressed as:

$$De = Dv \, \varepsilon \, \delta / \tau^2 \qquad\qquad (2)$$

The relationship shown in Eq. (2) has been used by Neretnieks [1] and others to describe diffusion of ionic species in rock. The equation assumes a constant proportionality between $De$ and $Dv$. To check the validity of this assumption, $Dv$'s for uranyl, strontium and iodide under the experimental conditions were estimated by taking into account mode of diffusion (salt diffusion or tracer diffusion), concentration of the diffusing species and ionic strength of the solution and temperature. The diffusivity of $UO_2^{2+}$ at infinite dilution [18] can be used as the diffusivity in bulk solution because the concentration of uranium was much lower than that of KCl, which assured tracer

diffusion. The ionic strength of the solution was 0.1 mol/L, which gives an uncertainty of 3% to $Dv$ [19]. The temperature was room temperature (20 - 25°C), which gives an uncertainty of 13% to $Dv$ [18]. The $Dv$ of $UO_2^{2+}$ under the condition was estimated to be $(4.3 \pm 0.6) \times 10^{-10}$ m²/s as shown in Table 8. The strontium diffusion in reference 10 is considered to be not tracer-diffusion but salt-diffusion. The diffusivity of $SrCl_2$ in infinite dilution is $1.30 \times 10^{-9}$ m²/s [18]. The concentration of $SrCl_2$ in the previous study [10] was 0.1 mol/L, which would reduce the diffusivity by 17% on the basis of the data for $CaCl_2$ [20]. The Sr source solution [10] contained $Ba(NO_3)_2$, $MgCl_2$, $CoCl_2$ and $NiCl_2$ in 0.1 mol/L. The uncertainty on $Dv$ due to these salts are estimated to be 3% based on the difference between the $CaCl_2$ diffusivity in a 0.5 mol/L solution and that in a 0.1 mol/L solution [20]. The $Dv$ of $Sr^{2+}$ under the condition was estimated to be $(1.08 \pm 0.03) \times 10^{-9}$ m²/s. The iodide diffusion in the granite is also considered to be salt diffusion. The diffusivity of 0.1 mol/L KI is $1.86 \times 10^{-9}$ m²/s [20]. The $Dv$ of iodide under the condition was estimated to be $(1.9 \pm 0.2) \times 10^{-9}$ m²/s taking into account the 13% uncertainty due to temperature.

Experimentally obtained $De$'s for iodide, strontium and uranyl are plotted versus $Dv$ in Fig. 41. Although there is a positive correlation between the effective diffusivity of these ions and their bulk diffusivity in solution, the slope of this relationship is much greater than unity. The experimental result do not support the relationship shown by Eq. (2): the $De/Dv$ ratios are $1.1 \times 10^{-3}$, $3.4 \times 10^{-4}$ and $8.5 \times 10^{-5}$ for $I^-$, $Sr^{2+}$ and $UO_2^{2+}$, respectively.

Skagius and Neretnieks [2] measured the effective diffusivity in the Finnsjön granite for several ions and discussed the $De/Dv$ ratios. They obtained ratios of $4.9 \times 10^{-5}$ for $I^-$ and $5 \times 10^{-6}$ for uranine and concluded that the difference in the ratio was due to the uncertainty in the $Dv$ value for uranine that had been estimated by the Hayduk-Laudie equation. The $Dv$ for uranine is evaluated here by another method. The relationship between the diffusivity of an ion in solution at infinite dilution and its hydrated ion radius is derived from the Nernst equation (Eq. (3)) and the corrected Stokes equation (Eq. (4)) [21, 22] as shown in the Eq. (5).

$$D^0 = RT \lambda^0 / (\ |Z| \ F^2)$$  (3)

$$r = |Z| \ F^2 (r/r_s) / (6N \eta^0 \lambda^0)$$  (4)

$$D^0 = RT (r/r_s) / (6N \eta^0 r)$$  (5)

where  $D^0$ : Limiting ionic diffusion coefficient (m²/s)

$R$ : Gas constant (=8.314 J/mol/K)

$T$ : Absolute temperature (K)

$\lambda^0$ : Limiting ionic equivalent conductivity ($m^2$/equiv)

$Z$ : Valence of ion

$F$ : Faraday's constant (=96,480 As/mol)

$r$ : Hydrated ion radius (m)

$r/r_s$ : Correction factor

$N$ : Avogadro's number (=6.02×$10^{23}$ $mol^{-1}$)

$\eta^0$ : Viscosity of water (Ns/$m^2$)

Uranine is an aromatic organic compound, $C_{20}H_{10}O_5Na_2$, with a molecular weight of 376.28. Uranine molecules are only slightly hydrated in water because of their large size and low charge. The radius of uranine molecule in water is estimated to be 0.5-0.6 nm based on the C-C bonding length (0.139 nm). The correction factor, $r/r_s$, is 1.0 for species whose radius is larger than 0.5 nm [21] . $D^0$ of uranine is estimated to be (4-5)×$10^{-10}$ $m^2$/s from Eq. (5). This agrees with the diffusivity estimated using the Hayduk-Laudie equation. The effective diffusivities of $I^-$ and uranine in Finnsjön granite [2] are also shown in Fig. 41. $De$ is not proportional to $Dv$ for either the Inada or Finnsjön granite. The change in $De$ is larger than the change in $Dv$ for the both rocks.

Skagius and Neretnieks [3] and Lever [23] pointed out that the ratio $De/Dv$ is independent of the diffusing species provided no size factors or pore size and/or size of the diffusing species influence the diffusion. The effect of the size factors has been unknown. Although the hydrated ion radii of the diffusing species studied in this paper can be estimated (0.33, 0.42 and 0.58 nm for $I^-$, $Sr^{2+}$ and $UO_2^{2+}$, respectively, from Eq. (4)), interaction between rock pores and diffusing species cannot be discussed here because of information on the pore space geometry is not available. Further study is needed for quantitative understanding of the diffusivity of ions in rocks.

## IV. CONCLUSION

An effective diffusivity of $UO_2^{2+}$ in Inada granite of (3.6±1.6)×$10^{-14}$ $m^2$/s was obtained in 0.1 mol/L KCl solution. A positive correlation between effective diffusivity of dissolved species in the granite and diffusivity in bulk solution was obtained. These values increased in the order of $UO_2^{2+}$ ～ uranine < $Sr^{2+}$ < $I^-$. This order agrees with their diffusion coefficient in bulk solution. However, the ratio $De/Dv$ was found to be not constant but increased with $De$ or $Dv$. The same trend was found for a Swedish

granite. Since experiments to determine the effective diffusivity in porous material is very time consuming, it is tempting to estimate $De$ values from a single $De$ and the knowledge of $Dv$ based on the proportionality between $De$ and $Dv$. The results of this work indicate that this approach may introduce large errors.

ACKNOWLEDGMENTS

The authors express their appreciation to Dr. M. Magara (JAERI) for the preparation of the $^{233}U$.

REFERENCES

( 1 ) NERETNIEKS, I. : Diffusion in the Rock Matrix; An Important Factor in Radionuclide retardation?, J. Geophys. Res. 85, 4379 (1980).

( 2 ) SKAGIUS, K., NERETNIEKS, I. : Diffusion in cystalline rocks of some sorbing and nonsorbing species, KBS-TR-82-12, SKBF/KBS, Stockholm 1982.

( 3 ) SKAGIUS, K., NERETNIEKS, I. : Porosities and Diffusivities of Some Nonsorbing Species in Crystalline Rocks, Water Resour. Res. 22, 389 (1986).

( 4 ) SKAGIUS, K., NERETNIEKS, I. : Measurement of Cesium and Strontium Diffusion in Biotite Gneiss, Water Resour. Res. 24, 75 (1988).

( 5 ) NISHIYAMA, K., NAKASHIMA, S., TADA, R., UCHIDA, T. : Diffusion of an Ion in Rock Pore Water and its Relation to Pore Characteristics, Mining Geol. (in Japanese) 40, 323 (1990).

( 6 ) KUMATA, M., IWAI, T., SAGAWA, T., SUZUKI, T., NISHIYAMA, K. : Diffusion Experiment of a Radionuclide in Granitic Rock Cores, JAERI-M 90-179 (in Japanese), 1990.

( 7 ) TSUKAMOTO, M., OHE, T. : Intraparticle Diffusion of Cesium and Strontium Cations into Rock Materials, Chem. Geol. 90, 31 (1991).

( 8 ) IDEMITSU, K., FURUYA, H., MURAYAMA, K., INAGAKI, Y. : Diffusivity of Uranium(VI) in Water-Saturated Inada Granite, Material Research Society Symposium Proceedings, Pittsburgh, Vol. 257, p. 625 (1992).

( 9 ) BRAKEL, J. V., HEERTJES, P. M. : Analysis of Diffusion in Macroporous Media in Terms of a Porosity, a Tortuosity and a Constrictivity Factor, Int. J. Heat Mass Transfer 17, 1093 (1974).

(10) YAMAGUCHI, T., SAKAMOTO, Y., SENOO, M. : Consideration on Effective Diffusivity of Strontium in Granite, J. Nucl. Sci. Technol. 30, 796 (1993).

(11) KITA, H., IWAI, T., NAKASHIMA, S. : Diffusion Coefficient Measurement of an Ion in

Pore Water of Granite and Tuff, J. Jpn. Soc. Eng. Geol. (in Japanese) 30, 84 (1989).

(12) WANNER, H., FOREST, I. : *Chemical Thermodynamics of Uranium*, North-Holland, Amsterdam 1992.

(13) KRAMER-SCHNABEL, U., BISCHOFF, H. XI, R. H., MARX, G. : Solubility Products and Complex Formation Equilibria in the Systems Uranyl Hydroxide and Uranyl Carbonate at 25℃ and $I$ = 0.1 M, Radiochim. Acta 56, 183 (1992).

(14) CHOPPIN, G. R., MATHUR, J. N. : Hydrolysis of Actinyl(VI) Cations, Radiochim. Acta 52/53, 25 (1991).

(15) CRANK, J. : *The Mathematics of Diffusion*, 2nd ed., Oxford Univ. Press, London 1975, p. 50.

(16) IDEMITSU, K., FURUYA, H., INAGAKI, Y., SATO, S. : Migration of Uranium(VI) in Laboratory Scale Granite, Proceedings of the Third International Symposium on Advanced Nuclear Energy Research, Mito, Japan, p. 207 (1991).

(17) IDEMITSU, K., FURUYA, H., MURAYAMA, K., ASAO, T., INAGAKI, Y. : Primary Diffusion Path or Uranium(VI) in Laboratory Scale Water Saturated Inada Granite, Proceedings of the 1993 International Conference on Nuclear Waste Management and Environmental Remediation, Vol. 1, p. 207 (1993).

(18) LI, Y. H., GREGORY, S. : Diffusion of ions in sea water and in deep-sea sediments, Geochim. Cosmochim. Acta 38, 703 (1974).

(19) MILLS, R. : Trace-Ion Diffusion in Electrolyte Solutions, Rev. Pure Appl. Chem. 11, 78 (1961).

(20) ROBINSON, R. A., STOKES, R. H. : *Electrolyte Solutions*, Butterworths, London 1955, p. 513.

(21) ROBINSON, R. A., STOKES, R. H. : *Electrolyte Solutions*, Butterworths, London 1955, p. 120.

(22) NIGHTINGALE, E. R. : Phenomenological Theory of Ion Solvation. Effective Radii of Hydrated Ions, J. Phys. Chem. 63, 1381 (1959).

(23) LEVER, D. A. : Some Notes on Experiments Measuring Diffusion of Sorbed Nuclides through Porous Media, AERE-R-12321, 1986.

Table 7 Eqilibrium constants for U(VI) hydrolysis species in 0.1 mol/L KCl solution. Equilibrium constants at 25°C and I=0 are taken from Wanner and Forest [12] unless otherwise noted, and corrected for ionic strength to 0.1 mol/L by using the method recommended in the literature [12].

| Species | $LogK_{sp}$ | $Log \beta$ [a] |
|---|---|---|
| $UO_2(OH)_2 \cdot H_2O$ | $-22.21 \pm 0.01$ [b] | |
| $UO_2(OH)^+$ | | $-5.4 \pm 0.3$ |
| $UO_2(OH)_2^0$ | | $-12.43 \pm 0.09$ [c] |
| $UO_2(OH)_3^-$ | | $-19.2 \pm 0.4$ |
| $UO_2(OH)_4^{2-}$ | | $-33 \pm 2$ |
| $(UO_2)_2(OH)^{3+}$ | | $-2.5 \pm 1.0$ |
| $(UO_2)_2(OH)_2^{2+}$ | | $-5.84 \pm 0.04$ |
| $(UO_2)_3(OH)_4^{2-}$ | | $-12.3 \pm 0.3$ |
| $(UO_2)_3(OH)_5^-$ | | $-16.21 \pm 0.12$ |
| $(UO_2)_3(OH)_7^-$ | | $-31 \pm 2$ |
| $(UO_2)_4(OH)_7^+$ | | $-22.8 \pm 1.0$ |

(a) equilibrium constant for $mUO_2^{2+} + nH_2O = (UO_2)_m(OH)_n^{2m-n} + nH^+$

(b) taken from K-Schnabel et al [13].

(c) taken from Choppin and Mathur [14].

Table 8 Effective diffusivity (De) and rock capacity factor $(\varepsilon + \rho R_d)$ of species in Inada granite.

| Species | De(m²/s) | $\varepsilon + \rho R_d$ [a] | Solution | Temperature | Reference | $D_v$(m²/s) |
|---|---|---|---|---|---|---|
| $UO_2^{2+}$ | $(2.2 \pm 0.2) \times 10^{-14}$ | $0.011 \pm 0.010$ | 0.1M KCl | room temp. | this work | $(4.3 \pm 0.6) \times 10^{-10}$ |
| | $(4.2 \pm 0.2) \times 10^{-14}$ | $0.025 \pm 0.016$ | pH=4 | | | |
| | $(4.4 \pm 0.4) \times 10^{-14}$ | $0.012 \pm 0.028$ | | | | |
| | avg. $(3.6 \pm 1.6) \times 10^{-14}$ | | | | | |
| $I^-$ | $1.9 \times 10^{-12}$ | $0.07 \pm 0.06$ [c] | 0.1M KI | room temp. | (11) | $(1.9 \pm 0.2) \times 10^{-9}$ |
| | $2.6 \times 10^{-12}$ | $0.05 \pm 0.06$ [c] | | | | |
| | avg. $(2.3 \pm 0.4) \times 10^{-12}$ | | | | | |
| $Sr^{2+}$ | avg. $(2.7 \pm 0.6) \times 10^{-13}$ | $0.013 \pm 0.008$ | 0.1M KCl [d] pH=4 | 25℃ | (10) | $(1.08 \pm 0.03) \times 10^{-9}$ |
| $NpO_2^+$ | $2.1 \times 10^{-13}$ | 0.016 | ground water | room temp. | (6) | no available data |
| | $2.9 \times 10^{-13}$ | 0.004 | pH=7.2~7.5 | | | |
| | avg. $(2.5 \pm 0.4) \times 10^{-13}$ | | I=0.077 | | | |
| uranine | $3.5 \times 10^{-14}$ | 0.017 | 1% uranine | room temp. | (6) | $(4.5 \pm 0.6) \times 10^{-10}$ |
| | $4.7 \times 10^{-14}$ | 0.015 | solution | | | |
| | $5.0 \times 10^{-14}$ | 0.071 | | | | |
| | avg. $(4.4 \pm 0.9) \times 10^{-14}$ | | | | | |

(a) Rock capacity factors obtained from through diffusion experiments may contain large errors due to extraporating of the linear portion of the diffusion curves to t =0. $\varepsilon$ and $\rho$ for the Inada granite are 0.007 and $2.6 \times 10^3$ kg/m³, respectively.

(b) see text

(c) The published values are 0.13 and 0.09. Rock samples used in the study had extra volume for ions to diffuse into; the effective cross section for ions to diffuse through was 30 mm$\phi$ while the rock sample was 40 mm$\phi$. It seems that the published rock capacity factors are overestimated because ions are stored in the extra volume. Their data have an intrisic uncertainty of $\sigma$=0.06 accompanied with fitting.

(d) multi-tracer diffusion experiment of Ba, Co, Mg, Ni, Sr
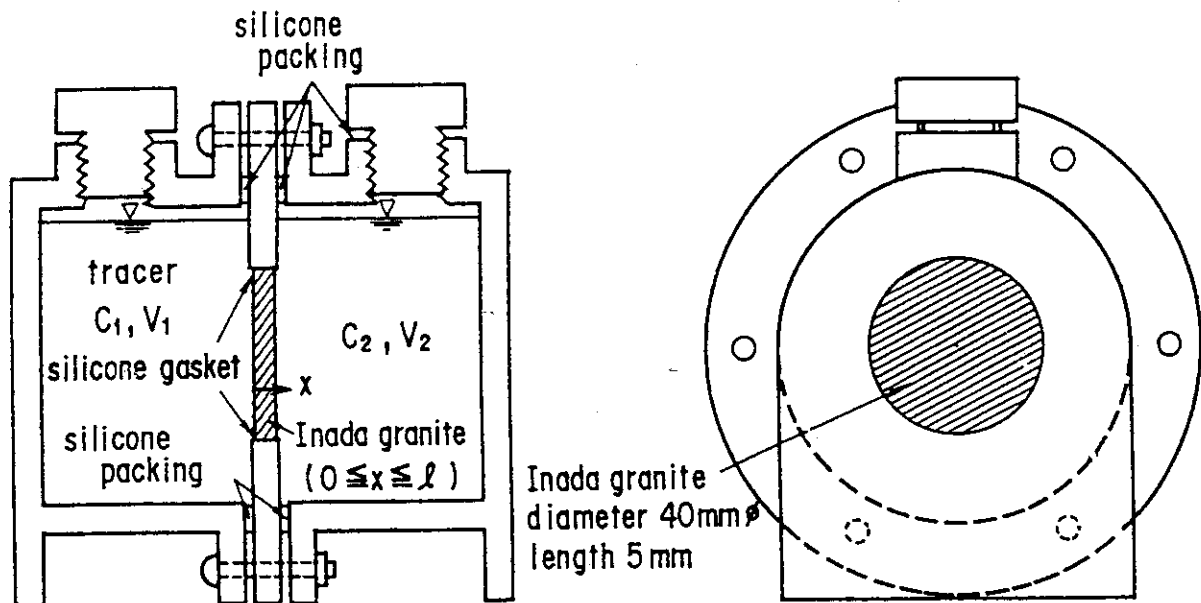
silicone
packing

tracer
$C_1$, $V_1$

silicone gasket

$C_2$, $V_2$

$x$

silicone
packing

Inada granite
$(0 \leqq x \leqq \ell)$

Inada granite
diameter 40mmφ
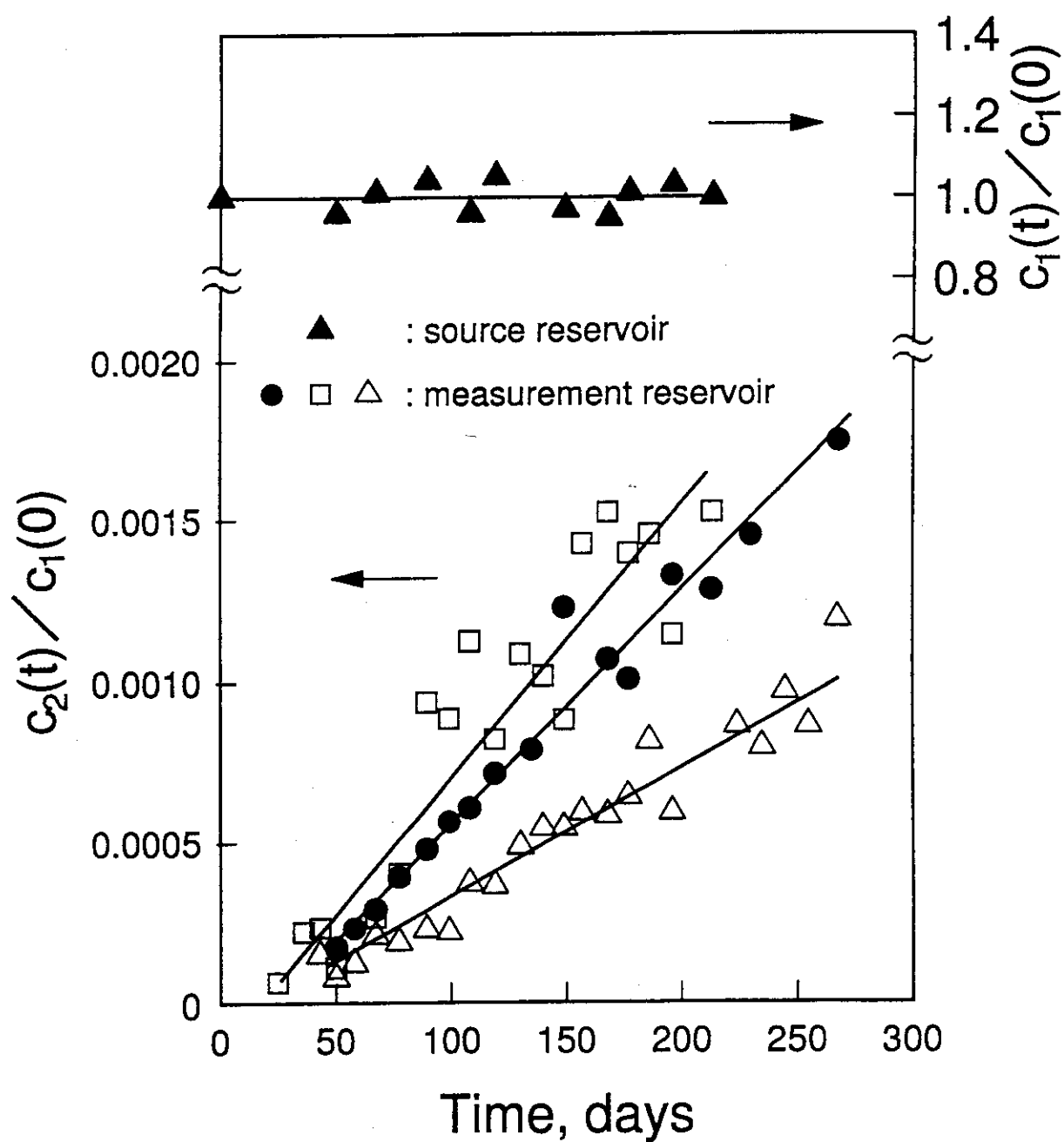length 5mm

Fig. 39 Diffusion cell used in experiment.

Fig. 40  Diffusion curves of uranium through 5-mm thick Inada granite disk in triplicate. Time dependence of the uranium concentration in a source reservoir is presented by closed triangles.
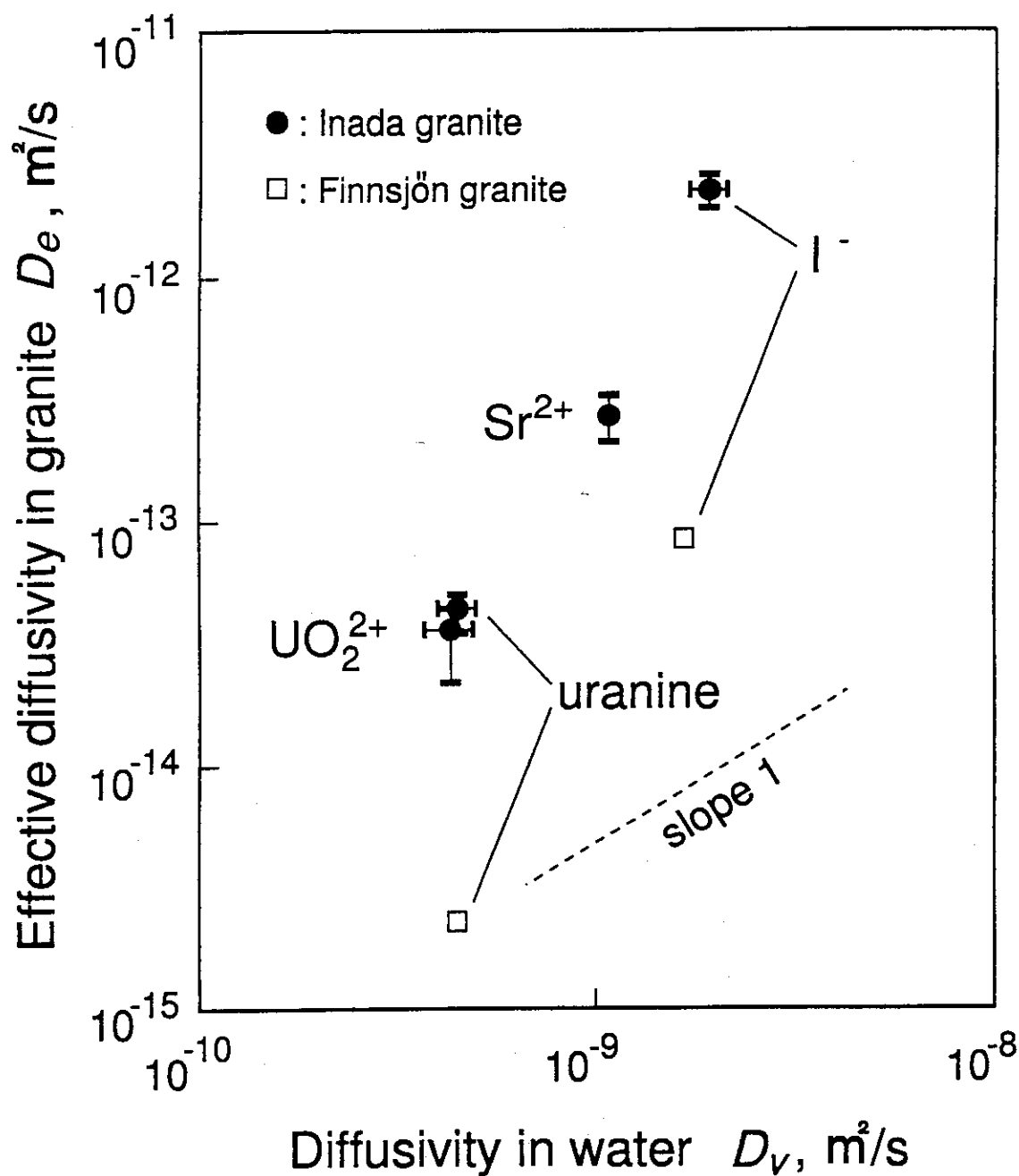
Fig. 41 Correlation between effective diffusivity of species in Inada granite and diffusivity in solution. Effective diffusivities for I⁻ and uranine in Swedish Finnsjön granite[2] are shown for comparison.

## 3.2.2 Nuclide Migration Experiments Using Fractured Rock under Deep Geological Conditions

M. Kumata

In order to study the migration of radionuclides under the conditions expected in the rock mass surrounding a disposal vault, an experimental system should represent deep geological conditions. Migration experiments using columns under deep geological conditions have been performed in a specially designed experimental room at the 240 level of the Underground Research Laboratory (URL), Manitoba, Canada, under JAERI/AECL cooperation. The results from these experiments showed that Tc and TRU elements such as Np, Pu, Am were strongly retained in columns under deep geological conditions [1-4]. Through these experiments it was convinced that the experimental system used is representing in-situ conditions very well.

New experimental plan was stated March 1994, under JAERI/AECL collaboration Phase 2. Large blocks of granite with dimensions of about $1 \times 1 \times 0.7$ m and containing part of the natural water-bearing fracture will be taken from the wall of a new room at the 240 level of the URL. The blocks will be placed under in-situ conditions. Migration experiments with groundwater from the fracture will be carried out using the blocks. Radionuclides such as Np and Pu will be injected in to the fracture of the block to study the radionuclides migration behavior through a fracture under deep geological conditions at a given flow field. Phase 2 will be completed September 1998.

REFERENCES

(1) Kumata, M. and T.T.Vandergraaf. 1992. 29th International Geological Congress, Kyoto, Japan, 1992 August 24-September 3.

(2) Kumata, M. and T.T.Vandergraaf. 1993. Radioactive Waste Management and the Nuclear Fuel Cycle, vol.17, No.2, pp.107-117.

(3) Kumata, M., T.T.Vandergraaf, and D.G.Juhnke. 1993. Migration '93, Charleston, SC, USA, 1993 December 12-17.

(4) Nakayama, S., T.T.Vandergraaf, and M.Kumata. 1994. Radioactive Waste Research, vol.1, No.1, pp.67-76 (in Japanese).

## 3.3 Natural Groundwater Flow System

### 3.3.1 Stable Isotope Hydrology

M. Kumata, M. Ohuchi, K. Watanabe and J. Shimada

INTRODUCTION

Groundwater will play an important role as a transport media of the radionuclide released from a vault of the radioactive wastes. Although, low flow and low permeable region is expected in a selection of an area for the radioactive wastes contained long lived radionuclides, a long-term groundwater flow is not negligible.

Stable isotope hydrology using deuterium and oxygen-18 contained in natural groundwater is considered as a useful tool for analysis and prediction of a long-term groundwater flow in a wide area.

Isotopic concentrations are expressed as $\delta$‰ values and refer to Standard Mean Ocean Water (SMOW) for international comparison.

$$\delta\text{‰} = \frac{R_{sample} - R_{SMOW}}{R_{SMOW}} \times 1000$$

where the R's are the $^{18}O/^{16}O$ or the $^{2}H/H$ isotope concentration ratios.

From the set of two values of $\delta^{18}O$ and $\delta D$ for each sample an origin of the groundwater will be analyzed. Based on the groundwater orgin, global water flow can be analyzed in a certain area.

ISOTOPIC RATIO

The $^{18}O/^{16}O$ and the $^{2}H/H$ in groundwater was analyzed by a gas mass spectrometer and expressed as $\delta^{18}O$ and $\delta D$, respectively. Pre-treatment of the groundwater samples is necessary to introduce gas samples to the mass spectrometer for the measurements of the isotopic concentrations. In the case of the $\delta D$ measurement, hydrophobic platinum catalyst was used to obtain the isotope equilibrium quickly between hydrogen gas and a water sample. In the case of the $\delta^{18}O$ measurement, $CO_2$ gas was equilibrated with water samples and introduced into the mass spectrometer.

An area was selected for the stable isotope hydrology in the central part of Japan and about 150 water samples were taken from the area. These samples were surface waters, shallow groundwaters and deep groundwaters. A big river is streaming from the west to

the east at the south boundary of the area.

The $\delta^{18}O$ and $\delta D$ values for each water samples from the area were plotted on a $\delta^{18}O$ - $\delta D$ diagram (Fig. 42). These values were distributed along the Local Meteoric Water Line obtained from the analysis of precipitation in Tokyo by IAEA. It is obviously clear that the groundwater in the area originate mainly in precipitation of this area. Further, the river water has different isotopic compositions from the groundwater in the area. Accordingly, the river water is not an origin of the groundwater. Considering with the local groundwater flow, groundwater movement from the river to the area is relatively less important than the vertical movement in the area.
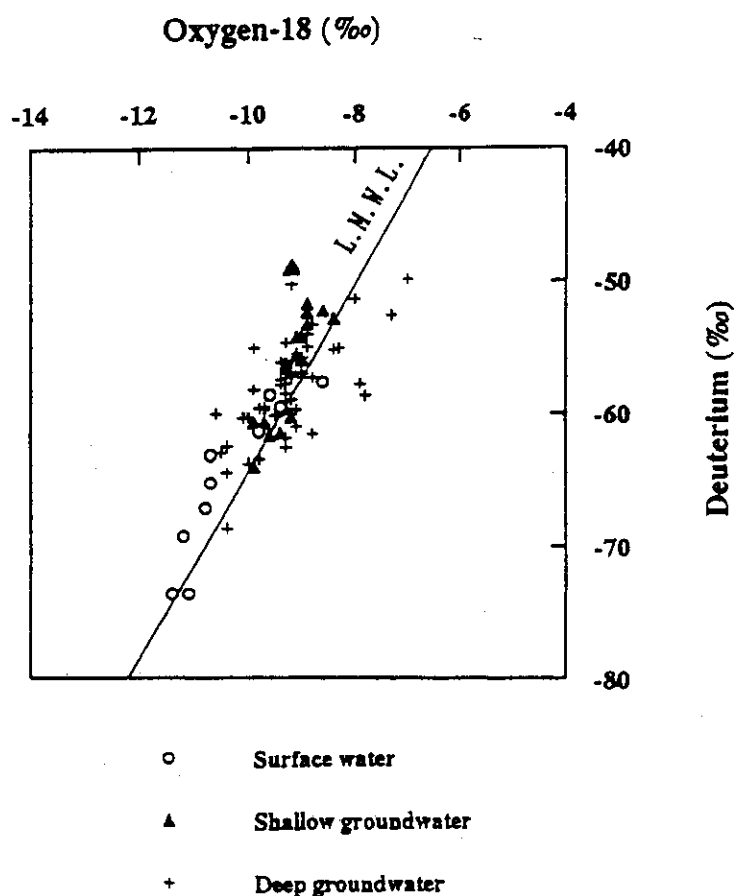
**Oxygen-18 (‰)**



Fig. 42   Relation between Oxygen-18(‰) and Deuterium(‰). The L. M. W. L. means the local meteoric water line obtained from the data analyzed for precipitation of Tokyo by IAEA during the period of from January 1964 to December 1979.

## 3.3.2 Basic Study on the Resistivity Tomography

M. Kumata, A. Chiba and R. Kubota

### INTRODUCTION

In the case of hard rock as a host rock of the HLW vault, fractures play an important role in the groundwater hydrology. Geotomography, the application of medical computed tomography to the underground survey, is one of the most effective technique to estimate rock fractures. Basic study of the resistivity tomography, one of techniques of geotomography, were carried out by using a tank filled with an NaCl solution for the physical model simulation tests.

Using the resistivity tomography, geological cross sections are visualized by reconstruction of the data obtained from measurements of the electrical potential in the ground. To fully understand the reconstructed cross section from the resistivity tomography, the detection limit and/or resolution of the technique should be discussed. Although numerical model calculations can handle the problem with digital computers, the verification of these results is difficult without supporting experimental work. For this purpose, an experimental approach was planned using a physical model simulation technique.

In earlier experiments performed for resolution investigations in electrical exploration work[1,2], it was pointed out that special construction of the tank walls is required to reduce wall effects that will perturb resistivity measurements[3]. The first step of our experiment was to examine the effect of the tank walls on the resistivity measurements to determine the area for which the wall effect is relatively small, so that further experiments could be performed with confidence.

The potential field in the tank was measured using a pole-pole array. Numerical experiments were carried out by using the 2.5 dimensional finite element method (FEM) and the results compared with the tank experiments.

### EXPERIMENTAL TANK

A steel tank 2×2 m square and 2.2 m high was prepared. Five 9 mm thick steel plates were used for the tank walls and placed inside a steel frame to support a water pressure of about 80 kPa. All surfaces of the tank walls were coated with a special insulating paint. Rubber sheets were placed between the bottom of the tank and the concrete floor to dampen vibration and avoid turbulence in the liquid.

The tank was filled to a depth of 2 m with a NaCl solution of resistivity 30 ohm-m. The surface in the cross section to be used in the experiments was set along the center line of the tank and two electrodes settled close to the wall surface in the tank to use as the infinite electrodes with in the pole-pole array. One was the infinite electrode of electric potential and the other was for current. The former electrode was a 1 mm diameter gold rod, while the latter was made of 2 mm diameter stainless steel. Both infinite electrodes penetrated 2 mm into the liquid.

ELECTRIC FIELD IN WHOLE TANK

A multi-electrode was prepared for the observation of the electric field in the whole tank. The multi-electrode contained twenty-seven pieces of 2 or 3 mm wide copper tape as potential electrodes. The multi-electrode was suspended in the NaCl solution with a weight. The top electrode was placed just on the solution surface and the lowest electrode was 180 cm beneath the liquid surface. Electrode spacings were varied from 2 cm to 20 cm depending on the location of the electrode. Each electrode of the multi-electrode was connected to measuring equipment, including a scanner and a transmitter. The electrodes were automatically scanned by the controlling equipment and measured values of electric potential were normalized using an applied current and recorded directly on to a floppy diskette.

Current was supplied to the liquid by the transmitter of equipment from the current source electrode settled in the center of the tank. The electrode was 2 mm diameter stainless steel as same as the infinite current electrode. Current conditions were as follows; square wave, 4 second period, 50% duty cycle and 200 mA amplitude.

The multi-electrode was moved and stopped 50 times along the center line of the tank to observe the electric field in the whole tank. Data were obtained totally at 1310 points on the section along the center line (Fig. 43). In an area close to the current source electrode, electric potential was too large to measure with the measuring equipment. The resistivity of the liquid in the tank was monitored during the observation, by measuring a voltage between the infinite electrode of electric potential and an electrode settled at 20 cm below the liquid surface. The electric potential field in the tank was obtained by plotting the measured potentials and drawing contour lines.

An equipotential contour map in the whole tank filled with a homogeneous media of resistivity 30 ohm-m was obtained by using a numerical model of 2.5 D finite element method (FEM). Boundary conditions of the model were based on the real tank. Electric

potentials were calculated on a 101× 101 mesh (2cm × 2cm) in the whole tank with triangular elements. Potentials were calculated by 2-D FEM for each wave number, then the potentials in the section were obtained by inverse Fourier transformation[4].

The calculated decreasing curve of potential for electric field was similar to the observed one. Therefore, the numerical model was thought to be a good representation of the tank, however, the observed electric field was larger than the calculated one.

## DETAILED OBSERVATION AROUND THE CURRENT SOURCE

The electric potential field around the current source electrode was observed in detail using an X-Y plotter settled above the electrode and a potential electrode made by a small rod of gold and a 30 cm long insulated fine pole. The potential electrode was located within 26 × 26 cm square are surrounding the current source point. The potential electrode was stepped in 5 mm increments both vertically and horizontally by the controlling plotter with a location accuracy of 0.1 mm.

A square wave current of 4 second duration and 100% duty cycle was transmitted at 1 mA into the liquid from the current source electrode. A small transmitter was used as the current source instead of the measurement equipment. Measured potentials and applied currents were converted to digitized time series data by a 12 bit A/D converter and then recorded to floppy diskette. Both potential and current was amplified and conditioned by 30 Hz low pass filter.

The electric potential field was calculated by applying the theory of images. Graphs showing the observed values and the theoretical curve are given in Fig. 44. Comparison of the observed and the calculated potential invariably showed that the observed values were larger than those calculated one. The theoretical curve well fitted with the observed values with a factor of 1.57.

An area sized 20 × 20 cm square was selected within the selection of the fine measured area described above. Sixty-one electrodes were arranged around the area for further investigation of the electric field. Again, calculations of the field strength were carried out using the numerical model for 2.5 D FEM and by applying the theory of images. Graphs showing the observed values and the calculated curves are shown in Fig. 45. Correspondence in shape of curves is very well. The calculated results derived from the numerical model and the theoretical curve are in good agreement, however, the observed potentials were larger in all instances. The factor was 1.40 to fit the FEM curve to the observed one.

CONCLUSION

Electric potentials were measured in the tank filled with a NaCl solution using a pole-pole array. The observed electric field was about 1.5 times larger than the calculated one. The theoretical field agreed with the 2.5 D FEM results suggesting the numerical model was representing the tank well.

FUTURE PLAN

On the basis of these experimental results, resolution and detection limits will be investigated using the tank and some other physical models representing low resistivity anomalies examined.

REFERENCES

(1) Apparao, A., 1979, Model Tank Experiments on Resolution of Resistivity Anomalies Obtained Over Buried Conducting Dykes - Inline and Broadside Profilling: Geophysical Prospecting, 27, 835-847.

(2) Karwatowski, J. and Habberjam, G. M., 1981, A Tunnel Resolution Investigation using an Automated Resistivity Tank Analog: Geophysical Prospecting, 29, 891-905.

(3) Goudswaad, W., 1959, On the effect of the tank wall material in geoelectrical model experiments: Geophysical Prospecting, 5, 272-281.

(4) Coggon, J. H., 1971, Electromagnetic and electrical modeling by the finite element method: Geophysics, 36, 132-155.
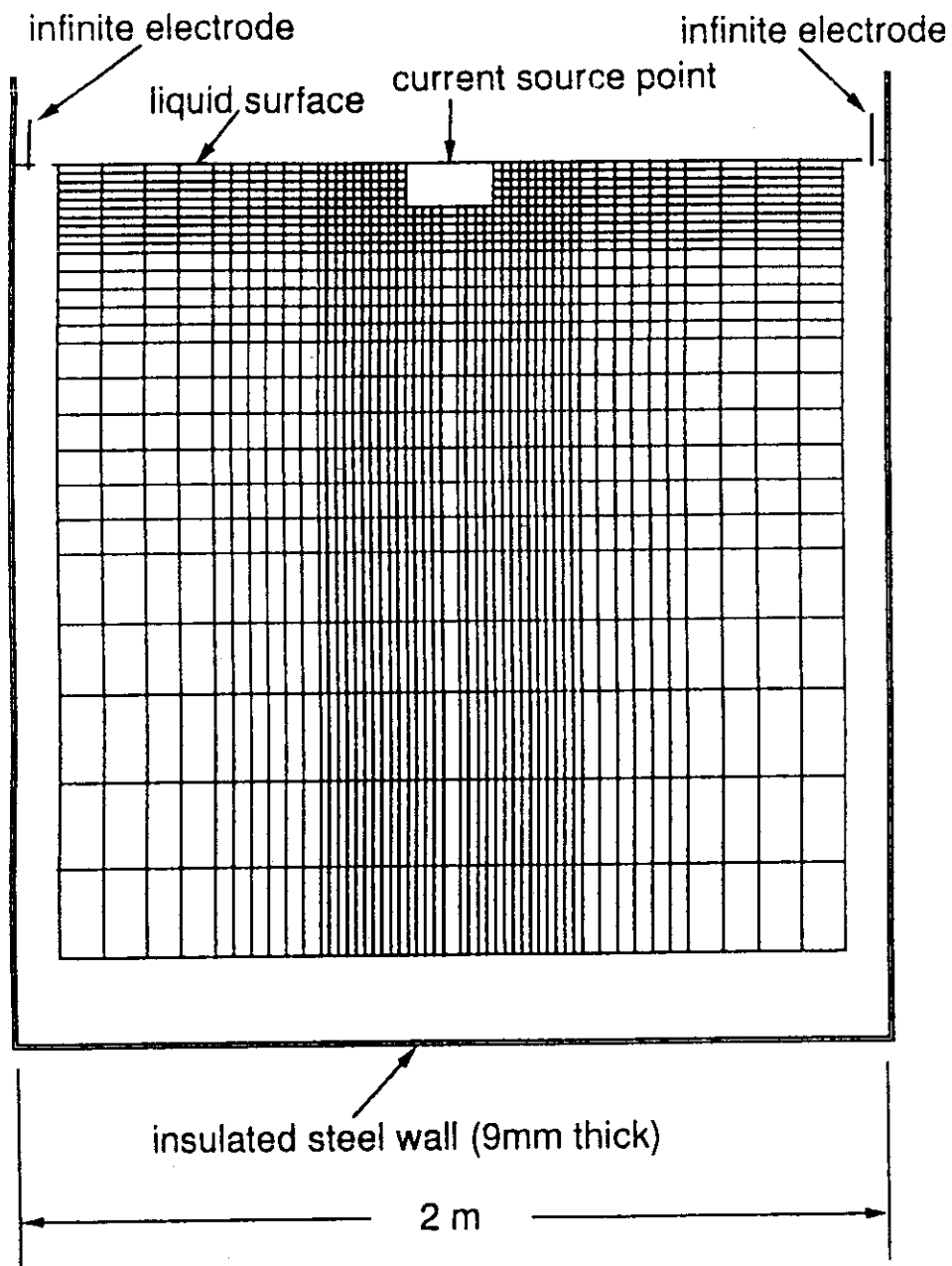
Fig. 43  Schematic diagram of the experimental tank showing the points of potential
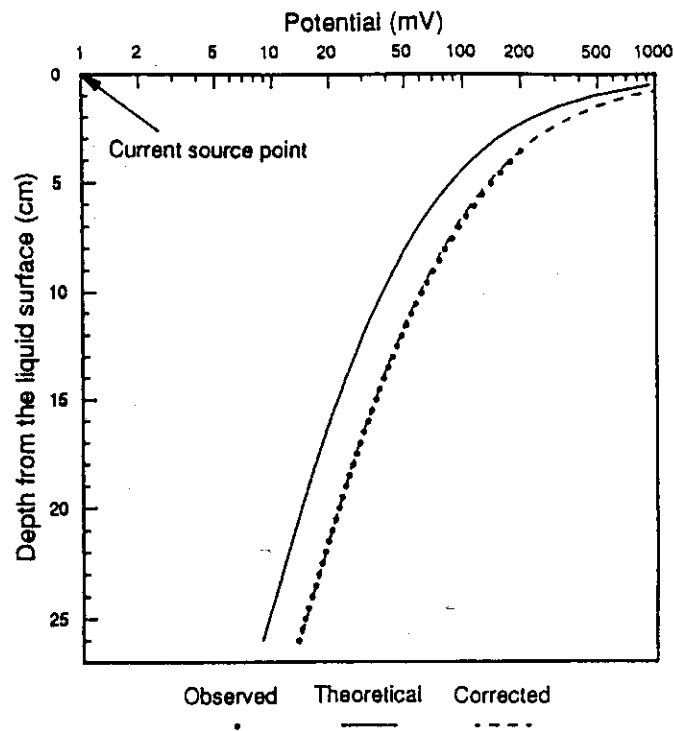measurement in the investigating section.

Fig. 44  Observed electric potentials and theoretical curve as a function of the distance from the liquid surface.
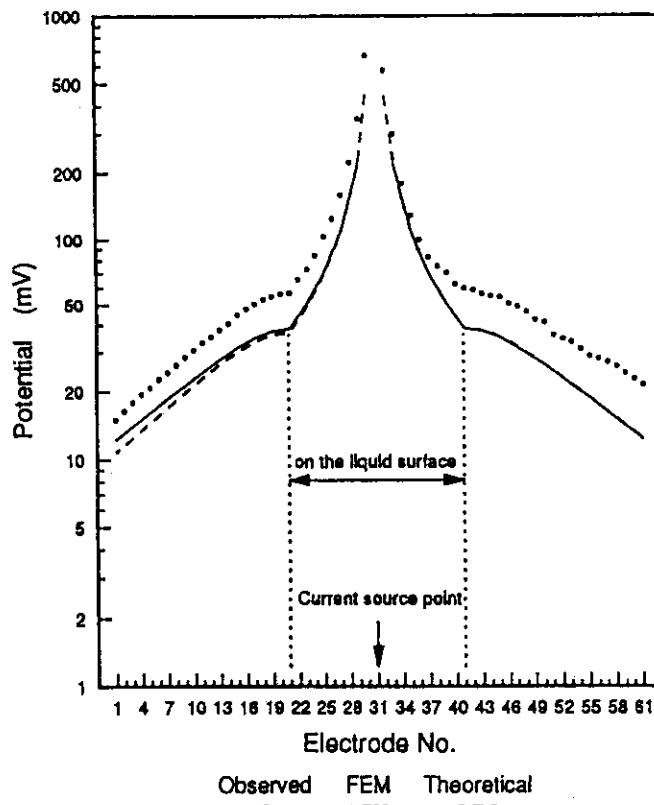


Fig. 45  Observed electric potentials, theoretical curve of the potentials and the 2.5 D FEM results.

### 3.3.3 Study on Relationship between Rock Resistivity and Pore Fluid Resistivity

H. Iwamoto, M. Kumata and H. Ii

INTRODUCTION

The geotomography technique visualizes the geological cross sections from the information for the invisible underground rock mass. Therefore it is expected that this technique will be available for the evaluation of the rock mass around the high level waste repository.

There are the seismic tomography, the radar tomography, the resistivity tomography and so on in the geotomography technique. Especially, the resistivity tomography is thought the most suitable technique for an examination of the water-bearing fractures by reason that this tomography is based on the sharp contrast between the high resistivity of the rock and the low resistivity of the underground water in the fractures.

In order to prepare tha basic data for the resistivity tomography, we have measured resistivity of granite which is one of crystalline rocks considered as candidate hosts for high level waste repositories [1-4]. Based on these data, the relationship between rock resistivity and pore fluid resistivity was studied.

EXPERIMENT

Fifteen cylindrical shaped granite samples were taken from the boring core of single borehole. The diameter of each sample is 5 cm and the length is 8 cm and porosity of samples varies from 0.55% to 2.66%. The samples were saturated with several different concentrations of KCl solution ranging from 220 ppm to 32500 ppm. After that, the rock samples were held in a box to prevent drying and to allow for stable measurement of the resistivity (Fig. 46). A square wave current of 30 second duration and 100% duty cycle was transmitted at 3V into the sample from the current source electrode [1]. Measured voltage and applied currents were converted to digitized time series data by a A/D converter and then recorded to floppy disk. The currents was amplified and conditioned by 20 Hz low pass filter. The rock resistivity is calculated by equation (1).

$$\rho = \frac{S}{L} \cdot \frac{\Delta V}{I} \qquad (1)$$

$\rho$ : resistivity of rock sample ($\Omega$m)

I : current in rock sample (A)

$\Delta V$ : voltage difference in axial direction (V)

S   : section area of rock sample ($m^2$)

L   : length of rock sample (m)

## RESULTS AND DISCUSSION

The resistivity of rock sample saturated with pore fluid increased with increasing pore fluid resistivity and became almost constant (Fig. 47). This result indicates that ARCHIE's formula (equation (2))[5] suggested for sand stone cannot be applied to granite when the pore fluid resistivity is high.

$$\rho_R = F \cdot \rho_W \qquad\qquad (2)$$

$\rho_R$ : rock resistivity ($\Omega m$)

$\rho_W$ : pore fluid resistivity ($\Omega m$)

$F$   : formation resistivity factor

KATSUBE and HUME[6] had proposed parallel circuit model expressed by equation (3) for gneiss.

$$\frac{1}{\rho_R} = \frac{1}{F \cdot \rho_W} + \frac{1}{\rho_C} \qquad\qquad (3)$$

$\rho_C$ : resistivity depended on pore-surface conduction ($\Omega m$)

For granite sample, equation (3) is applicable[1]. Using this equation, granite rock resistivity is well represented at all range of pore fluid resistivity (Fig. 47). The pore-surface resistivity ($\rho_C$) agrees with an asymptote which $\rho_R$ approaches when $\rho_W$ is infinite. A linear regresssion analysis of $1/\rho_R$ versus $1/\rho_W$ determines values of $F$ and $\rho_C$.

Figure 48 shows the relationship $F$ versus porosity of samples ($\phi$) and Fig. 49 shows the relationship $\rho_C$ versus $\phi$ on a log-log scale. Both $F$ and $\rho_C$ correlate with $\phi$, and following two regression curves are obtained.

$$F = 13.52 \; \phi^{-1.08} \qquad\qquad (4)$$

$$\rho_C = 3.19 \; \phi^{-1.52} \qquad\qquad (5)$$

These regression curves are substituted for equation (3), the following equation is obtained in case of fifteen rock samples.

$$\frac{\rho_R}{\rho_W} = \frac{1}{\dfrac{1}{13.52}\phi^{1.08} + \rho_W \cdot \dfrac{1}{3.19}\phi^{1.52}} \qquad (6)$$

Equation (6) shows the relationship among $\rho_R$, $\rho_W$ and $\phi$.

The porosity of rock mass around a borehole is predictable with equation (6) and the resistivity of rock mass from insitu electrical logging. There are two points to notice in this usage. One is how to practically know the resistivity of fluid solution in rock mass. The other is that the coefficient of equation (6) is available for only a borehole where fifteen samples were taken from. For using equation (6) for the sample taken from the other borehole, the study on the general value of coefficient are required.

REFERENCES

(1) A. Chiba and M. Kumata (1994): Resistivity Measurement for Granite and Tuff Samples - Influence of Pore Fluid Resistivity on Rock Resistivity -, BUTSURI-TANSA Vol. 47 No. 3, pp. 161-172.

(2) M. Kumata, H. Ii, H. Iwamoto and A. Chiba (1994): Rock resistivity and porosity of granite core samples, Proceedings of the 91st SEGJ Conference, pp. 298-300

(3) H. Iwamoto, M. Kumata, H. Ii and A. Chiba(1994): Relation between Resistivity of Granite Samples with Porosity and Pore Fluid, Proceedings of the 50th Annual Conference of the Japan Society of Civil Engineers, 3-(A), pp. 64-65.

(4) H. Iwamoto, M. Kumata, H. Ii and A. Chiba(1995): Prediction of Porosity Distribution in a Borehole Based on Resistivity of Rock Samples and Insitu Electrical Logging, The 27th symposium for Rock Mechanics.

(5) Archie, G. E. (1942): The electrical resistivity log as an aid in determining some reservoir characteristics, Trans. A. I. M. E., 146, pp. 54-67.

(6) Katsube, T. J. and Hume, J. P. (1983): Electrical resistivities of rocks from Chalk River, Proc. Ws. Geophys. Geosci. Res. at Chalk River, pp. 105-114.
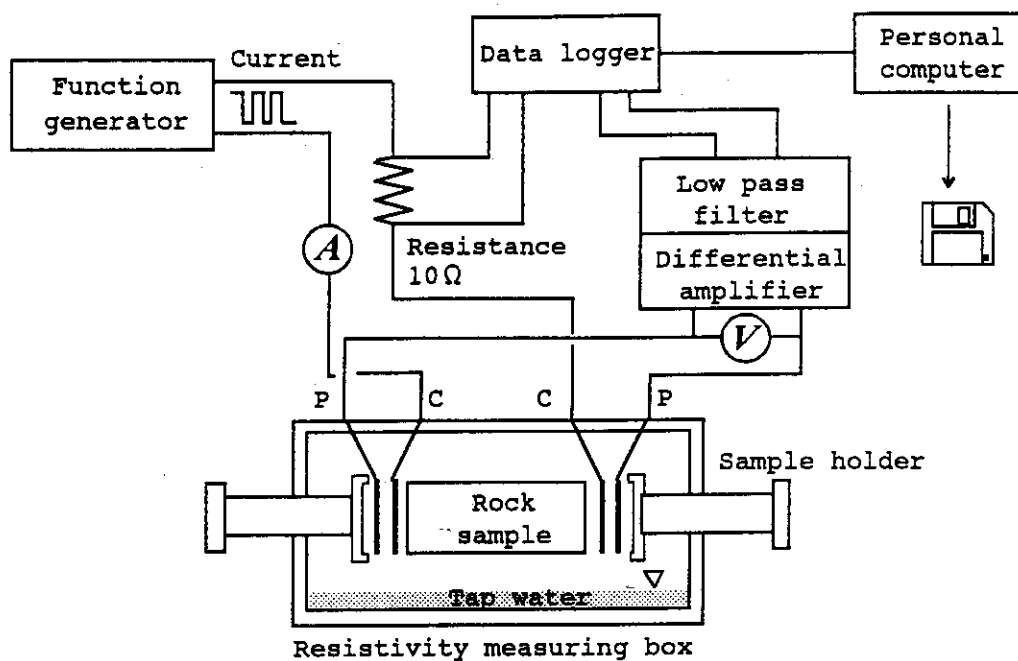
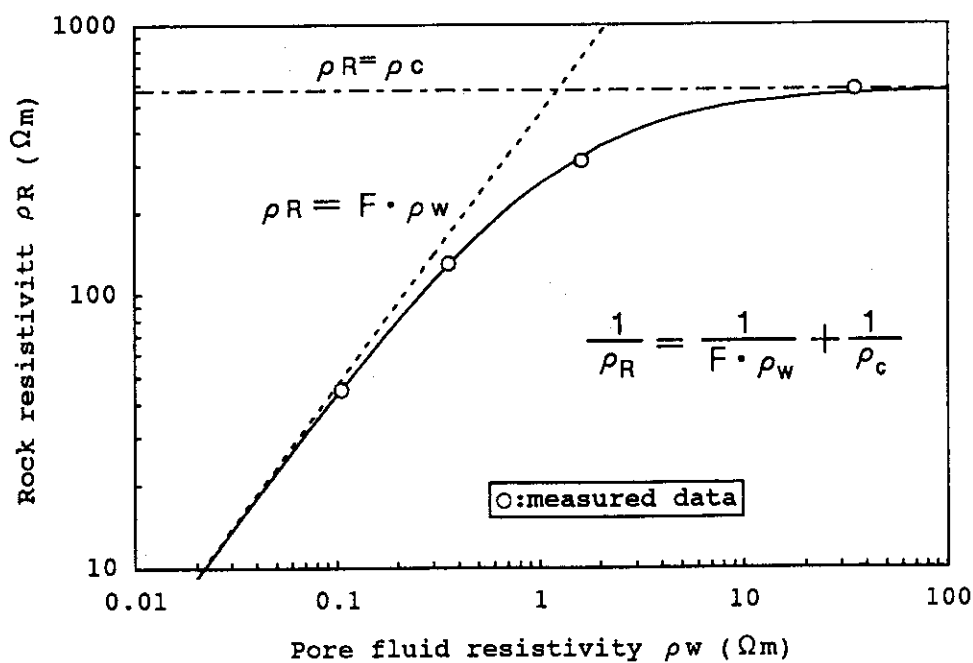Fig. 46   Schematic diagram of resistivity measurement system.



$$\frac{1}{\rho_R} = \frac{1}{F \cdot \rho_w} + \frac{1}{\rho_c}$$

Fig. 47   Example of relationship between rock resistivity and pore fluid resistivity.
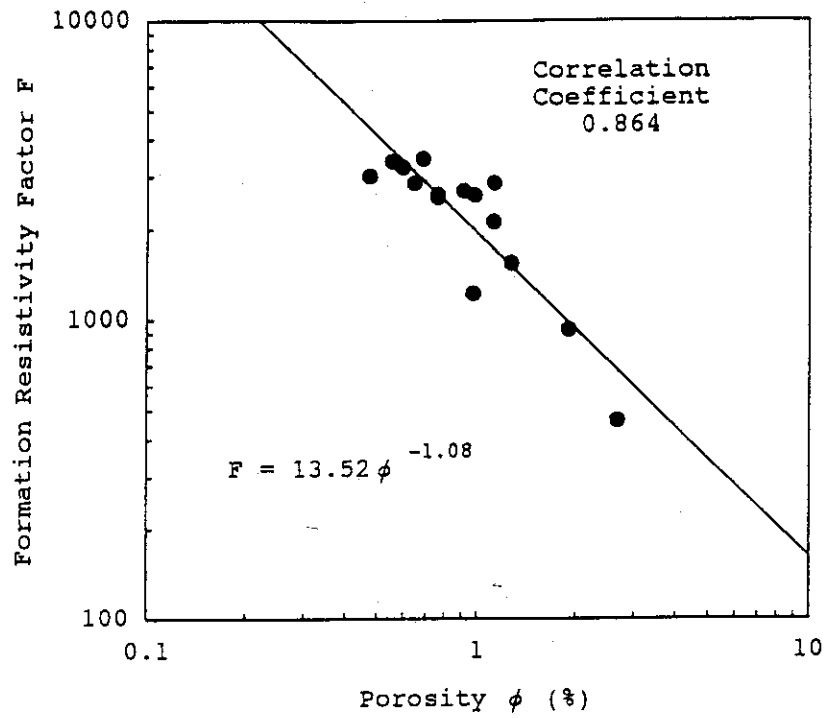
Fig. 48 Relationship between F and $\phi$.



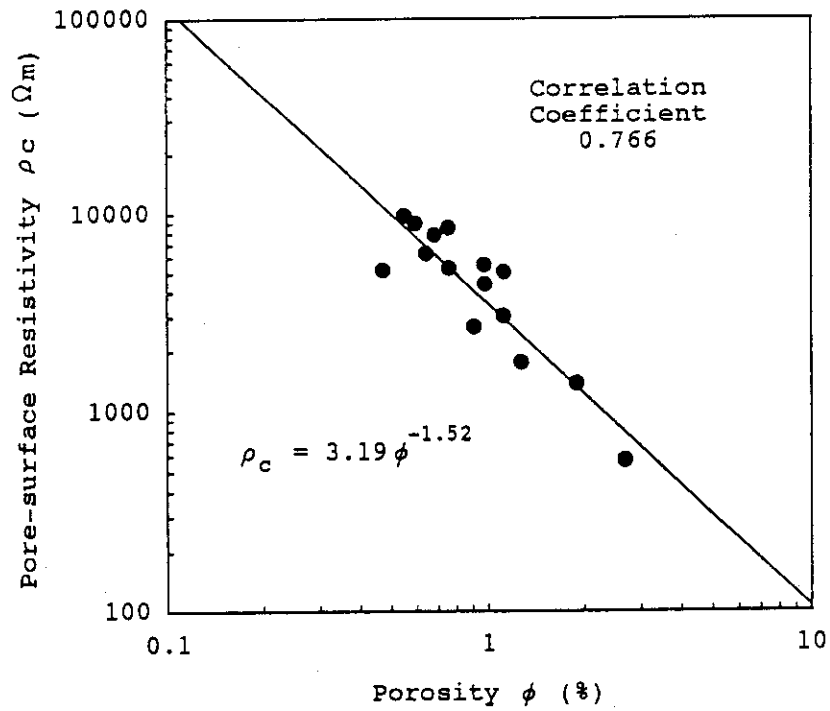Fig. 49 Relationship between $\rho_c$ and $\phi$.

# 3. 4  Natural Analogue

## 3.4.1  Natural Analogue Study

T. Ohnuki, N. Yanase, H. Isobe, T. Sato and K. Sekine

Analogue Studies in Alligator Rivers Region (ASARR) has been started in this year. ASARR is followed by Alligator Rivers Analogue Project (ARAP), one of the OECD/NEA projects. In ARAP, we have examined the processes, mechanisms, and kinetics of the chlorite weathering, and the uranium concentrations in minerals by various methods; X-ray diffraction analysis, scanning electron microscopy, electron microprobe analylsis, transmission electron microscopy, autoradiography, visible spectroscopy, and alpha and gamma spectrometry. The observed results were compared to those calculated, obtained based on the two models developed in ARAP. The results indicate that the water-rock interactions have resulted in weathering of chlorite, and uranyl in the groundwaters precipitates with the weathered products, and some of uranium is fixed to iron minerals occurred by the weathering.

We have also clarified the sequence of uranium minerals in and around both the primary and secondary ore deposits. Uraninite occurred in the primary ore deposit is dissolved by the oxidized water then is precipitated to form sklodowskite, uranyl silicate minerals. Sklodowskite also converts to kasolite with lead generated by radiogenic decay of uranium in sklodowskite. Sklodowskite alters to saléeite, uranyl phosphate minerals at apatite.

These results clearly indicate that the fixation mechanisms of uranium at Koongarra are the association with iron minerals occurred by the weathering of chlorite and the formation of uranium minerals.

However, all of iron minerals have not crystallised at the weathered zone. The anormary of activity ratio of $^{234}U/^{238}U$ in the residual fraction in the selective sequential extraction tests was observed. And the retardation mechanisms of uranium at the downgrandient of the secondary ore deposit have not yet clarified. Thus, the weathering process and mechanisms of chlorite and other minerals at Koongarra, and the migration behaviour of uranium and its daughter nuclides are not ideally clarified.

In ASARR, in order to refine the mechanisms of the weathering of chlorite and fixation of uranium, we have been conducting the sub projects of mineralogy, development of uranium series disequilibria at Koongarra, alteration of uranium minerals. Then, the migration mechanisms of uranium and its daughter nuclides is completed.

a) Mineralogy

Mineralogical study has begun for the 60 samples from DDH-85, -62, -58, -60, -87 and -92 by optical microscopy (OM), XRD and SEM/EDX/WDX and for a few samples by SIMS. Microscopic observations of the thin sections and XRD investigations for the whole rock and <2 $\mu$m fraction samples were almost brought to an end. These OM and XRD studies have made it clear a mineral alteration by weathering and a way of iron mineral formation. Moreover, the difference in resistence of the constituent minerals against weathering and in crystallinity of iron-minerals are revealed by micro infrared (IR) and visible (VIS) spectroscopy. For the same samples, uranium concentrations and activity ratio of some uranium series radionuclides have been measured by $\gamma$-spectrometry.

From the results of ARAP studies, iron minerals at Koongarra appear to influence the distribution of uranium and may have an important role in long-term fixation of U and its daughter radionuclides. At Koongarra, as pointed out by R. Edis in the final report of ARAP, iron minerals occur as coating clays, fissures and remnant schistosity planes, and form nodules. From our OM observations, it was also confirmed that these two occurrences are typical manners of iron mineral formation in weathered zone at Koongarra. The iron nodules are found at only centre and downgrandient of the dispersion fan.

Uranium concentration associated with iron minerals is different between these two manners (about 7% as $UO_3$ in the nodules and < 1% in the coatings). The crystallinity of iron minerals in the nodules is higher than the coatings. The concentrations of uranium in the nodules are correlated to those of copper and phosphorous. Ion mappings by SIMS show that the distribution of U corresponds to that of copper. These correlations probably suggest that the uranium forms a torbernite ($CU(UO_2)_2(PO_4)_2$) micro-crystalline in iron nodules. On the other hand, no correlation is gotten for the coatings iron minerals by EDX. Therefore, the different forms of iron oxide probably play different roles in the capture and storage of uranium. From these results, the iron minerals in nodules play as a most effective substance of uranium retention at downgrandient of economic uranium one.

Kaolinites, secondary altered minerals from chlorite, are major minerals in weathered zone. Some kaolinites are pregnant with the iron nodules. It can be defined that parents of the kaolinites are Fe-rich chlorites covered with Mg-rich chlorites from the observations based on sizes, inclusion minerals, textures. The Fe-chlorites are different in alteration process of the weathering from the Mg-chlorite. The Fe-chlorites are dissolved and converted to iron minerals. The Mg-chlorites are converted

to kaolinite, leaving their texture unchanged. The kaolinites from the Mg-chlorite can play role in pregnancy of the nodules like a womb. This pregnancy suggests that the formation of iron nodules is attributed to the texture and chemical composition of parent minerals.


b) The Development of Uranium Series Disequilibria at Koongarra

From the results of ARAP and partly ASARR, following scenario of weathering and uranium migration can be likely occurred at the Koongarra deposit. At the first stage of weathering, weathering proceeds through a path with high flow rate of groundwater such as fracture, grain boundary, rock matrix with high permeability, and the uranium in the primary ore deposit starts migration. Then the uranium in groundwater is coprecipitated with and deposited in the secondary minerals such as iron oxide minerals on the fracture surface, and in the grain boundary and rock matrix. The deposited uranium irradiate an alpha particle and partly contribute to the weathering by an increasing damage of crystal structure by alpha-ray irradiation and alpha recoil effect. In the ARAP, many microscopic observations which demonstrate these mechanisms were obtained. However, such data have not been linked to the macroscopic data which also indicate the uranium migration path. In the shallower zone (3-10 m), uranium concentration of rock is relatively low and smectite and vermiculite are still exist. These conditions are very different with that of DDH52-PH94 cross section where chlorite is fully weathered to kaolinite from the surface to the depth of about 25 m.

The activity ratios of uranium- and actinium series radionuclides in rock are changed depend on the geochemical condition due to difference of elemental characteristic, half-life, decay process of radionuclides. Figure 50 shows a two dimensional distribution of $^{230}Th/^{238}U$ activity ratios on the cross section of DDH85-92 line. Upgradient and downgradient in the shallow zone, and upgradient of the primary ore body, $^{230}Th/^{238}U$ activity ratios were greater than unity. This indicates that uranium leaching has occurred in this area. In the primary and secondary ore deposit, $^{230}Th/^{238}U$ activity ratios were approximately unity. At the depth of 15-25 m of DDH85 hole where uranium leaching may be occurred, $^{230}Th/^{238}U$ activivy ratios were unexpectedly unity. Downgradient of primary ore body and at the depth of 18-24 m under the secondary ore body, $^{230}Th/^{238}U$ activity ratios were less than unity which indicate uranium deposition have occurred in this area.


c) Alteration of Uranium Minerals

In ARAP, the alteration processes of uraninite to saléeite through sklodowskite are

clarified at transition zones of primary ore zone. Scope of the studies of alteration process of uranium minerals in ASARR has been concentrated in two fields in 1995. One is the microcrystallization of uranium minerals of uranyl phosphate minerals around iron minerals in the secondary ore zone downgradient. Another is alteration and formation processes of uraninite and uranyl-lead oxides and uranyl silicate minerals in the unweathered and transition zones of the primary ore zone.

A rock specimen, collected at the downstream of the secondary ore deposit, was examined mainly by high resolution transmission electron microscopy to understand a uranium fixation mechanism. Uranium was found to exist as saléeite $(Mg(UO_2)_2$ $(PO_4)_2.10H_2O)$ microcrystals of 1 - 20 nm in size scattered between iron minerals (mainly goethite and hematite) of 2 - 50 nm in size. The microtextural relationship between saléeite and the iron minerals reveals that the iron minerals function as catalyst for the formation of saléeite. The saléeite microcrystals show intermediately metamict microstructures, suggesting that they formed $5 \times 10^5$ to $4 \times 10^6$ years ago. Uranium has been fixed as saléeite at the downstream as in the secondary ore deposit. Saléeite samples in the secondary ore deposit showed completely periodic to fully metamict microstructures, suggesting that the saléeite a major uranium mineral in the secondary ore deposit, probably began to form a few million years ago and continued to form in a period of a million years since then.

In the transition zone, recently growing uraninite grains in veins with graphite were observed. Reduction of uranium by graphite and formation of uraninite have an important role to fix uranium from groundwater in the current transition zone.

d) Fixation Mechanisms of Uranium to Minerals

In ARAP, we have clarified that the water-rock interactions have resulted in weathering of chlorite, and uranyl in the groundwaters is sorbed on the weathered products, and precipitates and/or is sorbed on amrophous iron minerals which is one of the weathered products. Then, the uranium sorbed and/or precipitated with amrophous iron minerals are fixed to crystaline iron minerals during the crystallization.

By the activities in 1995, we have obtained some additional informations to refine the migration model of uranium and actinium series nuclides migration. Additional data compiled for the refinement are as follows:

i ) From our OM observations, it was confirmed that there are two different manners of iron minerals observed in weathered zone. One is iron minerals occur as coating clays, fissures and remnant schistosity planes. And the other is iron minerals occur as nodules. The iron nodules are found at only centre and downgrandient of the

dispersion fan. The crystallinity of iron minerals in the nodules is higher than the coatings.

Uranium concentration associated with iron minerals is different between these two manners (about 7% as $UO_3$ in the nodules and $< 1\%$ in the coatings). The concentrations of uranium in the nodules are correlated to those of copper and phosphorus. Ion mappings by SIMS show that the distribution of U corresponds to that of copper. These correlations probably suggest that the uranium is fixed in iron nodules as a torbernite $(Cu(UO_2)_2(PO_4)_2)$ micro-crystalline. On the other hand, no correlation is gotten for the coatings iron minerals by EDX. Therefore, the different forms of iron oxide probably play different roles in the capture and storage of uranium.

ii) Uranium was found to exist as saléeite $(Mg(UO_2)_2(PO_4)_2.10H_2O)$ microcrystals of 1 – 20 nm in size scattered between iron minerals (mainly goethite and hematite) of 2 – 50 nm in size in the downgradient of the secondary ore deposit. The microtextural relationship between saléeite and the iron minerals reveals that the iron minerals function as catalyst for the formation saléeite
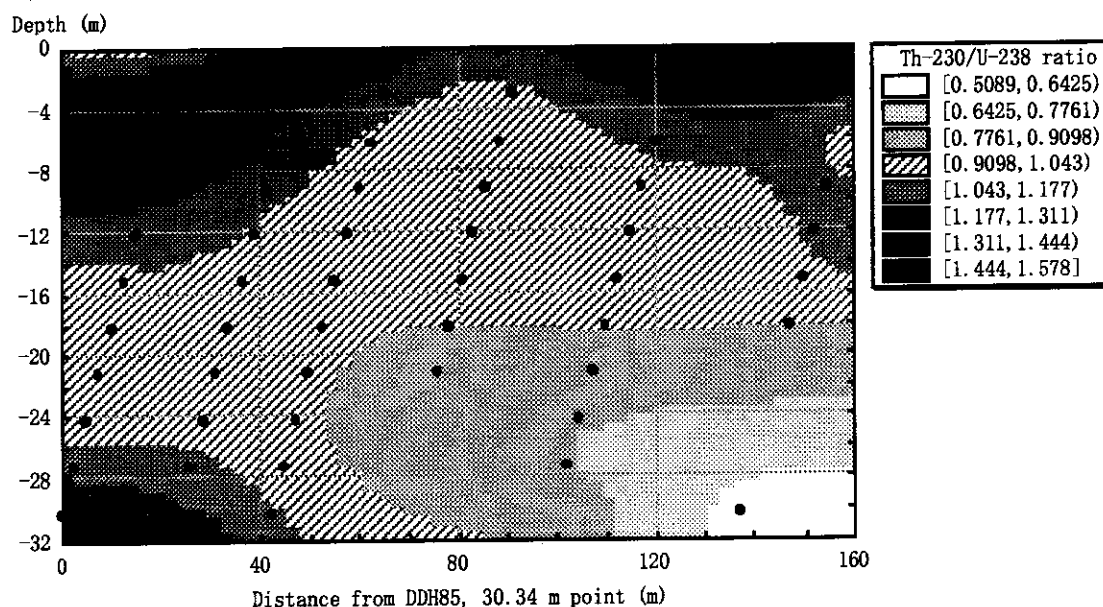


Fig. 50 Contour map of $^{230}Th/^{238}U$ activity ratios along the DDH85-DDH92 cross section. Closed circles show data points.